論文 / 著書情報
Article / Book Information

題目(和文)	素粒子標準模型を超える物理の宇宙論的相転移について
Title(English)	Cosmological Phase Transitions in Physics Beyond the Standard Model of Particle Physics
著者(和文)	藤倉浩平
Author(English)	Kohei Fujikura
出典(和文)	学位:博士(理学), 学位授与機関:東京工業大学, 報告番号:甲第11879号, 授与年月日:2021年3月26日, 学位の種別:課程博士, 審査員:山口 昌英,伊藤 克司,慈道 大介,今村 洋介,須山 輝明
Citation(English)	Degree:Doctor (Science), Conferring organization: Tokyo Institute of Technology, Report number:甲第11879号, Conferred date:2021/3/26, Degree Type:Course doctor, Examiner:,,,,
学位種別(和文)	博士論文
Type(English)	Doctoral Thesis

Ph.D. Thesis

January, 2021

Cosmological Phase Transitions in Physics Beyond the Standard Model of Particle Physics

Kohei Fujikura

Affiliation: Tokyo Institute of Technology

Abstract

One of the most important notions in modern particle physics is spontaneous symmetry breaking. The idea is that the underlying symmetries of nature are not manifest at the ground state, but the Lagrangians themselves are invariant. The cosmological history of spontaneous symmetry breaking provides us with rich information of underlying physics. Since the very early universe is filled with thermal plasma, the thermal effect plays an important role. When the temperature of the Universe is sufficiently higher than a certain scale of a symmetry breaking, a broken symmetry is restored. As the temperature decreases due to the cosmic expansion, cosmological phase transitions associated with rearrangement of the ground state take place.

If cosmological phase transitions are of first order, they proceed via nucleations of bubbles. They expand and eventually coalesce with each other until they fill the Universe. During this process, stochastic gravitational wave backgrounds are generated by bubble collisions, sound waves and turbulence of thermal plasma. Generated gravitational wave backgrounds are good target of future-planned experiments such as LISA, DECIGO and BBO.

Unfortunately, within the SM framework, the electroweak phase transition associated with electroweak symmetry breaking is not of first order confirmed by lattice studies, and hence, there is no production of the gravitational wave background. However, many theories beyond the Standard Model of particles physics have been proposed based on various motivations, *e.g.* naturalness of the electroweak symmetry breaking, origins of dark matter, neutrino masses and baryon asymmetry, and so on. In general, cosmological phase transitions realized in such theories can be of the first order, and thus, we can test these theories by the detection of gravitational wave backgrounds.

In this thesis, we consider two models of physics beyond the Standard Model of particle physics. One is the twin Higgs models which are motivated for solving the little hierarchy problem. The another model is the minimal scotogenic model where origins of dark matter and neutrino masses are simultaneously addressed. We study these models at finite-temperature and discuss cosmological phase transitions as well as their implications on electroweak baryogenesis and production of gravitational wave backgrounds.

In the twin Higgs models, it is shown that the expectation value of the Standard Model Higgs field at the critical temperature of the electroweak phase transition is much smaller than the critical temperature, which indicates two important facts: (i) the electroweak phase

transition cannot be analyzed perturbatively (ii) the electroweak baryogenesis is hardly realized in the typical realizations of twin Higgs models. We also analyze the phase transition associated with the global symmetry breaking, through which the Standard Model Higgs is identified with one of the pseudo-Nambu-Goldstone bosons in terms of its linear realization, with and without supersymmetry. For this phase transition, we show that, only in the supersymmetric case, there are still some parameter spaces, in which the perturbative approach is validated and the phase transition is of the first order. However, gravitational wave backgrounds, generated by the first-order phase transition, is impossible to be detected by LISA, DECIGO, BBO and ultimate-DECIGO in the linear realization and in the decoupling limit. The detection of the stochastic gravitational wave background with the feature of first order phase transition, therefore, will give strong constraints on twin Higgs models.

In the scotogenic model, there are two dark matter candidates: an electromagnetically neutral scalar component of an additional scalar $\mathrm{SU(2)_W}$ doublet (the scalar dark matter scenario), and a right-handed neutrino (the fermion dark matter scenario). The scalar dark matter scenario is similar to the inert scalar doublet extension of the Standard Model where a strong first-order electroweak phase transition favors a portion of the low mass regime of dark matter which is disfavored by the latest direct detection constraints. In the fermion dark matter scenario, we obtain a parameter space that favors strong first-order electroweak phase transition as the restriction on mass ordering within inert scalar doublet that can be relaxed. While the fermion dark matter remains safe from stringent direct detection constraints, the newly allowed low mass regime of the charged scalar can leave tantalizing signatures in collider experiments and induce charged lepton flavor violation processes within the reach of future experiments. We obtain such new parameter space satisfying dark matter relics, a strong first-order electroweak phase transition with detectable gravitational waves, light neutrino mass and other relevant constraints.

Contents

Chapter 1

Introduction

Results from collider experiments, including the discovery of the Standard Model-like Higgs boson at the Large Hadron Collider (LHC) experiments, strongly indicate that the Standard Model (SM) of particle physics can explain phenomenologies around and below the electroweak scale. In spite of this fact, SM would not be a theory of everything because it has some difficulties. For example, dark matter (DM), a matter and anti-matter asymmetry, tiny but non-zero neutrino masses and naturalness of the electroweak symmetry breaking remain as unsolved problems. For this reason, several physics beyond the SM has been proposed so far.

In physics beyond the SM, the thermal history of the very early Universe can differ from the standard one. When the temperature of the Universe was the order of the electroweak scale, the electroweak phase transition associated with the electroweak symmetry breaking is expected to occur. Within the SM framework, the electroweak phase transition is known to be crossover [1, 2, 3] confirmed by lattice studies. However, in physics beyond the SM, since the Higgs sector is significantly different from the SM, it is non-trivial whether the electroweak phase transition is of first order, or not. Furthermore, physics beyond the SM usually has additional spontaneous symmetry breaking different from the ordinary electroweak symmetry breaking. Hence cosmological phase transitions associated with such additional symmetry breaking can be of first order.

If cosmological phase transitions including the ordinary electroweak phase transition are of first order, they proceed via nucleations of bubbles. After nucleations of bubbles, they expand and eventually coalesce with each other leading to the completion of phase tran-

sitions. During this process, gravitational wave (GW) signals are generated from bubble collisions [4, 5, 6, 7, 8], sound waves [9, 10, 11, 12], and turbulence of the plasma [13, 14, 15, 16, 17, 18]. The typical peak frequencies of GW signals generated by the first order phase transition associated with the electroweak symmetry breaking are around $\mathcal{O}(10^{-3} \sim 10)$ Hz, which are good targets of space-based interferometers such as LISA, [14], DECIGO [19] and BBO [20]. Therefore, if first-order cosmological phase transitions take place in physics beyond the SM, they can be tested by these astrophysical observations. Moreover, if the SM Higgs vacuum expectation value (VEV) at the critical temperature is larger than the critical temperature, inside the bubble, the electroweak phase transition is called *strong first order* and the sphaleron decoupling condition is satisfied. (See Sec. 3.3.3 for the definitions of a first order phase transition and a strong first order phase transition.) The strong first-order electroweak phase transition accommodates electroweak baryogenesis [21, 22], so that the present baryon asymmetry of the Universe can be explained. In this thesis, we explore the possibility of GW production generated by cosmological first-order phase transitions and realization of the strong first-order electroweak phase transition in physics beyond the SM.

Naturalness of the electroweak symmetry breaking has been a good guideline to explore physics beyond the SM. Popular scenarios of physics beyond the SM include supersymmetry (SUSY) and composite Higgs, which are still promising solutions to the (large) hierarchy problem, since they remove the sensitivity of the weak scale to quadratically divergent quantum effects from physics at high energy scales such as the Planck scale and the grand unification scale. However, the discovery of the SM-like Higgs boson and nothing else at the LHC poses a problem for naturalness. No new colored particles predicted in these popular scenarios have been observed so far at the LHC, which already leads to fine-tuning in the Higgs potential at sub-percent level. Although we do not know whether nature takes thought for this little hierarchy problem or not, it is interesting to pursue possibilities to ameliorate this fine-tuning and to explore their implications for particle phenomenology and cosmology.

The twin Higgs mechanism [23] is an attractive idea to provide a solution to the little hierarchy problem without introducing new colored states. There are several variations to realize this idea, but every twin Higgs model starts with the assumption that the SM Higgs field can be considered as one of the pseudo-Nambu-Goldstone bosons (pNGBs) arising from spontaneous breaking of a global symmetry $\mathcal{G}$, such as U(4) symmetry, that contains $\mathrm{SU}(2)_\mathrm{A} \times \mathrm{SU}(2)_\mathrm{B}$ symmetry in its subgroups, to a smaller group $\mathcal{H}$, such as U(3). Here

$SU(2)_A$ and the mirror (or twin) $SU(2)_B$ are gauged and interchanged under a (approximate) $\mathbf{Z}_2$ symmetry. The $SU(2)_A$ gauge symmetry is identified with the $SU(2)_W$ symmetry in the SM and spontaneously broken by the vacuum expectation value (VEV) of the Higgs field. By introducing a $SU(3)_{\widehat{C}}$ mirror color symmetry and mirror fermions that are charged under $SU(3)_{\widehat{C}} \times SU(2)_B$, quadratic divergence to the Higgs potential coming from the SM colored particles (and $SU(2)_W$ gauge bosons) are canceled by the mirror colored particles (and $SU(2)_B$ gauge bosons).

We find that in the non-supersymmetric twin Higgs models, thermal potential around both the electroweak and global symmetry breaking cannot be analyzed perturbatively, which suggests that both phase transitions are unlikely to be first order and hence we can expect for neither the electroweak baryogenesis nor the generation of GW signals. Even in the case with supersymmetric UV completion, by limiting ourselves to the linear realization and the decoupling limit where only the mirror scalar top quarks are added to the non-supersymmetric model, we find that the electroweak symmetry breaking cannot still be analyzed perturbatively and the conclusion is still robust. For the global symmetry breaking, however, we show that, with an appropriate parameter choice, the phase transition associated with it can be of first order and the generated GW signals are generated, but unfortunately, it is too small to be detected by future planed experiments such as BBO, DECIGO and ultimate-DECIGO.

The scotogenic model, proposed by Ma in 2006 [24], is also one of promising candidates of physics beyond the SM. This model simultaneously gives solutions to origins of tiny neutrino masses and DM. In spite of significant experimental evidences confirming the non-vanishing yet tiny neutrino masses and the presence of a mysterious, non-luminous, non-baryonic form of matter, dubbed as DM [25], its origin remains unaddressed in the SM. While the latest experimental constraints on light neutrino parameters can be obtained from recent global fits [26, 27], the present DM abundance is quantified in terms of density parameter $\Omega_{\rm DM}$ and $h = 0.705 \pm 0.013$ as [28]: $\Omega_{\rm DM}h^2 = 0.120 \pm 0.001$ at 68% CL. The possibility of scalar DM in this model has been already studied in several works including [29, 30, 31, 32, 33, 34, 35, 36, 37, 38, 39, 40, 41, 42, 43], whereas that of thermal or non-thermal fermion DM has also been studied [44, 45]. The model can also account for the observed baryon asymmetry through successful leptogenesis in variety of different ways [46, 43, 47, 48, 49, 45, 50]. While the observational evidences suggesting the presence of DM are purely based on its gravitational

interactions, most of the particle DM models (including the scotogenic model) adopt a weak portal (but much stronger than gravitational coupling) between DM and the visible matter or the SM particles. If DM is of thermal nature, like in the weakly interacting massive particle (WIMP) paradigm, then such couplings between the SM particles and DM can be as large as the electroweak couplings. Hence such DM can leave imprint on direct search experiments. However, none of the direct detection experiments such as LUX [51], PandaX-II [52, 53] and Xenon1T [54, 55] have reported any positive signal yet, giving more and more stringent upper bounds on interactions between DM and nucleons.

Several works have studied such interplay of DM and first-order electroweak phase transition, specially in the presence of additional scalar doublet DM like we have in the present model [56, 57, 58, 59, 60, 61, 62]. While scalar doublet DM extension of the SM, popularly known as inert doublet model (IDM) allows a large parameter space supporting a first-order electroweak phase transition, most of this parameter space corresponds to sub-dominant DM [59] leaving a narrow window in low mass DM regime where both DM relic and strong first-order electroweak phase transition criteria can be simultaneously satisfied [57]. On the other hand, this low mass regime becomes increasingly in tension with direct search experiments as well as the collider constraints on invisible decay rate of the SM-like Higgs, where the former remains much more stringent. In fact, we show that the parameter space of scalar DM which satisfies strong first order electroweak phase transition is in reality disfavored by Xenon1T data of 2018. Extending IDM to scotogenic model not only addresses the origin of tiny neutrino masses, but also enlarges the parameter space that can simultaneously produce the observed DM relic density as well as the strong first-order electroweak phase transition. We discuss possibilities of both scalar and fermion DM in this model and constrain the parameter space from DM relic, strong first-order electroweak phase transition as well as light neutrino masses while incorporating relevant experimental and theoretical bounds. We then study the possibility of generating GW from the strong first-order electroweak phase transition and discuss the possibility of its detection in future experiments.

1.1 Organization

This thesis is organized as follows.

Chapter 2 is a review part of the SM of particle physics and its beyond. In Sec. 2.1, we construct the SM Lagrangian density based on the gauge principle and rernormalizability and summarize several features of the SM. In Sec. 2.2, we discuss three difficulties of the SM, which are naturalness of the SM Higgs mass parameter, origins of DM and the non-zero but tiny neutrino masses. In Sec. 2.3 is a review of twin Higgs models, which give the attractive solution to the little hierarchy problem. In particular, we study the dynamics of the EWSB at zero-temperature. In Sec. 2.4, we introduce minimal scotogenic model, which simultaneously addresses origins of the DM and neutrino masses. Several collider and precision constraints on this model are also summarized.

Chapter 3 is a review part of physics in the early Universe. In Sec. 3.1, we review a dynamics of an expanding Universe by solving the Friedmann equation. It will turn out that the Universe was filled by hot plasma, and hence, the standard thermodynamics plays a key role to understand physics occurred in the early Universe. We also clarify a local equilibrium condition based on the Boltzmann equation. In Sec. 3.2, we explain the standard freeze-out DM production mechanism. The annihilation cross section in the presence of the coannihilation is also presented. In Sec. 3.3, we compute the zero-temperature effective potential as well as finite temperature effective potential and discuss a resummation calculation and higher-order corrections from non-Abelian gauge fields. In Sec. 3.4, order of cosmological phase transitions is discussed. A calculation method of bounce action and formulae of GW signals produced by first-order phase transitions are shown.

Chapter 4 is based on my original work [63]. In Sec. 4.1, we explain motivation to consider cosmological phase transitions in twin Higgs models and outline of calculation method. In Sec. 2.3, we explain the thermal history realized in twin Higgs models and explain assumptions of two-step phase transition. In Sec. 4.3, we study twin Higgs models with and without SUSY at non-zero temperature and examine how the electroweak symmetry breaking proceeds. In Sec. 4.4, we examine how the global symmetry breaking proceeds and show that in supersymmetric twin Higgs models the first order phase transition can be realized for appropriate parameter choices but the resultant gravitational wave background is undetectable at planned gravitational wave detectors. Sec. 4.5 is devoted to our concluding

remarks and comments of twin Higgs models.

Chapter 5 is based on my original work [64]. In Sec. 5.1, we explain motivation to consider cosmogical phase transition realized in minimal scotogenic model. In Sec. 5.2, we explain the thermal history realized in minimal scotogenic model and explicitly show several physical quantities, which are necessarily to compute the thermal effective potential. In Sec. 5.3, we discuss our results both of scalar and fermion dark matter scenarios. We investigate parameter space leading to the strong first-order electroweak phase transition and explicitly derive GW signals. In the parameter search, we impose phenomenological constraints such as the dark matter direct detection constraints and the charged lepton flavor violation processes. We finally conclude in Sec. 5.4.

Finally, conclusion of this thesis is devoted to the Chapter 6.

Chapter 2

Physics beyond the Standard Model

This chapter is a review part related to physics beyond the SM. We first review the SM Lagrangian density and explain its basic features. After the review, we summarize three difficulties of the SM, which are the naturalness of the Higgs mass parameter, a generation of non-zero neutrino masses and the DM. To address these difficulties, we introduce physics beyond the SM. In particular, we first consider twin Higgs models to ameliorate a fine-tuning to the SM Higgs mass parameter. Second, we introduce minimal scotogenic model, which simultaneously gives solutions to origins of the DM and neutrino masses.

2.1 Standard Model of Particle Physics

In this section, we review SM of particle physics. We construct the SM Lagrangian density allowed by gauge symmetry and renormalizability with given matter content. Here, renormalizability implies that all operators appearing the Lagrangian density should have mass dimensions smaller than four.

The SM gauge symmetries are $\mathrm{SU(3)_C} \times \mathrm{SU(2)_W} \times \mathrm{U(1)_Y}$. Under these gauge symmetries, charge assignments of the SM leptons, quarks and Higgs are listed in Table. 2.1. In the table, ν_{nL}, $e_{nL(R)}$, $u_{nL(R)}$ and $d_{nL(R)}$ are the left-handed neutrinos, the left (right)-handed charged leptons, the left (right)-handed up-type quarks and the left (right)-handed down-type quarks, respectively. Here, all fermion fields are Dirac fermions. The suffix n represents

SM particles	$\mathrm{SU(3)_C}$	$\mathrm{SU(2)_W}$	T_3	Y	Q_{EM}
G^A_μ	**8**	**1**	–	–	–
W^I_μ	**1**	**3**	–	–	–
B_μ	**1**	**1**	–	–	–
$L_n = \begin{pmatrix} \nu_{nL} \\ e_{nL} \end{pmatrix}$	**1**	**2**	$+1/2$ $-1/2$	$-1/2$	0 -1
e_{nR}	**1**	**1**	0	-1	-1
$Q_n = \begin{pmatrix} u_{nL} \\ d_{nL} \end{pmatrix}$	**3**	**2**	$+1/2$ $-1/2$	$+1/6$	$+2/3$ $-1/3$
u_{nR}	**3**	**1**	0	$+2/3$	$+2/3$
d_{nR}	**3**	**1**	0	$-1/3$	$-1/3$
$H_{\mathrm{SM}} = \begin{pmatrix} \phi^+ \\ \phi^0 \end{pmatrix}$	**1**	**2**	$+1/2$ $-1/2$	$+1/2$	$+1$ 0
$(\nu_{nR}$	**1**	**1**	0	0	$0)$

Table 2.1: Matter content of the SM particles, and these dimensions of representations and charge assignments are listed. T_3, Y and Q_{EM} are the $\mathrm{SU(2)_W}$ isospin, the weak hypercharge and the electromagnetic charge. The right-handed neutrinos ν_{nR} are not introduced in the SM, but we show its charge assignment for later convenience.

the number of generations and runs 1 to 3. Concretely, these fields are given by

$$\begin{aligned} &n=1: \nu_{1L} \equiv \nu_{eL},\ e_{1L(R)} \equiv e_{L(R)},\ u_{1L(R)} \equiv u_{L(R)},\ d_{1L(R)} \equiv d_{L(R)}, \\ &n=2: \nu_{2L} \equiv \nu_{\mu L},\ e_{2L(R)} \equiv \mu_{L(R)},\ u_{2L(R)} \equiv c_{L(R)},\ d_{2L(R)} \equiv s_{L(R)}, \\ &n=3: \nu_{3L} \equiv \nu_{\tau L},\ e_{3L(R)} \equiv \tau_{L(R)},\ u_{3L(R)} \equiv t_{L(R)},\ d_{3L(R)} \equiv b_{L(R)}. \end{aligned} \tag{2.1}$$

In the above expressions, $\nu_{e,\mu,\tau L}$ is the left-handed electron, mu, τ-neutrinos. $e_{L(R)}$, $\mu_{L(R)}$ and $\tau_{L(R)}$ are the left (right)-handed electron, muon and tauon, respectively. $u_{L(R)}$, $c_{L(R)}$ and $t_{L(R)}$ are the left (right)-handed up, charm and top quarks, respectively. $d_{L(R)}$, $s_{L(R)}$ and $b_{L(R)}$ are the left (right)-handed down, strange and bottom quarks, respectively.

Note that the right-handed neutrinos ν_{nR} are absent in the SM because these existences have not yet been proved, but we show these charge assignment for later convenience. (We will discuss the right-handed neutrinos in Sec. 2.2.2.) T_3, Y and Q_{EM} denote the $\mathrm{SU(2)_W}$

isospin, the weak hypercharge and the electromagnetic charges, respectively. We define the SM Higgs, the left-haded quark and lepton $\mathrm{SU(2)_W}$ doublets as follows.

$$H_{\mathrm{SM}} = \begin{pmatrix} \phi^+ \\ \phi^0 \end{pmatrix}, \; Q_n = \begin{pmatrix} u_{nL} \\ d_{nL} \end{pmatrix}, \; L_n = \begin{pmatrix} \nu_{nL} \\ e_{nL} \end{pmatrix}. \tag{2.2}$$

The SM Lagrangian density, $\mathcal{L}^{\mathrm{SM}}$, can be schematically decomposed into following pieces:

$$\mathcal{L}^{\mathrm{SM}} = \mathcal{L}^{\mathrm{SM}}_{\text{gauge boson}} + \mathcal{L}^{\mathrm{SM}}_{\text{fermion}} + \mathcal{L}^{\mathrm{SM}}_{\text{Higgs}}. \tag{2.3}$$

where $\mathcal{L}^{\mathrm{SM}}_{\text{gauge bosons}}$, $\mathcal{L}^{\mathrm{SM}}_{\text{Yukawa}}$ and $\mathcal{L}^{\mathrm{SM}}_{\text{Higgs}}$ are the Lagrangian densities of the SM gauge boson sector, the SM fermion sector and the SM Higgs sector. These precise expressions will be given in the following subsubsections.

The SM gauge sector

The Lagrangian density of the gauge bosons sector is given by

$$\mathcal{L}^{\mathrm{SM}}_{\text{gauge boson}} = -\frac{1}{4}\mathrm{Tr}\left[G^A_{\mu\nu}G^{A\mu\nu}\right] - \frac{1}{4}\mathrm{Tr}\left[W^I_{\mu\nu}W^{I\mu\nu}\right] - \frac{1}{4}B_{\mu\nu}B^{\mu\nu}, \tag{2.4}$$

where $G^A_{\mu\nu}$, $W^B_{\mu\nu}$ and $B_{\mu\nu}$ are field strength of the $\mathrm{SU(3)_C}$, $\mathrm{SU(2)_W}$ and $\mathrm{U(1)_Y}$ gauge bosons defined by

$$\begin{aligned} G^A_{\mu\nu} &\equiv \partial_\mu G^A_\nu - \partial_\nu G^A_\mu + g_3 f_{ABC} G^B_\mu G^C_\nu, \\ W^I_{\mu\nu} &\equiv \partial_\mu W^I_\nu - \partial_\nu W^I_\mu + g_2 \epsilon_{IJK} W^J_\mu W^K_\nu, \\ B_{\mu\nu} &\equiv \partial_\mu B_\nu - \partial_\nu B_\mu. \end{aligned} \tag{2.5}$$

In these expressions, $G^A_\mu \equiv G_\mu \lambda^A/2$ (λ_A: Gell-Mann matrices with $A = 1, 2, \cdots, 8$), $W^I_\mu \equiv W_\mu \sigma^I/2$ (σ^I: Pauli matrices with $I = 1, 2, 3$) and B_μ are the $\mathrm{SU(3)_C}$ $\mathrm{SU(2)_W}$ and $\mathrm{U(1)_Y}$ gauge fields, respectively. g_3, g_2 are gauge couplings of $\mathrm{SU(3)_C}$ and $\mathrm{SU(2)_W}$ gauge symmetries. f_{ABC} and ϵ_{IJK} are the structure constants of $\mathrm{SU(3)_C}$ and $\mathrm{SU(2)_W}$, respectively. Traces of first and second terms of Eq. (2.4) are taken over the matrices of λ_A and σ_I, respectively. $\mathcal{L}^{\mathrm{SM}}_{\text{gauge bosons}}$ is the canonically normalized kinetic terms for $\mathrm{SU(3)_C} \times \mathrm{SU(2)_W} \times \mathrm{U(1)_Y}$ gauge bosons and includes the self-interaction of non-Abelian gauge fields. We have omitted Lagrangian densities of the Faddeev-Popov ghosts for $\mathrm{SU(3)_C} \times \mathrm{SU(2)_W}$.

The SM fermion sector

The Lagrangian density of the SM fermion sector $\mathcal{L}^{\rm SM}_{\rm fermion}$ can be further decomposed into following pieces:

$$\mathcal{L}^{\rm SM}_{\rm fermion} = \mathcal{L}^{\rm SM}_{\rm fermion\ gauge} + \mathcal{L}^{\rm SM}_{\rm Yukawa}. \tag{2.6}$$

The first term includes the kinetic terms of the SM fermions and couplings between the SM fermion and gauge fields, while the second term gives the Yukawa coupling between the SM Higgs and the SM fermions.

$\mathcal{L}^{\rm SM}_{\rm fermion\ gauge}$ is explicitly given by

$$\begin{aligned}\mathcal{L}^{\rm SM}_{\rm fermion\ gauge} &= i\bar{L}_n \not{D} L_n + i\bar{e}_{nR}\not{D} e_{nR} + i\bar{Q}_n \not{D} Q_n + i\bar{u}_{nR}\not{D} u_{nR} + i\bar{d}_{nR}\not{D} d_{nR}, \\ \not{D} &\equiv \gamma^\mu D_\mu,\end{aligned} \tag{2.7}$$

where γ^μ are the gamma matrices. They are 4×4 matrices and are given by

$$\gamma^\mu = \begin{pmatrix} 0 & \sigma^\mu \\ \bar{\sigma}^\mu & 0 \end{pmatrix}. \tag{2.8}$$

Here, $\sigma^\mu \equiv (\mathbf{1}, \boldsymbol{\sigma})$ and $\bar{\sigma} = (\mathbf{1}, -\boldsymbol{\sigma})$, where $\mathbf{1}$ is the 2×2 unit matrix and $\boldsymbol{\sigma} \equiv (\sigma_1, \sigma_2, \sigma_3)$ is the Pauli matrices. For fermion field Ψ, we define the Dirac adjoint as $\bar{\Psi} \equiv \Psi^\dagger \gamma^0$. D_μ is the covariant derivative of $\mathrm{SU(3)_C} \times \mathrm{SU(2)_W} \times \mathrm{U(1)_Y}$ defined by

$$D_\mu \Psi_{\rm SM} \equiv \left(\partial_\mu - i g_3 T_3^A G_\mu^A - i g_2 T_2^I W_\mu^I - i g_1 Y B_\mu/2\right) \Psi_{\rm SM}. \tag{2.9}$$

In the above expression, $\Psi_{\rm SM}$ is the SM (Dirac) fermion field. The SM quarks belong to the fundamental representation of $\mathrm{SU(3)_C}$, while the SM lepton is singlet under the $\mathrm{SU(3)_C}$. It follows that $T_3^A = \lambda_A/2$ for the SM (left and right-handed) quarks and $T_3^A = 0$ for the SM (left and eight-handed) leptons. Since $\mathrm{SU(2)_W}$ gauge boson couples to the left-handed fermions (and the SM Higgs), $T_2^I = \sigma^I/2$ for the left-handed SM quarks and leptons, and $T_2^I = 0$ for the SM right-handed quarks and leptons. g_1 and Y are the $\mathrm{U(1)_Y}$ gauge coupling and its weak hypercharge of the SM fermions, which can be explicitly seen from Table. 2.1. Note that all gauge interactions are diagonal for generations of the SM quarks and the SM leptons.

Next, the Lagrangian density of Yukawa couplings between the SM Higgs and the fermions, $\mathcal{L}^{\rm SM}_{\rm Yukawa}$, are given by

$$\mathcal{L}^{\rm SM}_{\rm Yukawa} = -\left(Y^e_{mn}\bar{L}_m H_{\rm SM} e_{nR} + Y^d_{mn}\bar{Q}_m H_{\rm SM} d_{mR} + Y^u_{mn}\bar{Q}_m \tilde{H}_{\rm SM} u_{nR} + \text{h.c.}\right). \tag{2.10}$$

In this expression, Y^e_{mn}, Y^d_{mn} and Y^u_{mn} are Yukawa couplings, which are in general complex and non-diagonal. $\tilde{H}_{\rm SM}$ is defined by

$$\tilde{H}_{\rm SM} \equiv \begin{pmatrix} (\phi^0)^* \\ -(\phi^+)^* \end{pmatrix}. \tag{2.11}$$

$\tilde{H}$ is transformed **2** under the $\mathrm{SU(2)_W}$ and its weak hypercharge is $Y = -1/2$, and hence, Yukawa coupling between the SM Higgs and the up-type quarks corresponding to the third term of Eq. (2.10) is allowed.

We can confirm that $\mathcal{L}^{\rm SM}_{\rm fermion}$ is invariant under the following U(1) transformations:

$$\mathrm{U(1)_B} : q_{L,R} \to e^{i\theta_B/3} q_{L,R}, \tag{2.12}$$

$$\mathrm{U(1)_{L_e}} : (e_{L,R}, \nu_{eL}) \to e^{i\theta_{L_e}} (e_{L,R}, \nu_{eL}), \tag{2.13}$$

$$\mathrm{U(1)_{L_\mu}} : (\mu_{L,R}, \nu_{\mu L}) \to e^{i\theta_{L_\mu}} (\mu_{L,R}, \nu_{\mu L}), \tag{2.14}$$

$$\mathrm{U(1)_{L_\tau}} : (\tau_{L,R}, \nu_{\tau L}) \to e^{i\theta_{L_\tau}} (\tau_{L,R}, \nu_{\tau L}). \tag{2.15}$$

In these expressions, $q_{L,R}$ denotes the all SM quark fields. θ_{B,L_e,L_μ} and $\theta_{\theta_{L_\tau}}$ are (global) parameters for each transformations. According to the Noether's theorem, there exists global conserved charges associated with above transformations. In particular, global conserved charge associated with $\mathrm{U(1)_B}$ is the baryon number B and is given by

$$B = \frac{1}{3}\left(N_q - \bar{N}_q\right), \tag{2.16}$$

where N_q and $\bar{N}_q$ are the quark and anti-quark numbers of all types, respectively. Here, the normalization of baryon number is defined in such a way that a baryon number of the proton which consists of two up-quarks and one down-quark is unity. On one hand, global conserved charges associated with $\mathrm{U(1)_{L_e}}$, $\mathrm{U(1)_{L_\mu}}$ and $\mathrm{U(1)_{L_\tau}}$ are the lepton numbers for each generations and are given by

$$\begin{aligned} L_e &= N_e + N_{\nu_e} - \left(\bar{N}_e + \bar{N}_{\nu_e}\right), \\ L_\mu &= N_\mu + N_{\nu_\mu} - \left(\bar{N}_\mu + \bar{N}_{\nu_\mu}\right), \\ L_\tau &= N_\tau + N_{\nu_\tau} - \left(\bar{N}_\tau + \bar{N}_{\nu_\tau}\right). \end{aligned} \tag{2.17}$$

Here, $N_{e,\mu,\tau}$, $N_{\nu_{e,\mu,\tau}}$ are numbers of electron, muon, tauon and electron, mu, tau-neutrinos, and $\bar{N}_{e,\mu,\tau}$, $\bar{N}_{\nu_{e,\mu,\tau}}$ are numbers of these anti-particles.

It should be noted that we do not impose any principles to make the SM Lagrangian invariant under these symmetries. Indeed, we construct the SM Lagrangian by imposing gauge principles and renormalizability. Hence such global symmetries are accidental. This implies that these global charges characterize the SM and violations of these symmetries are direct signals of deviations from the SM. For this reason, it is worthwhile to study consequences of these global symmetries. First of all, baryon number conservation ensures the stability of the lightest particles having non-zero baryon numbers because decay of such a particle needs to break the baryon number. The lightest particle having non-zero baryon numbers is the proton. Therefore, if the baryon number conservation is exact, the life-time of the proton is infinite. The proton decay has not yet been observed, and an experimental limit on the proton life-time τ_{proton} is

$$\tau_{\text{proton}} > 10^{33}\,\text{years}. \tag{2.18}$$

This bound puts stringent constraint on the grand unification scale, which we will be important for discussion in Sec. 2.2.1.

Second, lepton number conservations in each generations imply that there is no process changing the lepton flavor. Therefore, charged lepton flavor violation processes such as

$$\mu \to e + \gamma, \tag{2.19}$$

$$\mu \to e + e + e, \tag{2.20}$$

$$\mu + \text{Ti} \to e + \text{Ti}, \quad (\text{Ti} : \text{Titanium}) \tag{2.21}$$

are forbidden because these processes obviously violate L_e and L_μ conservations. γ is the photon field. Present bounds of branching ratios (BR) of above processes are summarized as follows:

- $\text{BR}(\mu \to e + \gamma) < 4.2 \times 10^{-13}$[65],
- $\text{BR}(\mu \to e + e + e) < 1.0 \times 10^{-12}$ [66],
- $\text{BR}(\mu + \text{Ti} \to \text{e} + \text{Ti}) < 4.3 \times 10^{-12}$ [67].

While the future sensitivity of the first two processes are around one order of magnitude lower than the present branching ratios, the μ to e conversion (Ti) sensitivity is supposed to increase by six order of magnitudes [68]. New physics leading to the charged lepton flavor

violation are therefore stringently constrained. In fact, minimal scotogenic model, which will be introduced in Sec. 2.4, is constrained by these experiments.

We have discussed lepton number conservations within the SM framework and argued that the charged flavor violation processes are absolutely forbidden. However, as we will discuss in Sec. 2.2.2 that lepton numbers defined by Eq. (2.17) is in reality violated by a presence of neutrino mixings. Hence the charged lepton flavor violation processes can be occurred via the neutrino mixings. Although, these processes occur at one-loop level and significantly suppressed by the tiny neutrino mass. For example, an explicit calculation showed $\mathrm{BR}(\mu \to e\gamma) < 10^{-54}$ [69], which is many order magnitude smaller than the current constraint. Thus, charged lepton flavor violation processes caused by neutrino oscillations are negligible amount and we can safely neglect it.

The SM Higgs sector

The Lagrangian density of the SM Higgs sector is given by

$$\mathcal{L}^{\mathrm{SM}}_{\mathrm{Higgs}} = D_\mu H^\dagger_{\mathrm{SM}} D^\mu H_{\mathrm{SM}} - V_{\mathrm{SM}}\left(|H_{\mathrm{SM}}|\right). \tag{2.22}$$

The covariant derivative in the above expression is given by $D_\mu \equiv \partial_\mu - ig_2\sigma^I W^I_\mu/2 - ig_1 B_\mu/2$. The SM Higgs potential $V_{\mathrm{SM}}(|H_{\mathrm{SM}}|)$ is given by

$$V_{\mathrm{SM}}(|H_{\mathrm{SM}}|) = \lambda_{SM}\left(|H_{\mathrm{SM}}|^2 - \frac{v^2_{\mathrm{SM}}}{2}\right)^2. \tag{2.23}$$

where $v_{\mathrm{SM}} \simeq 246\,\mathrm{GeV}$ and the self-coupling $\lambda_{\mathrm{SM}} \simeq 0.131$. Since this potential has a minimum at $H_{\mathrm{SM}} = v_{\mathrm{SM}}$, which is different from the origin, the SM Higgs obtain the vacuum expectation value (VEV). The SM Higgs is charged under the $\mathrm{SU(2)_W} \times \mathrm{U(1)_Y}$ and hence the gauge symmetry is spontaneously broken. After this symmetry breaking, it is convenient to parameterize H_{SM} field as follows:

$$H_{\mathrm{SM}} = \begin{pmatrix} 0 \\ \frac{v_{\mathrm{SM}}}{\sqrt{2}} + \frac{h^0_{\mathrm{SM}}(x)}{\sqrt{2}} \end{pmatrix}. \tag{2.24}$$

Here, $h^0_{\mathrm{SM}}(x)$ is a real scalar field, whose mass is given by $m_h = \sqrt{2\lambda_{\mathrm{SM}}} v_{\mathrm{SM}} \simeq 125\,\mathrm{GeV}$.

Let us next see a consequence of the symmetry breaking associated with the Higgs condensate $H_{\mathrm{SM}} = v_{\mathrm{SM}}$. We first put expression Eq. (2.24) into the first term of Eq. (2.22) and

neglect the term involving $h^0_{\rm SM}(x)$. Then the quadratic terms for $\mathrm{SU(2)_W \times U(1)_Y}$ gauge bosons corresponding to the mass terms are given by following matrix form:

$$(W^1_\mu,\ W^2_\mu,\ W^3_\mu,\ B_\mu) \begin{pmatrix} g_2^2\frac{v_{\rm SM}^2}{4} & 0 & 0 & 0 \\ 0 & g_2^2\frac{v_{\rm SM}^2}{4} & 0 & 0 \\ 0 & 0 & g_2^2\frac{v_{\rm SM}^2}{4} & -g_2g_1\frac{v_{\rm SM}^2}{4} \\ 0 & 0 & -g_2g_1\frac{v_{\rm SM}^2}{4} & g_1^2\frac{v_{\rm SM}^2}{4} \end{pmatrix} \begin{pmatrix} W^{1\mu} \\ W^{2\mu} \\ W^{3\mu} \\ B^\mu \end{pmatrix}. \tag{2.25}$$

We can easily see from the above expression that mass terms for (W^3_μ, B_μ) are not diagonalized. It is possible to diagonalize mass terms by the following orthogonal transformation:

$$\begin{pmatrix} Z_\mu \\ A_\mu \end{pmatrix} = \begin{pmatrix} \cos\theta_W & -\sin\theta_W \\ \sin\theta_W & \cos\theta_W \end{pmatrix} \begin{pmatrix} W^3_\mu \\ B_\mu \end{pmatrix}, \tag{2.26}$$

where θ_W is the weak mixing angle defined by

$$\tan\theta_W = \frac{g_1}{g_2}. \tag{2.27}$$

Also, $W^{1,2}_\mu$ fields are often parameterized by $W^\pm_\mu$ fields defined by

$$W^\pm_\mu = \frac{1}{\sqrt{2}}\left(W^1_\mu \pm iW^2_\mu\right). \tag{2.28}$$

In the basis $(W^+_\mu, W^-_\mu, Z_\mu, A_\mu)$, the mass matrix is explicitly given by

$$(W^+_\mu,\ W^-_\mu,\ Z_\mu,\ A_\mu) \begin{pmatrix} g_2^2\frac{v_{\rm SM}^2}{4} & 0 & 0 & 0 \\ 0 & g_2^2\frac{v_{\rm SM}^2}{4} & 0 & 0 \\ 0 & 0 & (g_1^2+g_2^2)\frac{v_{\rm SM}^2}{4} & 0 \\ 0 & 0 & 0 & 0 \end{pmatrix} \begin{pmatrix} W^{+\mu} \\ W^{-\mu} \\ Z^\mu \\ A^\mu \end{pmatrix}. \tag{2.29}$$

It is apparent that three gauge bosons, Z_μ, becomes massive, while the gauge boson A_μ, which is given by the linear combination of W^3_μ and B_μ, is still massless after the symmetry breaking. The massless gauge boson A_μ is photon associated with unbroken U(1) gauge symmetry, which is identified with the electromagentic gauge symmetry $\mathrm{U(1)_{EM}}$. Hence the electroweak symmetry $\mathrm{SU(2)_W \times U(1)_Y}$ is spontaneously broken to $\mathrm{U(1)_{EM}}$ by the Higgs condensation. This phenomenology is called the *electroweak symmetry breaking* (EWSB).

Let us next discuss the fermion sector with the SM Higgs condensation. Putting expression Eq. (2.24) into the Yukawa couplings given by Eq (2.10) and neglecting a terms, which

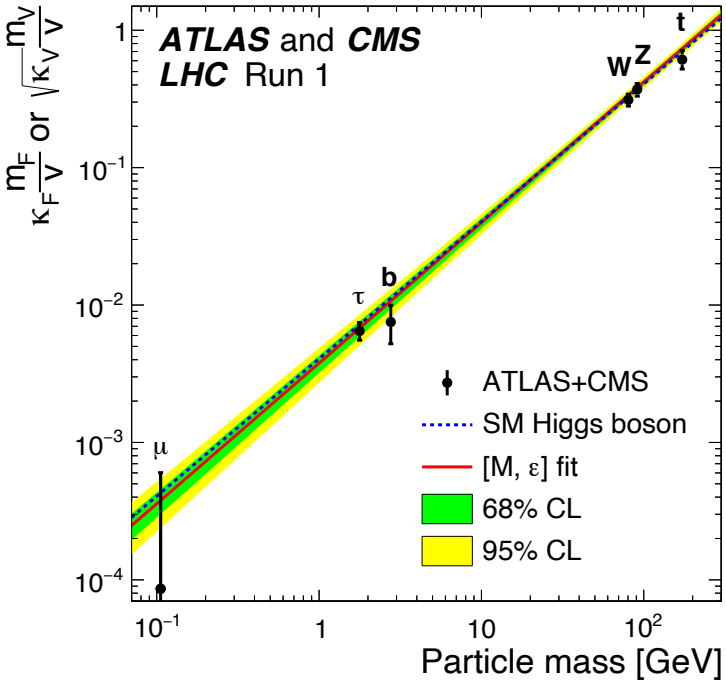

Figure 2.1: Results from ATLAS and CMS collaboration [70] is shown. The vertical axis indicates the couplings with the SM Higgs boson, while the horizontal axis is the observed mass spectra of the SM particles.

are proportional to $h^0_{\rm SM}(x)$, we obtain

$$\mathcal{L}^{\rm SM}_{\rm Yukawa} = -\left(M^e_{mn}\bar{e}_{Lm}e_{Rn} + M^u_{mn}\bar{u}_{Lm}u_{Rn} + M^d_{mn}\bar{d}_{mL}d_{nR} + \text{h.c.}\right), \tag{2.30}$$

$$M^e_{mn} \equiv Y^e_{mn}\frac{v_{\rm SM}}{\sqrt{2}},\ M^{u(d)}_{mn} \equiv Y^{u(d)}_{mn}\frac{v_{\rm SM}}{\sqrt{2}}, \tag{2.31}$$

where $M^{e,u,d}_{mn} \equiv Y^{e,u,d}_{mn}v_{\rm SM}/\sqrt{2}$. We can easily see that the charged leptons, up-type and down-type quarks obtain their masses through the SM Higgs condensation. Similar to the discussion of mass terms for $\mathrm{SU(2)_W \times U(1)_Y}$ gauge bosons, we can make $M^{e,u,d}_{mn}$ as a diagonalized matrix by acting unitary transformations to the quark and lepton fields. However, the left-handed neutrinos are still massless after the EWSB. This fact is not consistent with the observation of the neutrino oscillations, which we shall discuss in Sec. 2.2.2.

We have seen that SM particles except the left-handed neutrinos and gluon obtain their masses through the SM Higgs condensation. Since their masses are proportional to $v_{\rm SM}$ times coupling constants with the SM Higgs, observed mass spectra should maintain this proportionality as long as the SM is valid. Fig. 2.1 shows the observed mass spectra of

SM particles confirmed by the ATLAS and CMS collaborations [70]. As is easily seen from this figure, the observed mass spectra indicates that coupling constants of the SM particles proportional to these masses. Therefore, this result strongly supports the validity of the EWSB within the SM framework. At 2012, the SM Higgs boson $h^0_{\rm SM}(x)$ was finally observed at the LHC, and thus, the SM elegantly explains phenomena around the electroweak scale.

2.2 Difficulties of the Standard Model

In this section, we discuss some difficulties of the SM. In particular, we consider the naturalness of the SM Higgs mass parameter, the DM and non-zero neutrino masses and mixings. In Sec. 2.2.1, we define the measure of the tuning of the physical parameter and show that the SM Higgs mass parameter must be fine-tuned if there is no new physics around the TeV scale. In Sec. 2.2.2, we show that the left-handed neutrino can obtain mass by introducing the right-handed neutrinos, and summarize current constraints on neutrino masses and its mixings. In Sec. 2.2.3, we explain some evidences of the DM and summarize conditions of the DM.

2.2.1 Naturalness

In this subsection, we discuss the theoretical problem of the SM so-called the *hierarchy problem*. To give a precise statement of the hierarchy problem, we need to explain a notion of the naturalness.

Let us first give a definition of the measure of the tuning, The definition is given by [71]

$$\Delta(p_i) \equiv \left| \frac{\partial \log O(p_i)}{\partial \log p_i} \right|^{-1}, \tag{2.32}$$

where p_i are the model parameters and $O(p_i)$ are observables. In this measure, smaller $\Delta(p_i)$ means that larger fine-tuning is required. Thus $\Delta(p_i)$ should not be too small for the naturalness, say, at least all the measures should satisfy $\Delta(p_i) > \mathcal{O}(10^{-1})$. If a measure in the model is too small, $\Delta(p_i) \leq \mathcal{O}(10^{-1})$, we conclude the model is unnatural.

It is widely known that the SM Higgs mass parameter requires the fine-tuning against radiative corrections if an energy scale of new physics is much larger than the electroweak scale. To see this, let us decompose the SM Higgs bare mass, $m_{h\,\rm bare}$ into the renormalized

mass and its radiative correction (counterterm) as follows.

$$m_{h\,\mathrm{bare}}^2 = m_h^2 + \delta m_h^2. \tag{2.33}$$

In this expression, m_h and δm_h are the renormalized (observed) Higgs mass and the radiative correction. The SM Higgs boson mass receives one-loop quadratically divergent mass corrections from the top quark, $\mathrm{SU}(2)_\mathrm{W}$ gauge bosons and Higgs itself through the quartic coupling as

$$\delta m_h^2 = -\frac{3y_t^2}{4\pi^2}\Lambda_\mathrm{UV}^2 + \frac{9g_2^2}{32\pi^2}\Lambda_\mathrm{UV}^2 + \frac{\lambda_\mathrm{SM}}{4\pi^2}\Lambda_\mathrm{UV}^2. \tag{2.34}$$

Here, we have regularized the momentum integration by inserting the hard cut-off, Λ_UV. Then, we discuss the degree of the tuning to obtain the observed Higgs mass against quantum corrections given by Eq. (2.34). According to the definition of the tuning measure Eq. (2.32), we obtain

$$\begin{aligned}\Delta(\delta m_h^2) &= \left|\frac{\partial \log m_h^2}{\partial \log \delta m_h^2}\right|^{-1} \\ &= \frac{m_h^2}{\delta m_h^2}.\end{aligned} \tag{2.35}$$

Thus, $\Delta(\delta m_h^2) < 0.1$ corresponds to the cut-off scale

$$\Lambda_\mathrm{UV} \geq 1.5\mathrm{TeV}. \tag{2.36}$$

Therefore, if the SM is valid up to higher than the energy scale $\Lambda_\mathrm{UV} \sim \mathcal{O}(1)\,\mathrm{TeV}$, the SM Higgs mass parameter requires unnatural fine-tuning.

The Large Hierarchy Problem

The cut-off scale Λ_UV represents an energy scale of new physics instead of the SM. At least, we expect that quantum gravity effects becomes important at the Planck scale, and hence, the SM Lagrangian density does not give correct description of physics around that scale. Since all parameters in the SM Lagrangian density do not have Landau poles, they are well-defined up to the Planck scale. Hence, for simplicity, let us first assume that the SM is valid up to the Planck scale, that is, there is no new physics between the electroweak scale and the Planck scale, which is sometime called the *great desert*. In this case, the cut-off scale is

identified with the Planck scale $\Lambda_{\rm UV} = M_{\rm Pl} \sim 10^{19}\,{\rm GeV}$ and the SM Higgs mass parameter must be fine-tuned with the degree of

$$\Delta(\delta m_h^2) \sim 10^{-34},\ \Lambda_{\rm UV} \sim 10^{19}\,{\rm GeV}. \tag{2.37}$$

This fact tells us that the SM Higgs mass parameter is extremely fine-tuned at the Planck scale otherwise the observed Higgs mass cannot be realized.

An another popular candidate of new physics is the grand unification theory. We shall here discuss a particular energy scale of the grand unification theory and required tuning to the SM Higgs mass parameter at that scale. In the SM, as was seen in the previous section, the baryon as well as the lepton numbers are classically conserved at the renormalizable level, and thus, the proton is stable. However, in that theory, the quark and the lepton generally belong to the same representation under the unified gauge symmetry, which usually explicitly breaks the baryon number. Hence it is widely believed that the proton decay occurs in the that theory. Therefore, a measurement of a life-time of the proton puts a stringent constraint on the energy scale of the grand unification theory. From Eq. (2.18), the energy scale of the grand unification theory is roughly expected to be $M_{\rm GUT} \sim 10^{15}\,{\rm GeV}$. Assuming the SM is valid up to this scale $\Lambda_{\rm UV} = M_{\rm GUT}$, the SM Higgs mass parameter must be fine-tuned with the degree of

$$\Delta(\delta m_h^2) \sim 10^{-26},\ \Lambda_{\rm UV} = M_{\rm GUT}. \tag{2.38}$$

It is milder than the required tuning given by Eq. (2.37), but fine-tuning is still needed.

We have learned from above arguments that the SM Higgs mass parameter must be fine-tuned if there is no new physics between the electroweak and the Planck (or the grand unification scale). These fine-tuning problems are obviously caused by the "large" hierarchy between these scales. Therefore, this problem is called by the *large hierarchy problem*. This fact strongly suggests an existence of physics beyond the SM. For instance, in the supersymmetric extension of the SM, quadratic divergent mass corrections Eq. (2.34) to the SM Higgs mass are canceled by the supersymmetric partner. Hence if the supersymmetry exists not far above the cut-off scale given by Eq. (2.36), the large hierarchy problem can be addressed. For this reason, the supersymmetric extension of the SM is regarded as a promising candidate for physics beyond the SM and many people believed its existence at the electroweak scale.

The Little Hierarchy Problem

In particular, supersymmetric partners of the top quark called the scalar top quark plays an essential role to address the little hierarchy problem. This is because the most dominant contribution to the quadratic divergent mass correction to the SM Higgs mass parameter Eq. (2.34) comes from the top quark, which can be canceled by the scalar top quark correction. The scalar top quark is colored and (electromagnetically) charged state, and hence, it is easy to produce by the LHC experiments as long as its mass is within reach of the energy scale of it. Therefore, the scalar top quark is a good target of the collider experiments. Note that the scalar top quark mass should be around the electroweak scale to ameliorate the fine-tuning because cancellation mechanism does not take place for an energy scale lower than the scalar top quark mass.

However, current experiments have not yet observed any direct signals of these new colored particles and puts stringent constraints on $\Lambda_{\rm UV}$. Moreover, precision measurements of the SM also gives bounds on $\Lambda_{\rm UV}$, which is order of TeV scale [72]. Thus, supersymmetry is very difficult to ameliorate the fine-tuning up to $\Lambda_{\rm UV}$ given by Eq. (2.36). Since this fine-tuning problem related to the "little" hierarchy between the electroweak scale and the TeV scale, which is much smaller than the large hierarchy, it is called the *little hierarchy problem*. It should be emphasized that if supersymmetry exists an energy scale just above the TeV scale which is not within reach of present collider experiments, the large hierarchy problem between the TeV scale and the Planck (or the grand unification) scale can be addressed. However, to solve the little hierarchy problem, we need physics beyond the SM, which must be consistent with the current collider experiments. Twin Higgs models are promising theories such beyond the SM and we shall explain its mechanism in Sec. 2.3. We will also explain the essential reason why these models can provide the solution to the little hierarchy problem.

2.2.2 Neutrino masses

As we saw in Sec. 2.1 and Eq. (2.30), the left-handed neutrinos are still massless after the EWSB. Also, there is no neutrino flavor changing process because of the lepton number conservations Eq. (2.17). However, observations of neutrino oscillations imply that there are non-zero neutrino masses and these mixings. In this subsection, we first show that the

left-handed neutrinos can obtain their mass by introducing right-handed neutrinos into the SM. After that, we summarize some constraints on neutrino masses and these mixings from observations of neutrino oscillations.

Let us introduce the right-handed neutrinos, ν_{nR}, into the SM Lagrangian. Its charge assignment and dimensions of gauge group representation were already listed in Table 2.1. Since ν_{nR} are singlet under all SM gauge group, following Majorana mass terms and additional Yukawa couplings between the SM Higgs and leptons are allowed:

$$\mathcal{L}_{\nu_R} = \bar{\nu}_{nR}\partial\!\!\!/\nu_{nR} + \frac{1}{2}\left(M_{\nu_R}\right)_{mn}\left(\bar{\nu}^c_{nR}\nu_{mR} + \text{h.c.}\right) - \left(Y^{\nu}_{mn}\bar{L}_n\tilde{H}_{\text{SM}}\nu_{nR} + \text{h.c.}\right), \tag{2.39}$$
$$\partial\!\!\!/ \equiv \gamma^\mu\partial_\mu.$$

Here, M_{ν_R} and Y^{ν}_{mn} are 3×3 Majorana mass and the Yukawa coupling matrices, respectively. ν^c_{nR} is the charge conjugation of ν_{nR}. After the EWSB, the second term of the above expression gives a Dirac mass term for the neutrinos by the Higgs condensation, which is similar to the quark sector.

Let us here study the consequence of non-zero neutrino masses. As we discussed in the previous subsection, the lepton sector of the SM Lagrangian Eq. (2.10) possesses three independent conserved lepton numbers given by Eq. (2.17). The second term explicitly breaks the global $\mathrm{U(1)_{L_e}}$, $\mathrm{U(1)_{L_\mu}}$ and $\mathrm{U(1)_{L_\tau}}$, but does not break the $\mathrm{U(1)_L}$ symmetry defined by the transformation of phase rotation with respect to all lepton fields. This fact implies that the lepton flavor can be broken via the neutrino masses, and in the massless limit, the lepton flavor is absolutely recovered. Furthermore, the presence of the Majorana mass terms breaks not only $\mathrm{U(1)_{L_e}}$, $\mathrm{U(1)_{L_\mu}}$ and $\mathrm{U(1)_{L_\tau}}$, but also breaks the $\mathrm{U(1)_L}$ symmetry. Therefore, in the presence of the neutrino mass terms, the lepton flavor violation processes can be allowed. We took into account this fact when we discuss the charged lepton flavor violation in Sec. 2.

Constraints on the neutrino mixing parameters

Generally, in the basis where electroweak gauge interactions $\mathrm{SU(2)_W}\times\mathrm{U(1)_Y}$ are diagonal with respect to generations of leptons called the *flavor basis*, the lepton mass matrix becomes non-diagonal, which implies that neutrino flavors can be changed via the mass matrix (or via the non-diagonal Yukawa couplings). In the basis where the mass matrix is diagonal, the electroweak gauge interaction $\mathrm{SU(2)_W}\times\mathrm{U(1)_Y}$ becomes non-diagonal, and hence, neutrino flavors can be changed by the gauge interaction. Of course, physics does not depend on the

basis. Both basis should lead to the same result, but it is convenient to work in the mass basis because observational constraints on neutrino masses and mixings are given in this basis.

Neutrinos in the mass basis ν_i where $i = 1, 2, 3$ is related to the flavor basis ν_n ($n = e, \mu, \tau$) via the unitary matrix:

$$\nu_n = U_{ni}\nu_i. \tag{2.40}$$

Here, the 3×3 unitary matrix U_{in} is the mixing matrix of the neutrino sector, which is called Pontecorvo-Maki-Nakagawa-Sakata (PMNS) matrix. Parameterization of the PMNS matrix is explicitly given by

$$U = \begin{pmatrix} c_{12}c_{13} & s_{12}c_{13} & s_{13}e^{-i\delta} \\ -s_{12}c_{23} - c_{12}s_{23}s_{13}e^{i\delta} & c_{12}c_{23} - s_{12}s_{23}s_{13}e^{i\delta} & s_{23}c_{13} \\ s_{12}s_{23} - c_{12}c_{23}s_{13}e^{i\delta} & -c_{12}s_{23} - s_{12}c_{23}s_{13}e^{i\delta} & c_{23}c_{13} \end{pmatrix} U_{\rm Maj}, \tag{2.41}$$

where $c_{ij} = \cos\theta_{ij}$, $s_{ij} = \sin\theta_{ij}$ and δ is the leptonic Dirac CP phase. The diagonal matrix $U_{\rm Maj} = {\rm diag}(1, e^{i\xi_1}, e^{i\xi_2})$ contains the undetermined Majorana CP phases ξ_1, ξ_2. Observations of neutrino oscillation gives constraints on each components of PMNS matrix Eq. (2.41), which are explicitly given by [26, 27]

$$|U| = \begin{pmatrix} 0.79 - 0.88 & 0.47 - 0.61 & < 0.18 \\ 0.19 - 0.53 & 0,42 - 0.73 & 0.58 - 0.82 \\ 0.20 - 0.53 & 0.44 - 0.74 & 0.56 - 0.81 \end{pmatrix}, \tag{2.42}$$

with 3σ confidence level. Current constraints on the mixing angles are given by [26, 27]

$$0.82 \lesssim \sin^2 2\theta_{12} \lesssim 0.89, \tag{2.43}$$

$$\sin^2 2\theta_{13} \lesssim 0.19, \tag{2.44}$$

$$0.92 \lesssim \sin^2 2\theta_{23}. \tag{2.45}$$

Constraints on mass squared differences are given by

$$7.7 \times 10^{-5}{\rm eV}^2 \lesssim m^2_{\nu_2} - m^2_{\nu_1} \lesssim 8.4 \times 10^{-5}{\rm eV}^2, \tag{2.46}$$

$$1.9 \times 10^{-3}{\rm eV}^2 \lesssim m^2_{\nu_3} - m^2_{\nu_2} \lesssim 3.0 \times 10^{-3}{\rm eV}^2, \tag{2.47}$$

where $m_{\nu_{1,2}}$ and m_{ν_3} are masses of neutrinos in mass eigenstates $\nu_{1,2}$ and ν_3 and we have assumed that $m_{\nu_1} < m_{\nu_2} < m_{\nu_3}$. Furthermore, there is upper bound on the sum of neutrino masses [28]

$$\sum_{i=1}^{3} m_{\nu_i} \leq 0.11\,\mathrm{eV}, \tag{2.48}$$

from cosmological observations. When we consider new physics, which generate the non-zero neutrino masses, all constraints must be satisfied. All constraints listed in this section are important when we consider minimal scotogenic model, which will be discussed in Sec. 2.4.

2.2.3 Dark Matter

In this subsection, we discuss the basic properties of the DM except its production mechanism. Since a calculation of the relic abundance of the DM strongly depends on its production mechanism, we will discuss it in Sec. 3.2 after reviewing the standard cosmology.

DM is the one of dominant gravitationally attractive component of our Universe. The existence of the DM was first pointed out by Zwicky [73] more than eighty years before. He carefully analyzed movement of Coma clusters, which consists of around 1000 galaxies, and concluded that there must be a large amount of non-luminous matter inside the cluster. Recently, several astronomical and cosmological observations make great progress, and there are a lot of evidences of the DM. For example, observations of galactic rotation curves [74], gravitational lensing events [75] and cosmic microwave background [28] can be well described by the DM. In spite of this fact, we do not know what the DM consists of.

At least, we know that the DM should satisfy following conditions.

- (i) The DM must be non-luminous. In other word, it does not (or very weakly couples) to the photon.
- (ii) Since the galaxy is almost comprised by the DM, it must be stable (or its life-time must be longer than the age of the present Universe).
- (iii) The DM should be non-relativistic and massive otherwise it exceeds the escape velocity of the clumping baryons, and hence, it becomes inconsistent with the structure formation.

- (iv) The relic abundance of the DM must be consistent with observed value: $\Omega_{\rm DM}h^2 = 0.120 \pm 0.001$ (68% confidence level). ($\Omega_{\rm DM}$ and h will be defined in Sec. 3.1.1.)

It is natural to consider whether there is a DM candidate within the SM framework, or not, and we would like to discuss it here. Physically, condition (ii) can be regarded as a consequence of (approximate) symmetries because it guarantees the stability of particles. As we discussed in Sec. 2.1, the SM possesses accidental global symmetries, and as a result, the proton, and the charged leptons and the neutrinos, are stable. Among them, the proton and the charged leptons cannot be DM candidates because they conflict with the condition (i), while $\nu_{e,\mu}$ and ν_τ satisfy it. However, with constraints given in the previous subsection, it turned out that they cannot satisfy conditions (iii) and (iv) [76]. (Roughly speaking, massive neutrinos are too light to comprise the DM in the present Universe.) Therefore, unfortunately, there is no DM candidates within the SM framework. This fact also strongly suggests new physics beyond the SM and conditions listed above is a good guideline to build a model, which explains the DM. We will argue that, in minimal scotogenic model, there are (elementary particle) DM candidates, which satisfy all above conditions. [1]

2.3 Twin Higgs models

The main purpose of this section is to review twin Higgs models motivated by the little hierarchy problem discussed in Sec. 2.2.1. In Sec. 2.3.1, we briefly explain basic setup and its mechanism. In Sec. 2.3.2, we review the twin Higgs mechanism, which provides a solution to the little hierarchy problem [23, 78]. The Higgs mass formulae are also presented. We then discuss the degree of fine-tuning to realize the adequate EWSB in this scenario. In Sec. 2.3.3, we consider supersymmetric extension of the twin Higgs models to simultaneously address the little and the large hierarchy problems.

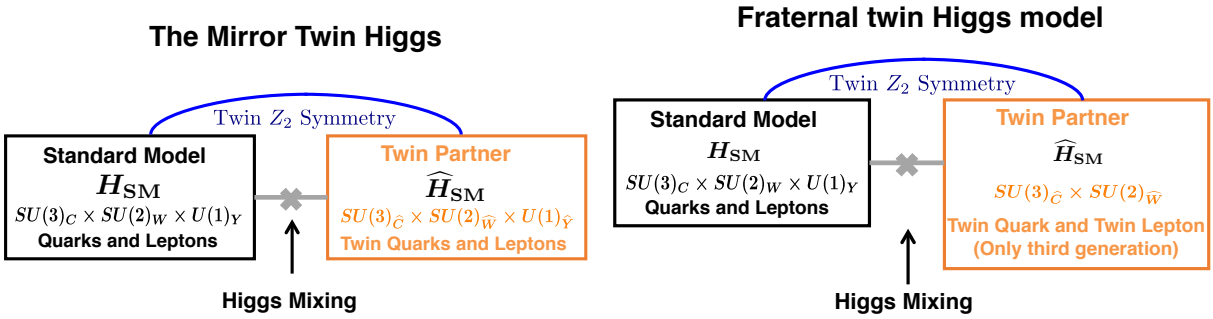

Figure 2.2: The matter content of the Mirror twin Higgs models (**the left panel**) and of the Fraternal Twin Higgs models (**the right panel**) are shown.

2.3.1 Overview of Twin Higgs Models

First of all, we would like to explain the essential reason why the twin Higgs models provide the solution to the little hierarchy problem different from the supersymmetry. It was discussed in Sec. 2.2.1 that supersymmetry is very difficult to provide the solution to it because the scalar top quark, which is necessarily to cancel the quadratic divergence, is colored state. However, as we will see, in twin Higgs models, the top quark partner called "twin top quark" is surprisingly uncolored and is electromagnetically neutral states. Hence it is very difficult to produce the collider experiments and hence constraints on the mass of the twin top quark is much milder than one of the scalar top. Thanks to this fact, the little hierarchy problem can be addressed without conflicting present collider and precision constraints.

Next, we would like to concretely explain the framework of the twin Higgs models. The original realization of the twin Higgs idea, which is now called the Mirror twin Higgs model [23], has a mirror copy of all the SM particle content related to the $\mathbf{Z}_2$ symmetry. On the other hand, the Fraternal (minimal) twin Higgs model [78] has a smaller twin particle content, that is, twin W bosons, twin gluons and twin fermions corresponding to the third generation. Other twin particles are not required since the corresponding SM particles give less important contributions to the Higgs potential. The matter content of the Mirror twin Higgs model and the Fraternal twin Higgs model are shown in Fig. 2.2. The SM particles and twin particles

[1]Note that primordial black hole is also attractive DM candidate, which does not require any modifications to the SM Lagrangian density. Also, E. Witten showed that there is a possibility that the DM can be produced within the SM framework if QCD chiral phase transition is of first order and some certain conditions are satisfied [77]. We do not discuss such possibilities in this thesis.

interact with each other only through Higgs mixing given by $|H_{\rm SM}|^2|\widehat{H}_{\rm SM}|^2$. Hence the most significant constraint on this model is SM precision tests rather than the direct detection in comparison to the supersymmetry. In particular, Higgs coupling measurements give most stringent constraint on this model.

In any case, due to the $\mathbf{Z}_2$ symmetry, the quadratic terms of the Higgs potential accidentally preserve the original global symmetry $\mathcal{G}$ and the pNGBs associated with $\mathcal{G} \to \mathcal{H}$ breaking are protected from radiative corrections, allowing the natural EWSB. Since every twin partner is not charged under the SM gauge group, this mechanism realizes the so-called neutral naturalness[2] and enables the model to evade stringent LHC bounds. In this mechanism, there still remains the large hierarchy problem, that is, the hierarchy between the global $\mathcal{G} \to \mathcal{H}$ breaking scale, expected to be up to 5-10 TeV, and the Planck scale (or the grand unification scale). It is expected to be addressed by the UV completion such as supersymmetry [80, 81, 82, 83, 84, 85, 86] or composite Higgs [87, 88, 89, 90, 91].

2.3.2 The non-supersymmetric twin Higgs

The twin Higgs mechanism and setup

In the twin Higgs mechanism, the SM Higgs field is identified with pNGBs arising from spontaneous breaking of an approximate U(4) symmetry (though it is explicitly broken by the Yukawa and gauge couplings).[3] Let us consider a linear realization of the mechanism and write a U(4) symmetric potential of a complex scalar field $H_{\rm twin}$ with the fundamental representation,

$$V(H) = -m^2 H_{\rm twin}^\dagger H_{\rm twin} + \lambda \left(H_{\rm twin}^\dagger H_{\rm twin} \right)^2 , \tag{2.49}$$

where $\lambda > 0$ is required from the stability of the potential. This potential drives the scalar field H to obtain a nonzero VEV, $f \equiv \langle |H_{\rm twin}| \rangle = m/\sqrt{2\lambda}$. Then, the global U(4) symmetry is broken down to U(3) yielding 7 NGBs. The U(4) symmetry contains the subgroups $\mathrm{SU}(2)_{\rm A} \times \mathrm{SU}(2)_{\rm B}$ and the scalar field can be decomposed as $H_{\rm twin} = (H_A, H_B)$, where H_A transforms as a doublet of $\mathrm{SU}(2)_{\rm A}$ while H_B does as a doublet of $\mathrm{SU}(2)_{\rm B}$. H_A is identified

[2] Another known realization of neutral naturalness is Folded SUSY [79].

[3] Here, we confine a global group G to U(4) symmetry as a concrete realization. However, our conclusion is still robust even for a generic gauge group G as long as we consider a Mexican-hat type potential given by (2.49).

with the SM Higgs doublet, $H_{\rm SM}$, and the $\mathrm{SU}(2)_{\rm A}$ symmetry is regarded as the ordinary $\mathrm{SU}(2)_{\rm W}$ gauge symmetry. The $\mathrm{SU}(2)_{\rm B}$ symmetry is gauged and becomes the twin $\mathrm{SU}(2)_{\widehat{\rm W}}$. Then, the 6 pNGBs are eaten by the gauge bosons after the symmetry breakings while the remaining one is the observed SM-like Higgs boson $h_{\rm SM}$, which is parameterized as Eq. (2.24). A physical heavy exotic Higgs $\widehat{h}$, corresponding to the radial direction, has the mass $m_{\widehat{h}} = \sqrt{2\lambda}f$ from Higgs mechanism. $\mathrm{SU}(2)_{\rm A}$ and the twin $\mathrm{SU}(2)_{\rm B}$ are interchanged under a $\mathbf{Z}_2$ symmetry. In the Fraternal twin Higgs model [78], only the $\mathbf{Z}_2$ partners of the third generation of quarks and leptons and the partners of gluons (twin gluons) as well as the twin $\mathrm{SU}(2)_{\widehat{\rm W}}$ gauge bosons are introduced. The twin Higgs doublet H_B has a Yukawa coupling similar to the SM top Yukawa coupling.

The two scalar doublets H_A and H_B receive quadratically divergent corrections from the top and twin top quarks respectively as well as corrections from the $\mathrm{SU}(2)_{\rm A}$ and $\mathrm{SU}(2)_{\rm B}$ gauge bosons at one loop. In addition, they receive corrections from the gluons and twin gluons at two-loop level. The quadratically divergent part of their potential is given by

$$V \supset \left(-\frac{3y_t^2}{8\pi^2} + \frac{9g_2^2}{64\pi^2} - \frac{y_t^2 g_3^2}{8\pi^4}\right)\Lambda_{\rm UV}^2|H_A|^2 + \left(-\frac{3\widehat{y}_t^2}{8\pi^2} + \frac{9\widehat{g}_2^2}{64\pi^2} - \frac{\widehat{y}_t^2\widehat{g}_3^2}{8\pi^4}\right)\Lambda_{\rm UV}^2|H_B|^2, \tag{2.50}$$

where g_2, $\widehat{g}_2$ are the $\mathrm{SU}(2)_{\rm W}$ and $\mathrm{SU}(2)_{\widehat{\rm W}}$ gauge couplings, y_t and $\widehat{y}_t$ are the top and the twin top couplings, g_3, $\widehat{g}_3$ are the $\mathrm{SU}(3)_{\rm C}$ and $\mathrm{SU}(3)_{\widehat{\rm C}}$ gauge couplings and $\Lambda_{\rm UV}$ is a cutoff scale. The exact $\mathbf{Z}_2$ symmetry leads to $\widehat{y}_t = y_t$, $\widehat{g}_2 = g_2$, $\widehat{g}_3 = g_3$ which guarantee that the quadratically divergent part of the potential respects the full U(4) symmetry. Then, the NG nature of the Higgs field is not explicitly broken by the quadratically divergent corrections, addressing the little hierarchy problem. However, the SM Higgs would be exactly massless and inconsistent with our Universe if the U(4) and $\mathbf{Z}_2$ symmetries are exact. Thus we need small breakings of these symmetries.

Let us consider the breaking of the U(4) and the $\mathbf{Z}_2$ symmetries to give the appropriate effective Higgs potential. First of all, the gauged $\mathrm{SU}(2)_{\rm A} \times \mathrm{SU}(2)_{\rm B}$ group has already broken the U(4) symmetry explicitly. In addition to the quadratically divergent corrections, this generates logarithmically divergent contributions to the quartic couplings of the form $(|H_A|^4 + |H_B|^4)$, which do not respect the U(4) symmetry and then contribute to the Higgs boson mass. The explicit $\mathbf{Z}_2$ symmetry breaking is also needed otherwise the hierarchy, $v_A^2 \ll f^2$, is not fulfilled, which is required to satisfy the constraint from the Higgs coupling measurement. We do not specify a mechanism to generate this breaking in this thesis, but

just encapsulate the breaking effect in the quadratic and quartic terms of H_A. The effective potential of the scalar field H we consider here is then summarized as

$$V^{\rm twin} = \lambda\left(|H_A|^2 + |H_B|^2 - \frac{f^2}{2}\right)^2 + \kappa_1\left(|H_A|^4 + |H_B|^4\right) + \sigma_1 f^2|H_A|^2 + \rho_1|H_A|^4. \quad (2.51)$$

The first term is the U(4) conserving term coming from the original potential Eq. (2.49) rewritten in terms of H_A and H_B and the corrections in Eq. (2.50), which determines the U(4) symmetry breaking scale f. The second term that breaks the U(4) symmetry includes the gauge (and top Yukawa) contributions in the Coleman-Weinberg potential. Thus κ_1 will be of order $g_2^4/16\pi^2 \log\left(\Lambda_{\rm UV}/g_2 f\right)$. The third and fourth terms are the $\mathbf{Z}_2$ breaking terms. The third term is induced, *e.g.,* by the quadratic corrections with $\mathbf{Z}_2$-breaking part in the gauge and matter sector. ρ_1 in the fourth term includes the contribution of the one-loop Coleman-Weinberg potential. In the Fraternal twin Higgs model, the fourth term could arise from the $\mathbf{Z}_2$ breaking effect such as the absence of the $\mathrm{U}(1)_{\rm Y}$ gauge symmetry in the twin sector. However, this effect is of order $g_1^4/16\pi^2$, where g_1 is the $\mathrm{U}(1)_{\rm Y}$ gauge coupling constant and tiny. In summary, we take $\lambda, f, \kappa_1, \sigma_1$ and ρ_1 to be the model parameters and require $\sigma_1,\ \kappa_1,\ \rho_1 < \lambda$ so that the second, third and the forth terms in Eq. (2.51) are regarded as perturbations to the first term.

The Lagrangian densities of the Mirror and Fraternal Twin Higgs models

Here, based on the previous discussion, let us concretely write down the Lagrangian densities of the twin Higgs models. The Lagrangian density of twin Higgs models, $\mathcal{L}^{\rm twin}$, can be decomposed into following forms:

$$\mathcal{L}^{\rm twin} = \mathcal{L}^{\rm SM}_{\text{gauge boson}} + \mathcal{L}^{\rm twin}_{\text{gauge boson}} + \mathcal{L}^{\rm SM}_{\rm fermion} + \mathcal{L}^{\rm twin}_{\rm fermion} + \mathcal{L}^{\rm twin}_{\rm Higgs}, \quad (2.52)$$

where $\mathcal{L}^{\rm SM}_{\text{gauge boson}}$ and $\mathcal{L}^{\rm SM}_{\rm fermion}$ are the Lagrangian densities of the gauge boson and fermion sectors, which were already defined by Eq. (2.4) and Eq. (2.6), respectively. We shall explicitly show concrete expressions of Lagrangian densities $\mathcal{L}^{\rm twin}_{\text{gauge boson}}$, $\mathcal{L}^{\rm twin}_{\rm fermion}$ and $\mathcal{L}^{\rm twin}_{\rm Higgs}$ in the following.

$\mathcal{L}^{\rm twin}_{\rm gauge\ boson}$ is the Lagrangian density of twin gauge bosons:

$$\mathcal{L}^{\rm twin}_{\rm gauge\ boson} = \begin{cases} -\frac{1}{4}{\rm Tr}\left[\widehat{G}^{\mathcal{A}}_{\mu\nu}\widehat{G}^{\mathcal{A}\mu\nu}\right] - \frac{1}{4}{\rm Tr}\left[\widehat{W}^{I}_{\mu\nu}\widehat{W}^{I\mu\nu}\right] - \frac{1}{4}\widehat{B}_{\mu\nu}\widehat{B}^{\mu\nu} & \text{(The Mirror twin Higgs model)} \\ -\frac{1}{4}{\rm Tr}\left[\widehat{G}^{\mathcal{A}}_{\mu\nu}\widehat{G}^{\mathcal{A}\mu\nu}\right] - \frac{1}{4}{\rm Tr}\left[\widehat{W}^{I}_{\mu\nu}\widehat{W}^{I\mu\nu}\right] & \text{(The Fraternal twin Higgs model)} \end{cases} . \tag{2.53}$$

In the above expressions, $\widehat{G}^{\mathcal{A}}_{\mu\nu}$, $\widehat{W}^{I}_{\mu\nu}$ and $\widehat{B}_{\mu\nu}$ are the field strengths of $\mathrm{SU}(3)_{\widehat{\mathrm{C}}}$, $\mathrm{SU}(2)_{\widehat{\mathrm{W}}}$ and $\mathrm{U}(1)_{\widehat{\mathrm{Y}}}$, respectively. Definitions of these field strengths are given by Eq. (2.5) with replacements of $G^{A}_{\mu} \to \widehat{G}^{\mathcal{A}}_{\mu}$, $W^{I}_{\mu} \to \widehat{W}^{I}_{\mu}$ and $B_{\mu} \to \widehat{B}_{\mu}$, and $g_3 \to \widehat{g}_3$ and $g_2 \to \widehat{g}_2$. Here, $\widehat{G}^{\mathcal{A}}_{\mu}$, $\widehat{W}^{I}_{\mu}$ and $\widehat{B}_{\mu}$ are the twin gluon, the twin $\mathrm{SU}(2)_{\mathrm{B}}$ gauge boson and the $\mathrm{U}(1)_{\widehat{\mathrm{Y}}}$ gauge boson, respectively. As we stated in the previous subsection, the $\mathrm{U}(1)_{\widehat{\mathrm{Y}}}$ gauge boson, which is the twin $\mathrm{U}(1)_{\mathrm{Y}}$ partner is absent in the Fraternal model. We have omitted the Lagrangian densities of Faddeev-Popov ghosts of $\mathrm{SU}(3)_{\widehat{\mathrm{C}}} \times \mathrm{SU}(2)_{\widehat{\mathrm{W}}}$.

$\mathcal{L}^{\rm twin}_{\rm fermion}$ is the Lagrangian density of the twin partner of the fermion sector. Due to the twin $\mathbf{Z}_2$ symmetry, fermion content and fermions charge assignments of the twin sector are almost same as the SM Lagrangian. Similar to the $\mathcal{L}^{\rm SM}_{\rm fermion}$, we further decompose $\mathcal{L}^{\rm twin}_{\rm fermion}$ into following pieces:

$$\mathcal{L}^{\rm twin}_{\rm fermin} = \mathcal{L}^{\rm twin}_{\rm fermion\ gauge} + \mathcal{L}^{\rm twin}_{\rm Yukawa}. \tag{2.54}$$

The first term includes the kinetic terms of the twin fermions and couplings between the twin fermion and twin gauge fields, while the second term gives the Yukawa coupling between the H_B Higgs and the twin fermions. $\mathcal{L}^{\rm twin}_{\rm fermion\ gauge}$ is explicitly given by

$$\mathcal{L}^{\rm twin}_{\rm fermion\ gauge} = \begin{cases} i\overline{\widehat{L}}_n \widehat{\not{D}} \widehat{L}_n + i\overline{\widehat{e}}_{nR} \widehat{\not{D}} \widehat{e}_{nR} + i\overline{\widehat{Q}}_n \widehat{\not{D}} \widehat{Q}_n + i\overline{\widehat{u}}_{nR} \widehat{\not{D}} \widehat{u}_{nR} + i\overline{\widehat{d}}_{nR} \widehat{\not{D}} \widehat{d}_{nR}. & \text{(The Mirror twin Higgs model)} \\ i\overline{\widehat{L}}_3 \widehat{\not{D}} \widehat{L}_3 + i\overline{\widehat{e}}_{3R} \widehat{\not{D}} \widehat{e}_{3R} + i\overline{\widehat{Q}}_3 \widehat{\not{D}} \widehat{Q}_3 + i\overline{\widehat{u}}_{3R} \widehat{\not{D}} \widehat{u}_{3R} + i\overline{\widehat{d}}_{3R} \widehat{\not{D}} \widehat{d}_{3R}. & \text{(The Fraternal twin Higgs model)} \end{cases} , \tag{2.55}$$

$\widehat{\not{D}} \equiv \gamma^{\mu} \widehat{D}_{\mu}$.

In the above expression, $\widehat{\Psi}_{\rm SM}$ represents the twin partner of the SM field denoted by $\Psi_{\rm SM}$, which was defined in Sec. 2. The definition of the covariant derivative with respect to the

twin gauge symmetries $\mathrm{SU}(3)_{\widehat{\mathrm{C}}} \times \mathrm{SU}(2)_{\widehat{\mathrm{W}}} (\times \mathrm{U}(1)_{\widehat{\mathrm{Y}}})$, $\widehat{D}_\mu$, is defined by

$$\widehat{D}_\mu \widehat{\Psi}_{\mathrm{SM}} \equiv \begin{cases} \left(\partial_\mu - i\widehat{g}_3 \widehat{T}_3^{\mathcal{A}} G_\mu^{\mathcal{A}} - i\widehat{g}_2 \widehat{T}_2^I \widehat{W}_\mu^I - i\widehat{g}_1 \widehat{Y} \widehat{B}_\mu\right) \widehat{\Psi}_{\mathrm{SM}} \text{ (The Mirror twin Higgs model)} \\ \left(\partial_\mu - i\widehat{g}_3 \widehat{T}_3^{\mathcal{A}} G_\mu^{\mathcal{A}} - i\widehat{g}_2 \widehat{T}_2^I \widehat{W}_\mu^I\right) \widehat{\Psi}_{\mathrm{SM}} \text{ (The Fraternal twin Higgs model)} \end{cases}, \tag{2.56}$$

Here, $\widehat{T}_3^{\mathcal{A}} = \lambda_{\mathcal{A}}/2$ ($\lambda_{\mathcal{A}}$ is the Gell-Mann matrices $\mathcal{A} = 1, 2, \cdots, 8$) for the twin quarks and $\widehat{T}_3^{\mathcal{A}} = 0$ for the twin leptons. Since $\mathrm{SU}(2)_{\mathrm{B}}$ gauge boson couples to the left-handed twin fermions (and the H_B Higgs), $\widehat{T}_2^I = \sigma^I/2$ for the left-handed twin quarks and the twin leptons, and $\widehat{T}_2^I = 0$ for the twin right-handed quarks and leptons. $\widehat{g}_1$ and $\widehat{Y}$ are the $\mathrm{U}(1)_{\widehat{\mathrm{Y}}}$ gauge coupling and its twin hypercharge of the twin fermions. Note that twin fermions are singlet under all SM gauge group. As we stated in the previous section, in the Fraternal twin Higgs model, only third generation of the quark and lepton are introduced. The Lagrangian density of the twin Yukawa sector $\mathcal{L}_{\mathrm{Yukawa}}^{\mathrm{twin}}$ is explicitly given by

$$\mathcal{L}_{\mathrm{Yukawa}}^{\mathrm{twin}} = \begin{cases} -\left(\widehat{Y}_{mn}^e \bar{\widehat{L}}_m H_B \widehat{e}_{nR} + \widehat{Y}_{mn}^d \bar{\widehat{Q}}_m H_B \widehat{d}_{Rm} + \widehat{Y}_{mn}^u \bar{\widehat{Q}}_m \tilde{H}_{\mathrm{B}} \widehat{u}_{Rn} + \mathrm{h.c.}\right). \text{ (The Mirror twin Higgs model)} \\ -\left(\widehat{Y}_{33}^e \bar{\widehat{L}}_3 H_B \widehat{e}_{3R} + \widehat{Y}_{33}^d \bar{\widehat{Q}}_3 H_B \widehat{d}_{R3} + \widehat{Y}_{33}^u \bar{\widehat{Q}}_3 \tilde{H}_{\mathrm{B}} \widehat{u}_{R3} + \mathrm{h.c.}\right). \text{ (The Fraternal twin Higgs model)} \end{cases}, \tag{2.57}$$

In the above expression, $\widehat{Y}_{mn}^e$, $\widehat{Y}_{mn}^d$ and $\widehat{Y}_{mn}^u$ are 3×3 Yukawa coupling matrices of the twin leptons, the twin down-type quarks and the twin up-type quarks, respectively. The definition $\tilde{H}_B$ is same as $\tilde{H}_A$. Again, it should be emphasized that, in the Fraternal twin Higgs models, only third generation of twin fermions are introduced.

Let us finally show the Lagrangian density of the Higgs sector.

$$\mathcal{L}_{\mathrm{Higgs}}^{\mathrm{twin}} = \left(D_\mu H_A\right)^\dagger \left(D^\mu H_A\right) + \left(\widehat{D}_\mu H_B\right)^\dagger \left(\widehat{D}^\mu H_B\right) - V^{\mathrm{twin}}. \tag{2.58}$$

The first term of the above expression is completely same as the gauge coupling and the kinetic term of the SM Higgs boson. For the second term, the covariant derivative is given by $\widehat{D}_\mu \equiv \partial_\mu - i\widehat{g}_2 \sigma^I \widehat{W}_\mu^I/2 - i\widehat{g}_1 \widehat{B}_\mu/2$ for the Mirror twin Higgs and $\widehat{D}_\mu \equiv \partial_\mu - i\widehat{g}_2 \sigma^I \widehat{W}_\mu^I/2$ for the Fraternal twin Higgs model. The tree-level Higgs potential V^{twin} is given by Eq. (2.51).

The electroweak symmetry breaking in the twin Higgs Models

At energies well below the symmetry breaking scale f, we can integrate out the Higgs field H_B, which enables us to work with an effective field theory of the SM Higgs field H_A. The effective potential of the SM Higgs field can be obtained by setting H_B as

$$|H_B|^2 = \frac{f^2}{2} - |H_A|^2. \tag{2.59}$$

Using this relation, V^{twin} can be calculated as

$$V_{\text{eff}}(H_A) = -(\kappa_1 - \sigma_1) f^2 |H_A|^2 + (2\kappa_1 + \rho_1)|H_A|^4. \tag{2.60}$$

This potential coincides with the SM Higgs potential when the parameters κ_1, σ_1 are identified with

$$2\kappa_1 + \rho_1 = \lambda_{\text{SM}}, \qquad \frac{\kappa_1 - \sigma_1}{2\kappa_1 + \rho_1} = \frac{v_A^2}{f^2}, \tag{2.61}$$

where $\lambda_{SM} \sim \frac{1}{8}$ is the SM Higgs self-coupling, $v_A = 246\,\text{GeV}$ is the VEV of the SM Higgs field. As denoted above, to satisfy the constraint from the Higgs coupling measurement, the VEV of the Standard Model Higgs field is required to be satisfactorily small compared to the $U(4)$ symmetry breaking scale, that is, $v_A^2 \ll f^2$.

Let us discuss the electroweak symmetry breaking conditions ($v_A \simeq 246\text{GeV}$ and $m_h \simeq 125\text{GeV}$) in the twin Higgs models precisely with the potential (2.51). By expressing the potential (2.51) in terms of the two physical modes ϕ_A and ϕ_B with $H_A \equiv (0, \phi_A/\sqrt{2})$ and $H_B \equiv (0, \phi_B/\sqrt{2})$ and requiring the minimization conditions, $\partial V/\partial\phi_A = \partial V/\partial\phi_B = 0$, we find the potential minimum given by

$$v_A^2 = \lambda f^2 \frac{-\sigma_1 + \kappa_1(1 - \frac{\sigma_1}{\lambda})}{\lambda\rho_1 + \kappa_1(2\lambda + \rho_1 + \kappa_1)}. \tag{2.62}$$

Evaluating the mass matrix $\partial V/\partial\phi_i\partial\phi_j (i, j = A, B)$ around the potential minimum, we obtain the mass eigenvalues of the system, that is, the SM Higgs boson h and the heavy exotic (global symmetry breaking) Higgs $\widehat{h}$ as [83, 84]

$$\begin{aligned} m_{\widehat{h},h}^2 &= \rho_1 v_A^2 + f^2(\lambda + \kappa_1)\left(1 \pm \sqrt{1 - A}\right), \\ A &\equiv 2\frac{v_A^2}{f^2}\frac{\lambda\rho_1 + \kappa_1(4\lambda + \rho_1 + 2\kappa_1)}{(\lambda + \kappa_1)^2} - \frac{v_A^4}{f^4}\frac{4\lambda\rho_1 + \rho_1^2 + \kappa_1(8\lambda + 4\rho_1 + 4\kappa_1)}{(\lambda + \kappa_1)^2}, \end{aligned} \tag{2.63}$$

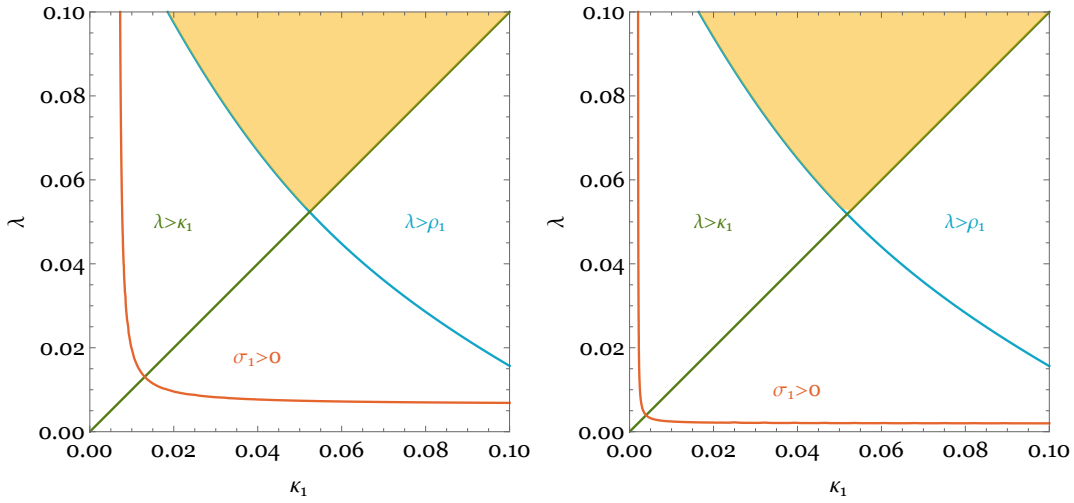

Figure 2.3: The (yellow) region that satisfies $\lambda > \rho_1,\ \kappa_1$ and $\sigma_1 > 0$ is shown for $v_A \simeq 246$ GeV, $m_h \simeq 125$GeV, and $v_A/f = 0.223$ (left) and 0.123 (right). The regions above the blue, green and red curves satisfy with the constraints $\lambda > \rho_1,\ \lambda > \kappa_1$ and $\sigma_1 > 0$, respectively.

where the plus sign in front of $\sqrt{1-A}$ corresponds to $m_{\hat{h}}^2$ and the negative sign corresponds to m_h^2. With $v_A^2/f^2 \ll 1$, the SM Higgs mass is approximately given by

$$m_h^2 \simeq 2\frac{\kappa_1^2 + 2\kappa_1\lambda + \kappa_1\rho_1 + \lambda\rho_1}{\kappa_1 + \lambda} v_A^2 \,. \tag{2.64}$$

Since we have five parameters $f,\ \lambda,\ \sigma_1,\ \kappa_1$ and ρ_1, after imposing the EWSB conditions $v_A \simeq 246$ GeV (2.62) and $m_h \simeq 125$GeV (2.63), the system is now described by three parameters. As noted above, we impose the conditions $\lambda > \sigma_1, \kappa_1, \rho_1$ to keep the philosophy of the twin Higgs models. Fig. 2.3 shows the parameter space that satisfies these conditions for $v_A/f = 0.223$ ($f = 1.1$ TeV) and 0.123 ($f = 2$ TeV). We also confirmed that the condition $\lambda > \sigma_1$ is always satisfied. Note that the parameters $\lambda,\ \kappa_1$ and ρ_1 cannot take arbitrary small values because tiny $\lambda,\ \kappa_1$ and ρ_1 cannot realize the SM-like Higgs mass. In fact, we can see from Fig. 2.3 that the smallest values of $\lambda,\ \kappa_1$ and ρ_1 are roughly given by $\lambda \simeq \kappa_1 \simeq \rho_1 \simeq 0.05$. This bound will play important roles when we analyze the dynamics of a phase transition as we will see in Sec. 4.4. The smallest values of $\lambda,\ \kappa_1,\ \rho_1$ are not sensitive to the breaking scale v_A/f and SM-like Higgs mass $m_h \simeq 125$GeV. $\sigma_1 > 0$ guarantees our assumption of the two-step phase transition as we will see later.

Let us finally examine the fine-tuning in this effective potential. In our effective potential,

the set of the observable and parameter that gives the smallest measure is the following one,

$$\Delta_{\sigma_1} \equiv \left| \frac{\partial \log \left(v_A^2/f^2\right)}{\partial \log \sigma_1} \right|^{-1} = \frac{2\frac{v_A^2}{f^2}}{1-2\frac{v_A^2}{f^2}} \simeq \frac{2v_A^2}{f^2}. \tag{2.65}$$

In this calculation, we simply assume the soft breaking scenario, $\sigma_1 \gg \rho_1$, which means that the twin $\mathbf{Z_2}$ symmetry is only broken by the soft term $\sigma_1 f^2$.[4] In order to solve the little hierarchy problem in twin Higgs models, Δ_{σ_1} should not take an arbitrary small value. Thus, the symmetry breaking scale f is bounded from above in light of naturalness. In other words, we cannot take the breaking scale f as large as the Planck scale (or the grand unification scale). Hence the twin Higgs mechanism cannot provide the solution to the large hierarchy problem, that is, the hierarchy between the breaking scale f and the Planck scale.

2.3.3 Supersymmetric twin Higgs models

To address the large hierarchy problem in the twin Higgs scenario, SUSY can provide an attractive solution. Parallel to the case of the ordinary Minimal Supersymmetric Standard Model (MSSM), where Higgs chiral multiplets consist of a pair of doublets, supersymmetric twin Higgs models generally contain four Higgs doublets,

$$H_u = \begin{pmatrix} H_u^A \\ H_u^B \end{pmatrix}, \qquad H_d = \begin{pmatrix} H_d^A \\ H_d^B \end{pmatrix}. \tag{2.66}$$

The chiral multiplets H_u, H_d are fundamental under the $U(4)$ symmetry and the U(4) multiplets are decomposed into the visible sector fields H_u^A, H_d^A and the twin sector fields H_u^B, H_d^B under the subgroups $\mathrm{SU(2)_A} \times \mathrm{SU(2)_B}$. The superpotential contains an extended version of the ordinary μ-term, $W \supset \mu(H_u^A H_d^A + H_u^B H_d^B)$. Including soft SUSY breaking mass terms, the quadratic part of the $U(4)$ symmetric potential in supersymmetric twin Higgs models is given by

$$\begin{aligned} V_{U(4)} \supset\ & \left(\widetilde{m}_{H_u}^2 + \mu^2\right)\left(|H_u^A|^2 + |H_u^B|^2\right) + \left(\widetilde{m}_{H_d}^2 + \mu^2\right)\left(|H_d^A|^2 + |H_d^B|^2\right) \\ & - b\left(H_u^A H_d^A + H_u^B H_d^B + \mathrm{h.c.}\right). \end{aligned} \tag{2.67}$$

The quartic part of the $U(4)$ symmetric potential is model dependent. The first term of (2.51) contains the quartic term $|H_A|^2|H_B|^2$. However, SUSY forbids this type of couplings

[4] For the hard breaking scenario, $\rho_1 \gg \sigma_1$, see Ref. [83].

without further modification of the Higgs sector. There are several proposals to obtain Higgs couplings with twin Higgs fields. Refs. [80, 81, 82, 83] have introduced a massive singlet chiral superfield S with a superpotential SH_uH_d. The effective theory after integrating out this singlet contains the quartic term $|H_uH_d|^2$. Ref. [84] has considered an additional contribution to the D-term potential from a new U(1) gauge symmetry, under which both the Higgs and the twin Higgs fields are charged. In our analysis, we do not go into the details of a specific supersymmetric twin Higgs model, instead, we simply assume the existence of an appropriate U(4) symmetric quartic term and try to extract general features of a supersymmetric twin Higgs scenario.

We next consider possible sources of the breaking of the U(4) and the $\mathbf{Z}_2$ symmetries in this scenario. In the non-supersymmetric minimal model, the U(4) symmetry breaking arises only from quantum corrections or from some explicit breaking terms. On the other hand, supersymmetric models have the D-term potential,

$$V_D = \frac{g_1^2 + g_2^2}{8}\left(|H_u^A|^2 - |H_d^A|^2\right)^2 + \frac{\widehat{g}_2^2}{8}\left(|H_u^B|^2 - |H_d^B|^2\right)^2, \tag{2.68}$$

which breaks the U(4) and the $\mathbf{Z}_2$ symmetries. Here we have assumed the minimal realization of the twin Higgs mechanism, where the twin partner of $\mathrm{U}(1)_\mathrm{Y}$ is not introduced. Unfortunately, the size of the $\mathbf{Z}_2$ breaking in the above D-term potential is insufficient to realize the required hierarchy between the electroweak breaking scale, v_A, and the U(4) breaking scale, f. Then, we simply assume the following $\mathbf{Z}_2$ breaking soft mass terms,

$$V_\mathrm{soft} = \Delta\widetilde{m}_{H_u}^2|H_u^A|^2 + \Delta\widetilde{m}_{H_d}^2|H_d^A|^2. \tag{2.69}$$

In order to make the discussion independent of the form of quartic couplings, we take the decoupling limit of the SUSY heavy Higgses and match the theory to the non-supersymmetric twin Higgs potential. In the decoupling limit, the four Higgs doublets can be written as follows in terms of H_A and H_B in the non-supersymmetric twin Higgs model,

$$\begin{aligned} H_u^A &= H_A \sin\beta_A, \qquad & H_u^B &= H_B \sin\beta_B, \\ H_d^A &= H_A^\dagger \cos\beta_A, \qquad & H_d^B &= H_B^\dagger \cos\beta_B. \end{aligned} \tag{2.70}$$

Here, $\tan\beta_A = v_u^A/v_d^A$ and $\tan\beta_B = v_u^B/v_d^B$ with $v_{u,d}^{A,B} \equiv \langle H_{u,d}^{A,B}\rangle/\sqrt{2}$. Thanks to the approximate $\mathbf{Z}_2$ symmetry, they are almost equal, $\tan\beta_A \simeq \tan\beta_B$. In the rest of the discussion, we simply assume $\beta_A = \beta_B = \beta$ and $\widehat{g}_2 = g_2$. Note that by taking the decoupling limit (2.70),

the structure of the Higgs potential is essentially the same as that of the potential given by (2.51) discussed in the previous subsection. When we require that the supersymmetric twin Higgs potential is matched with Eq. (2.51), we obtain the following relations,

$$\begin{aligned} -\lambda f^2 &= \widetilde{m}_{H_u}^2 \sin^2\beta + \widetilde{m}_{H_d}^2 \cos^2\beta + \mu^2 - b\sin 2\beta, \\ \sigma_1 f^2 &= (\sigma + \delta\sigma) f^2 = \Delta\widetilde{m}_{H_u}^2 \sin^2\beta + \Delta\widetilde{m}_{H_d}^2 \cos^2\beta + \delta\sigma f^2, \\ \kappa_1 &= \kappa + \delta\kappa = \frac{g_2^2}{8}\cos^2 2\beta + \delta\kappa, \\ \rho_1 &= \rho + \delta\rho = \frac{g_1^2}{8}\cos^2 2\beta + \delta\rho, \end{aligned} \tag{2.71}$$

where $\delta\sigma, \delta\kappa$ and $\delta\rho$ represent the radiative corrections. With these expressions, we can evaluate the SM-like Higgs mass from (2.63). Note that it is difficult to realize the SM-like Higgs mass only with the quartic couplings in the D-term potential, $\kappa = \frac{g_2^2}{8}\cos^2 2\beta$ and $\rho = \frac{g_1^2}{8}\cos^2 2\beta$. We simply assume that there is an additional contribution or a radiative correction to κ and ρ to realize the SM-like Higgs mass. As mentioned in the previous subsection, we impose the EWSB conditions and the conditions $\lambda > \sigma_1,\ \kappa_1,\ \rho_1$ to consider the general feature of SUSY twin Higgs models. In any case, after integrating out all supersymmetric partners, the effective Lagrangian density becomes the one given in the previous subsection.

2.4 Minimal Scotogenic Model

As we saw in the previous Sec. 2.2.3 and Sec. 2.2.2, to explain the DM and non-zero neutrino masses, we need physics beyond the SM. The scotogenic model [92] is one of the promising candidate for physics beyond the SM, which simultaneously explains the origin of neutrino masses and the DM.

The minimal scotogenic model is an extension of the SM with three right-handed neutrinos ν_{nR} and one $\mathrm{SU(2)_W}$-doublet scalar field S (called inert scalar doublet). Assuming that ν_{nR} and S particles are odd under discrete Z_2 symmetry, while the SM fields remain Z_2-even such that

$$\nu_{nR} \to -\nu_{nR}, \quad S \to -S, \quad A_{\mathrm{SM}} \to A_{\mathrm{SM}}\,, \tag{2.72}$$

where A_{SM} represents the SM particles. The total Lagrangian density of this model, $\mathcal{L}^{\mathrm{scotogenic}}$,

can be schematically decomposed into following form:

$$\mathcal{L}^{\text{scotogenic}} = \mathcal{L}^{\text{SM}}_{\text{fermion}} + \mathcal{L}^{\text{SM}}_{\text{gauge bosons}} + \mathcal{L}^{\text{scotogenic}}_{\text{scalar}} + \mathcal{L}^{\text{scotogenic}}_{\text{lepton}}. \tag{2.73}$$

In this expression, $\mathcal{L}^{\text{SM}}_{\text{fermion}}$ and $\mathcal{L}^{\text{SM}}_{\text{gauge bosons}}$ are the SM Lagrangian defined by Eq (2.7) and Eq. (2.4), respectively.

$\mathcal{L}^{\text{scotogenic}}_{\text{scalar}}$ is the Lagrangian density of the scalar sector of this model and is explicitly given by

$$\mathcal{L}^{\text{scotogenic}}_{\text{scalar}} = D_\mu S^\dagger D^\mu S + D_\mu H^\dagger_{\text{SM}} D^\mu H_{\text{SM}} - V^{\text{scotogenic}}_{\text{tree}}(S, H_{\text{SM}}). \tag{2.74}$$

The charge assignment of S is completely same as the SM Higgs doublet. Hence, the covariant derivative appearing above is defined by $D_\mu \equiv \partial_\mu - ig_2\sigma^I W^I_\mu/2 - ig_1 B_\mu/2$. The tree level scalar potential of the model, $V^{\text{scotogenic}}_{\text{tree}}$, is given by

$$\begin{aligned} V^{\text{scotogenic}}_{\text{tree}} =& V_{\text{SM}}(H_{\text{SM}}) + m_1^2|S|^2 + \lambda_1|H_{\text{SM}}|^2|S|^2 + \lambda_2(H^\dagger_{\text{SM}}S)\left(S^\dagger H_{\text{SM}}\right) \\ &+ \left[\lambda_3\left(H^\dagger_{\text{SM}}S\right)^2 + \text{h.c.}\right] + \lambda_S|S|^2. \end{aligned} \tag{2.75}$$

where $V_{\text{SM}}(H_{\text{SM}})$ is defined by Eq. (2.23). The unbroken Z_2 symmetry prevents the S to acquire any VEV, that is, $m_1^2 > 0$ otherwise Z_2 symmetry is spontaneously broken.

The Lagrangian density of the lepton sector $\mathcal{L}^{\text{scotogenic}}_{\text{lepton}}$ is given by

$$\mathcal{L}^{\text{scotogenic}}_{\text{lepton}} = \bar{\nu}_{nR}\partial\!\!\!/\nu_{nR} + \frac{1}{2}(M_{\nu_R})_{nm}\left(\bar{\nu}^c_{nR}\nu_{mR} + \text{h.c.}\right) + \left(Y^S_{nm}\,\bar{L}_n\tilde{S}\nu_{mR} + \text{h.c.}\right). \tag{2.76}$$

where $(M_{\nu_R})_{nm}$ and Y^S_{nm} are the Majorana mass and Yukawa coupling with the inert scalar doublet matrices, respectively. Compared to the expression Eq. (2.39), the Y^ν_{mn} term is absent since it is forbidden by the Z_2 symmetry Eq. (2.72), and hence, the left-handed neutrinos are massless (because S does not develop VEV) at classical level.

To compute mass spectrums of H_{SM} and S fields, let us parametrise those fields as follows.

$$H_{\text{SM}} = \begin{pmatrix} 0 \\ \frac{h_{\text{SM}}}{\sqrt{2}} \end{pmatrix}, \qquad S = \begin{pmatrix} S^+ \\ S_0 \end{pmatrix}. \tag{2.77}$$

For S^+ and S_0 fields, we have following mass terms:

$$m^2_\pm = m_1^2 + \frac{1}{2}\lambda_1 h^2_{\text{SM}}, \;\; \mathcal{M}^2_{S_0} = \begin{pmatrix} m_1^2 + \frac{1}{2}\left(\lambda_1 + \lambda_2 + 2\lambda_3\right)h^2_{\text{SM}}, & 0 \\ 0, & m_1^2 + \frac{1}{2}\left(\lambda_1 + \lambda_2 - 2\lambda_3\right)h^2_{\text{SM}} \end{pmatrix}. \tag{2.78}$$

Using $S_0 = (H + iA)/\sqrt{2}$ we obtain the physical masses as

$$\begin{aligned} n_\pm = 2 \ &: \ m_\pm^2 = m_1^2 + \frac{1}{2}\lambda_1 h_{\rm SM}^2, \\ n_H = 1 \ &: \ m_H^2 = m_1^2 + \frac{1}{2}\left(\lambda_1 + \lambda_2 + 2\lambda_3\right) h_{\rm SM}^2, \\ n_A = 1 \ &: \ m_A^2 = m_1^2 + \frac{1}{2}\left(\lambda_1 + \lambda_2 - 2\lambda_3\right) h_{\rm SM}^2, \end{aligned} \tag{2.79}$$

where m_H (m_A) and $m_\pm$ are the masses of CP-even (odd) component and the charged component of the inert scalar doublet, respectively, and $n_\pm$, n_H and n_A represent degrees of freedom of each fields. Present masses are obtained by $h_{\rm SM} = v_{\rm SM}$.

2.4.1 Generation of Neutrino masses in Scotogenic Model

Let us here consider the generation of the neutrino masses in minimal scotogenic model. Due to the Z_2 symmetry, we saw that the left-handed neturinos are classically massless. However, non-zero masses can be radiatively generated at one-loop level given by [24, 93]

$$\begin{aligned} (M_{\nu_R})_{nm} &= \sum_k \frac{Y^S_{nk} Y^S_{mk} M_k}{32\pi^2} \left(\frac{m_H^2}{m_H^2 - M_k^2} \ln \frac{m_H^2}{M_k^2} - \frac{m_A^2}{m_A^2 - M_k^2} \ln \frac{m_A^2}{M_k^2} \right) \\ &\equiv \sum_k \frac{Y^S_{nk} Y^S_{mk} M_k}{32\pi^2} \left[L_k(m_H^2) - L_k(m_A^2) \right] , \end{aligned} \tag{2.80}$$

where M_k is the mass eigenvalue of the mass eigenstate ν_{kR} in the internal line and the indices $n, m = 1, 2, 3$ run over the three neutrino generations as well as three copies of ν_{nR}. The function $L_k(m^2)$ is defined as

$$L_k(m^2) = \frac{m^2}{m^2 - M_k^2} \ln \frac{m^2}{M_k^2} . \tag{2.81}$$

It is important to ensure that the choice of Yukawa couplings as well as other parameters involved in light neutrino mass are consistent with the current constraints summerized in Sec. 2.2.2. In order to incorporate these constraints on model parameters, it is often useful to rewrite the neutrino mass formula given in equation (2.80) in a form resembling the type-I seesaw formula:

$$M_{\nu_R} = Y^S \Lambda^{-1} (Y^S)^T , \tag{2.82}$$

where we have introduced the diagonal matrix Λ with elements

$$\Lambda_i \;=\; \frac{2\pi^2}{\lambda_3}\zeta_i\frac{M_i}{v^2}\,, \tag{2.83}$$

$$\text{and}\quad \zeta_i \;=\; \left(\frac{M_i^2}{8(m_H^2-m_A^2)}\left[L_i(m_H^2)-L_i(m_A^2)\right]\right)^{-1}\,. \tag{2.84}$$

The light neutrino mass matrix (2.82) which is complex symmetric, can be diagonalized by the PMNS matrix U, [5] defined by Eq. (2.41). The diagonal light neutrino mass matrix is therefore,

$$D_\nu \;\equiv\; U^\dagger M_{\nu R} U^* \;=\; \text{diag}(m_{\nu_1}, m_{\nu_2}, m_{\nu_3})\,. \tag{2.85}$$

Since the inputs from neutrino data are only in terms of the mass squared differences and mixing angles, it would be useful for our purpose to express the Yukawa couplings in terms of light neutrino parameters. This is possible through the Casas-Ibarra (CI) parametrisation [94] extended to radiative seesaw model [68] which allows us to write the Yukawa coupling matrix satisfying the neutrino data as

$$Y^S \;=\; U D_\nu^{1/2} R^\dagger \Lambda^{1/2}\,, \tag{2.86}$$

where R is an arbitrary complex orthogonal matrix satisfying $RR^T = \mathbf{1}$.

2.4.2 Dark Matter in Scotogenic Model

The lightest Z_2 odd particle, if electromagnetically neutral, can be the DM candidate in the model because condition (i) listed in Sec. 2.2.3 is satisfied. Also, decay of new particles S and ν_{nR} are forbidden by the Z_2 symmetry, and thus, condition (ii) is also satisfied. We have seen that S particles have two electromagnetically neutral components, which are H and A particles. In this thesis, we only consider the case H is lighter than A if H is lighter than the right-handed neturinos. (The scenario, where A is the DM candidate, can be obtained by the simple replacement of $\lambda_3 \to -\lambda_3$.) We shall call this scenario as scalar DM scenario. We can also consider the case where the lightest right handed-neutrino ν_{1R} is the DM candidate, which is called the fermion DM scenario. The dark matter production mechanism for both scalar and fermion DM candidates will be explained in Sec. 2.4.2.

[5] Usually, the leptonic mixing matrix is given in terms of the charged lepton diagonalising matrix (U_l) and light neutrino diagonalising matrix U_ν as $U = U_l^\dagger U_\nu$. In the simple case where the charged lepton mass matrix is diagonal which is true in our model, we can have $U_l = \mathbf{1}$. Therefore we can write $U = U_\nu$.

2.4.3 Constraints on Model Parameters in Scotogenic Model

Precision measurements at LEP experiment forbids additional decay channels of the SM gauge bosons. For example, it strongly constrains the decay channel $Z \to HA$ requiring $m_H + m_A > m_Z$. Additionally, LEP precision data also rule out the region $m_H < 80$ GeV, $m_A < 100$ GeV, $m_A - m_H > 8$GeV [95]. We take the lower bound on charged scalar mass $m_\pm > 90$ GeV. If $m_{H,A} < m_h/2$, the LHC bound on invisible Higgs decay comes into play [96] which can constrain the SM Higgs coupling with H, A namely $\lambda_1 + \lambda_2 \pm 2\lambda_3$ to as small as 10^{-4}, which however remains weaker than DM direct detection bounds in this mass regime (See e.g. [97].).

The LHC experiment can also put bounds on the scalar masses in the model, though in a model dependent way. Depending upon the mass spectrum of its components, the heavier ones can decay into the lighter ones and a gauge boson, which finally decays into a pair of leptons or quarks. Therefore, we can have either pure leptonic final states plus missing transverse energy (MET), hadronic final states plus MET or a mixture of both. The MET corresponds to DM or light neutrinos. In several earlier works [98, 37, 99], the possibility of opposite sign dileptons plus MET was discussed. In [100], the possibility of dijet plus MET was investigated with the finding that inert scalar masses up to 400 GeV can be probed at high luminosity LHC. In another work [101], tri-lepton plus MET final states was also discussed whereas mono-jet signatures have been studied by the authors of [102, 103]. The enhancement in dilepton plus MET signal in the presence of additional vector like singlet charged leptons was also discussed in [104]. Exotic signatures like displaced vertex and disappearing or long-lived charged track for compressed mass spectrum of inert scalars and singlet fermion DM was studied recently by the authors of [105].

In addition to the collider or direct search constraints, there exists theoretical constraints also. For instance, the scalar potential of the model should be bounded from below in any field direction. This criteria leads to the following co-positivity conditions. [106, 107, 38, 108]:

$$\lambda_S > 0,\ \lambda_1 + 2\sqrt{\lambda_{\rm SM}\lambda_S} > 0,\ \lambda_1 + \lambda_2 - \frac{|\lambda_3|}{2} + 2\sqrt{\lambda_{\rm SM}\lambda_S} > 0. \tag{2.87}$$

The last condition comes from unitarity of the S-matrix elements [109, 110]. The coupling constants appeared in above expressions are evaluated at the electroweak scale, $v_{\rm SM}$. Also, in order to avoid perturbative breakdown, all dimensionless couplings like quartic couplings (λ_i),

Yukawa couplings (Y^S_{ij}), gauge couplings (g_i) should obey the the perturbativity conditions:

$$|\lambda_i| < 4\pi, |Y_{ij}| < \sqrt{4\pi}, g_i < \sqrt{4\pi}, \tag{2.88}$$

where indices run over appropriate numbers according to the Lagrangian.

2.4.4 Charged Lepton Flavor Violation in Scotogenic Model

We can easily see that $\mathcal{L}^{\text{scotogenic}}_{\text{lepton}}$ explicitly breaks the global $U(1)_{\text{L}_{e,\mu,\tau}}$ symmetries, and hence, charged lepton flavor violations cannot be avoided in this model. Since the couplings, masses involved in this process are the same as the ones that generate light neutrino masses and play a role in DM relic abundance, we can no longer choose them arbitrarily. The branching fraction for $\mu \to e + \gamma$ that follows from this one-loop contribution can be written as [111],

$$\text{Br}(\mu \to e + \gamma) = \frac{3(4\pi)^3 \alpha_{\text{em}}}{4G_F^2} |A_D|^2 \text{Br}(\mu \to e + \nu_\mu + \bar{\nu_e}). \tag{2.89}$$

Where α_{em} is the electromagnetic fine structure constant, e is the electromagnetic coupling and G_F is the Fermi constant. A_D is the dipole form factor given by

$$A_D = \sum_{i=1}^{3} \frac{Y^*_{ie} Y_{i\mu}}{2(4\pi)^2} \frac{1}{m^2_\pm} \left(\frac{1 - 6\xi_i + 3\xi_i^2 + 2\xi_i^3 - 6\xi_i^2 log\xi_i}{6(1-\xi_i)^4} \right). \tag{2.90}$$

Here the parameter ξ_i's are defined as $\xi_i \equiv M^2_{N_i}/m^2_\pm$. The MEG experiment provides the most stringent upper limit on the branching ratio $\text{Br}(\mu \to e + \gamma) < 4.2 \times 10^{-13}$ [65]. For analytical expressions of other flavour violating processes can be seen in Ref. [111]. Current constraints of charged lepton flavor violation processes were summarized in Sec. 2 and we will take account this constraint in Sec 5.3.2.

Chapter 3

The Early Universe

This chapter is a review part related to the early Universe. In the past, our Universe is dense so that interactions between the SM particles sufficiently occur to maintain thermal equilibrium. Due to the cosmic expansion, the temperature of the Universe cools down, which leads to the interesting phenomena in the early Universe such as the dark matter production and cosmological phase transitions. As we will see that the DM relic abundance can be calculated by solving the Boltzmann equation on the expanding Universe. We study the dynamics of cosmological phase transitions by computing the effective potential on the thermal background for generic scalar field. We also discuss higher-order corrections from non-Abelian gauge field at finite-temperature field theory. Based on the thermal effective potential at one-loop order with high-temperature expansion, order of a phase transition will be clarified. Finally, formulae of GW signals generated by cosmological first-oder phase transitions are summarized.

3.1 Cosmic Expansion and Thermodynamics

In this subsection, we review standard history of the expanding Universe. In Sec. 3.1.1, we review standard cosmology. We derive the Friedmann equation and explain the expanding Universe. In Sec. 3.1.2, we summarize basic properties of the standard thermodynamics to understand the early Universe surrouding by the thermal plasma. In Sec. 3.1.3, we discuss thermal (chemical) equilibrium condition in the expanding Universe. We also calculate the change of the number density of particles by considering the Boltzmann equation with taking

into account cosmic expasion.

3.1.1 Expanding Universe

Our Universe is known to be approximately homogeneous and isotropic. Under this symmetries, the metric of our Universe can be written as

$$ds^2 = -dt^2 + a(t)^2 d\boldsymbol{x}^2, \tag{3.1}$$

where t, $a(t)$ and $\boldsymbol{x} = (x, y, z)$ are cosmic time, the scale factor and the three dimensional Cartesian coordinates, respectively. We have assumed spatially flat Universe, which is consistent with the present observation. A dynamics of the Universe is governed by the Einstein equation given by

$$R_{\mu\nu} - \frac{1}{2} g_{\mu\nu} R + g_{\mu\nu}\Lambda = 8\pi G T_{\mu\nu}, \tag{3.2}$$

where $g_{\mu\nu}$, $R_{\mu\nu}$, R, Λ and $T_{\mu\nu}$ are the metric given by Eq. (3.1), Ricci tensor, Ricci scalar, the cosmological constant and the energy-momentum tensor, respectively. $(0, 0)$ component of the above equation is given by

$$\mathrm{H}^2 = \frac{8\pi G}{3}\rho. \tag{3.3}$$

In this expression, $T_{00} = \rho$ is the energy density of the Universe and H is called *Hubble parameter* defined by

$$\mathrm{H} \equiv \frac{\dot{a}}{a}, \tag{3.4}$$

where dot represets the time derivative. The inverse of the Hubble parameter, H^{-1}, represents the characteristic time scale of the cosmic expansion and it roughly gives the age of the Universe. The value of the present Hubble parameter denoted by H_0 is given by [28] [1]

$$\mathrm{H}_0 = (70.5 \pm 1.3)\frac{\mathrm{km}}{\mathrm{sec} \times \mathrm{Mpc}} \tag{3.5}$$

This quantity is conventionally parameterized as follows:

$$\mathrm{H}_0 = h \times 100 \frac{\mathrm{km}}{\mathrm{sec} \times \mathrm{Mpc}}, \ h \equiv 0.705 \pm 0.013. \tag{3.6}$$

[1] The unit Mpc is often used in the context of the astrophysics. Note that $1\,\mathrm{Mpc} \simeq 3.1 \times 10^{24}\,\mathrm{cm}$.

In order to realize homogenous and isotropic metric Eq. (3.1), the energy-momentum tensor $T_{\mu\nu}$, which is the right-hand side of the Einstein equation Eq. (3.2), should possess same symmetries. This implies that $T_{\mu\nu}$ should be diagonal and all spatial components should be equal. The simplest example, which satisfies this condition, is the energy momentum-tensor of the perfect fluid. It is given by

$$T_{\mu\nu} = \mathrm{diag}(\rho, p, p, p), \tag{3.7}$$

where p is the pressure of the perfect fluid. $\mu = 0$ component of the conservation of the energy momentum tensor $\nabla_\mu T^{\mu\nu} = 0$, where ∇_μ is the covariant derivative with respect to $g_{\mu\nu}$, leads to the following relation

$$\dot{\rho} + 3\mathrm{H}(\rho + p) = 0. \tag{3.8}$$

For given equation of state: $\rho = wp$, where the value of w depends on species of matter, the energy density evolves as

$$\rho \propto a^{-3(1+w)}. \tag{3.9}$$

Here, we have assumed that w does not depend on cosmic time t. By using the Friedmann equation Eq. (3.3), dependence of the energy density and the scale factor in terms of cosmic time are summarized as follows:

$$\begin{aligned}
&\text{Radiation domination}: \ w = \frac{1}{3}, \ \rho \propto a(t)^{-4}, \ a(t) \propto t^{\frac{1}{2}}, \\
&\text{Matter domination}: \ w = 0, \ \rho \propto a(t)^{-3}, a(t) \propto t^{\frac{2}{3}}, \\
&\text{Vacuum domination}: \ w = -1, \ \rho \propto \text{const}, \ a(t) \propto e^{Ht}.
\end{aligned} \tag{3.10}$$

In reality, energy density of our Universe is composed of the relativistic matter such as the photon and the neutrinos, the non-relativistic matter such as baryons and the DM, and the vacuum energy (or the dark energy). Hence, time evolution of our real Universe is governed by the Friedmann equation, where all energy densities are included. It is given by

$$\mathrm{H}^2 = \frac{8\pi}{3} G \rho_{\mathrm{tot}}, \tag{3.11}$$

where ρ_{tot} is the total energy density of the Universe defined by $\rho_{\mathrm{tot}} \equiv \rho_{\mathrm{rad}} + \rho_{\mathrm{matter}} + \rho_\Lambda$. G is the Newton constant. Here, ρ_{rad}, ρ_{matter} and ρ_Λ are the energy densities of the radiation,

non-relativistic matter and the vacuum energy. We introduce the critical density ρ_c, which is defined by

$$\rho_c \equiv \frac{3}{8\pi G}\mathrm{H}_0^2, \tag{3.12}$$

In other word, ρ_c is sum of the energy densities of the current Universe, $\rho_c = \rho_{\mathrm{rad},0} + \rho_{\mathrm{matter},0} + \rho_{\Lambda,0}$, where $\rho_{\mathrm{rad},0}$, $\rho_{\mathrm{matter},0}$ and $\rho_{\Lambda,0}$ are the present energy densities of the radiation, non-relativistic matter and the vacuum energy. Numerically, $\rho_c = 1.05 \times h^2 \times 10^{-5}\,\mathrm{GeV/cm^3}$. We also introduce cosmological parameters defined by

$$\Omega_{\mathrm{rad}} \equiv \frac{\rho_{\mathrm{rad},0}}{\rho_c},\ \Omega_{\mathrm{matter}} \equiv \frac{\rho_{\mathrm{matter},0}}{\rho_c},\ \Omega_\Lambda \equiv \frac{\rho_{\Lambda,0}}{\rho_c} \tag{3.13}$$

By definitions, $\sum_i \Omega_i = 1$. There are several independent observations to determine these cosmological parameters. Current values are summarized as [28]

$$\Omega_{\mathrm{rad}} \leq 10^{-4},\ \Omega_{\mathrm{matter}} \simeq 0.27,\ \Omega_{\mathrm{DM}} \simeq 0.73. \tag{3.14}$$

In particular, the present energy density of the non-relativistic component Ω_{matter} can be further decomposed into energy densities of baryon and the DM as follows.

$$\Omega_{\mathrm{matter}} = \Omega_{\mathrm{baryon}} + \Omega_{\mathrm{DM}}, \tag{3.15}$$

where $\Omega_{\mathrm{baryon}} \equiv \rho_{\mathrm{baryon}}/\rho_c$ and $\Omega_{\mathrm{DM}} \equiv \rho_{\mathrm{DM}}/\rho_c$ with ρ_{baryon} and ρ_{DM} being present energy densities of the baryon and the DM. These values are summarized as [28]

$$\Omega_{\mathrm{baryon}} \simeq 0.046,\ \Omega_{\mathrm{DM}} \simeq 0.23. \tag{3.16}$$

Strictly speaking, Ω_{matter} includes the contribution from lepton such as the electron and the (massive) neutrino. However, these contributions to Ω_{matter} is vanishingly small and is negligible amount.

By using cosmological parameters Ω_{rad}, Ω_{matter} and Ω_Λ, the Friedmann equation Eq. (3.11) becomes

$$\mathrm{H}^2 = \frac{8\pi G}{3}\rho_c \left(\Omega_{\mathrm{rad}}\left(\frac{a_0}{a}\right)^4 + \Omega_{\mathrm{matter}}\left(\frac{a_0}{a}\right)^3 + \Omega_\Lambda\right), \tag{3.17}$$

where a_0 is the scale factor at the present time. We have used Eq. (3.10) to derive the above equation.

In the present epoch $a(t) = a_0$, it is obvious that the cosmic expansion is mainly governed by the non-relativistic matter $\Omega_{\rm matter}$ and the vacuum energy Ω_Λ because $\Omega_{\rm matter}, \Omega_\Lambda \gg \Omega_{\rm rad}$. However, in the past, since the scale factor, $a(t)$, is very small so that the first term of the right-hand side of the Friedmann equation is dominated. This epoch is called radiation domination era. As scale factor $a(t)$ grows due to the cosmic expansion, the radiation component becomes vanishingly small and the second term of the right-hand side of the Friedmann equation dominates the Universe. This epoch is called the matter domination era. Eventually, the last term of the right hand-side of the Friedmann equation dominates the Universe.

In this thesis, we only consider cosmological phenomena occurred in the radiation domination era, and thus, we only review basic cosmology at this epoch. In this epoch, the Universe was highly dense so that the SM particles are expected to be in thermal equilibrium via these interactions. This fact is strongly supported by the observation of the cosmic microwave background. Therefore, the standard thermodynamics plays a key role in the radiation domination era. We will also discuss the thermal equilibrium condition on the expanding Universe in Sec. 3.1.3 and argue that an (elementary) particle DM can be thermally produced in the early stage of the Universe.

3.1.2 Equilibrium Thermodynamics

In this subsection, we briefly review the standard thermodynamics to understand the basic feature of the radiation dominated Universe.

A number density, n, an energy density, ρ, and a pressure, p of weakly-interacting gas of particles are given in terms of its phase space distribution function $f(\boldsymbol{p})$ as

$$n^{\rm eq} = g \int \frac{d^3p}{(2\pi)^3} f^{\rm eq}(\boldsymbol{p}), \tag{3.18}$$

$$\rho = g \int \frac{d^3p}{(2\pi)^3} E(\boldsymbol{p}) f^{\rm eq}(\boldsymbol{p}), \tag{3.19}$$

$$p = g \int \frac{d^3p}{(2\pi)^3} \frac{|\boldsymbol{p}|^2}{3E} f^{\rm eq}(\boldsymbol{p}), \tag{3.20}$$

where $\boldsymbol{p}$, $E(\boldsymbol{p}) = \sqrt{\boldsymbol{p}^2 + m^2}$, m and g are the spatial momentum, energy, mass and internal degrees of freedom of particles, respectively. The phase space distribution $f^{\rm eq}(\boldsymbol{p})$ is explicitly

given by

$$f^{\rm eq}(\boldsymbol{p}) = \frac{1}{e^{\frac{E-\mu}{T}} \pm 1}, \tag{3.21}$$

where μ is the chemical potential. In the denominator, $+1$ corresponds to the Bose-Einstein spcies and -1 corresponds to the Fermi-Dirac species. In the relativistic limit $T \gg m$ and $T \gg \mu$, ρ, n and p are given by

$$\rho = \begin{cases} \frac{\pi^2}{30} g T^4 \\ \frac{7}{8}\frac{\pi^2}{30} g T^4 \end{cases}, \tag{3.22}$$

$$n^{\rm eq} = \begin{cases} \frac{\zeta(3)}{\pi^2} g T^4 \\ \frac{3}{4}\frac{\zeta(3)}{\pi^2} g T^4 \end{cases}, \tag{3.23}$$

$$p = \frac{\rho}{3}. \tag{3.24}$$

Here, $\zeta(3) \simeq 1.202$ is the Riemann zeta function of 3. In the non-relativistic limit $m \gg T$, n, ρ and p are given by

$$n^{\rm eq} = \left(\frac{mT}{2\pi}\right)^{\frac{3}{2}} e^{-(m-\mu)/T}, \tag{3.25}$$

$$\rho = mn, \tag{3.26}$$

$$p = nT. \tag{3.27}$$

Above expressions are same for Bose and Fermi species. Note that $p \gg \rho$ in this limit, and hence the equation of state of the non-relativistic particles is given by $p = 0$. A total energy density $\rho_{\rm R}$ and a total pressure p_R are given by the sum of all species:

$$\rho_R \equiv \sum_i n_i = \sum_i T^4 \left(\frac{T_i^4}{T^4}\right) \frac{g_i}{2\pi^2} \int_{x_i}^{\infty} dz \frac{\sqrt{z^2 - x_i^2} z^2}{e^{z-y_i} \pm 1}, \tag{3.28}$$

$$p_R \equiv \sum_i \rho_i = \sum_i T^4 \left(\frac{T_i^4}{T^4}\right) \frac{g_i}{6\pi^2} \int_{x_i}^{\infty} dz \frac{(z^2 - x_i^2)^{\frac{3}{2}}}{e^{z-y_i} \pm 1}, \tag{3.29}$$

$$x_i \equiv \frac{m_i}{T}, \ y_i \equiv \frac{\mu_i}{T}, \tag{3.30}$$

where i represents the species of particle and T_i is the temperature of ith particle, which can in principle be different from the photon temperature, T, which is defined as the temperature of the Universe. [2] From expressions given by Eq. (3.27), it is obvious that contributions from

[2]For example, after the SM neutrinos decoupling, its temperature is different from the photon temperature.

non-relativistic particles are suppressed by the Boltzmann factor and is negligible amount compared to these from relativistic particles. One can therefore simply neglect contributions from non-relativistic particles and only take into account relativistic components. Under this approximation, above expressions are significantly simplified as follows.

$$\rho_R \simeq \frac{\pi^2}{30} g_* T^4, \tag{3.31}$$

$$p_R \simeq \frac{\pi^2}{90} g_* T^4 = \frac{\rho_R}{3}. \tag{3.32}$$

Here, g_* is called *effective number of degrees of freedoms*, which is defined by

$$g_* \equiv \sum_{i \text{ Boson}} g_i \left(\frac{T_i}{T}\right)^4 + \sum_{i \text{ Fermion}} g_i \frac{7}{8} \left(\frac{T_i}{T}\right)^4. \tag{3.33}$$

The sum runs over only relativistic particles.

The entropy density, s, is also important physical quantity which characterizes the thermal equilibrium system. In the absence of the chemical potential, the entropy density can be expressed as

$$s = \frac{\rho + p}{T}. \tag{3.34}$$

The assumption of the vanishing chemical potential is justified in the next subsection. From the above expression, the entropy density of relativistic ith particle, s_i, is given by

$$s = \frac{4}{3}\frac{\rho_i}{T} \begin{cases} g_i \frac{2\pi^2}{45} T^3, \text{ (boson)} \\ g_i \frac{7}{8} g_i \frac{2\pi^2}{45} T^3, \text{ (fermion)} \end{cases} \tag{3.35}$$

Since the non-relativistic contribution to the entropy density is also Boltzmann suppressed and is vanishingly small, the total entropy density s_R is safely approximated as the summation of the relativistic species:

$$s_R = g_{*S} \frac{2\pi^2}{45} T^3, \tag{3.36}$$

where g_*^S is the effective number of degrees of freedoms for the entropy density defined by

$$g_{*S} \equiv \sum_{i \text{ Boson}} g_i \left(\frac{T_i}{T}\right)^3 + \sum_{i \text{ Fermion}} g_i \frac{7}{8} \left(\frac{T_i}{T}\right)^3. \tag{3.37}$$

The sum runs over only relativistic particles.

In the radiation dominated Universe, cosmological quantities such as the scale factor and the Hubble parameter are related to the cosmic temperature, and hence, it is useful to express these quantities in terms of the cosmic temperature. According to the second law of the standard thermodynamics, entropy density in any closed system increases, or it remains constant. For the cosmic expansion, entropy inside the co-moving volume $a(t)^3$ is invariant. Indeed, one obtains

$$\frac{d}{dt}\left(a^3(t)s\right) = a^3(t)\left(\dot{\rho} + 3\mathrm{H}(\rho + p)\right) = 0. \tag{3.38}$$

In this calculation, we have used the thermodynamical relation $ds = d\rho/T$ (in the absence of the chemical potential) and Eq. (3.34). The last equality comes from Eq. (3.8). Then the cosmic temperature relates to the scale factor as

$$T(t) \propto g_{S*}^{-\frac{1}{3}} a^{-1}. \tag{3.39}$$

This relation implies that the cosmic temperature inversely decreases by the cosmic expansion. Furthermore, by putting into the radiation energy density Eq. (3.31) into the Friedmann equation Eq, (3.3), the Hubble parameter during the radiation domination era can be expressed in terms of the cosmic temperature as

$$\mathrm{H}(T) = \frac{T^2}{M_{\mathrm{Pl}}^*}. \tag{3.40}$$

where M_{Pl}^* is the reduced Planck mass defined by

$$M_{\mathrm{Pl}}^* = \sqrt{\frac{90}{8\pi^3 g_*}} M_{\mathrm{Pl}} \simeq \frac{1}{1.66\sqrt{g_*}} M_{\mathrm{Pl}}. \tag{3.41}$$

3.1.3 Local equilibrium condition

So far, we assumed that the radiation dominated Universe is filled with various species of interacting particles, which are in thermal equilibrium. However, as we saw in the previous subsection, the temperature of the Universe cools down due to the cosmic expansion. Hence it is questionable whether thermal equilibrium is really realized in the past Universe, or not. In fact, departure of the thermal equilibrium occurs and leads to the interesting phenomena such as dark matter production and cosmological phase transitions as we will argue in next section. In this subsection, we discuss a local thermal equilibrium condition in the expanding Universe.

Suppose that for a given particle species X, there is a reaction

$$X + j + \cdots \to l + m + \cdots . \tag{3.42}$$

where $j, l, m, \cdots$ represent particles species. The characteristic time scale of this process, τ_X, is roughly given by

$$\frac{1}{\tau_X} = \left| \frac{1}{n_X} \frac{dn_X}{dt} \right| . \tag{3.43}$$

If τ_X is smaller than the characteristic time scale of the cosmic expansion, $\tau_X \lesssim \mathrm{H}^{-1}$, this process is sufficient to occur, and hence, X couples to the thermal plasma and is soon in thermal (chemical) equilibrium. In comparison to this, if $\tau_X \gtrsim \mathrm{H}^{-1}$ is realized, this process is decoupled from the thermal plasma, and hence, X becomes out-of-thermal equilibrium.

The Boltzmann Equation

Let us here more quantitatively discuss above statement. In the expanding Universe, the time evolution of the number density of X is governed by the following Boltzmann equation:

$$\begin{aligned} \frac{dn_X}{dt} + 3\mathrm{H}n_X = & \sum_{j,l,m,\cdots} \int d\Pi (2\pi)^4 \delta^{(4)} \left(\sum_i P_i \right) \\ & \times \Big[|\mathcal{M}|^2_{(l+m+\cdots \to X+j+\cdots)} f_l f_m (1 \pm f_X)(1 \pm f_j) \cdots \\ & - |\mathcal{M}|^2_{(X+j+\cdots \to l+m+\cdots)} f_X f_j (1 \pm f_l)(1 \pm f_m) \cdots \Big] , \end{aligned} \tag{3.44}$$

$(+ :$ for Boson, $-$: for Fermion).

In this expression, $d\Pi$ is the product of the phase space volume elements defined by

$$d\Pi \equiv d\Pi_X \times d\Pi_j \times \cdots \times d\Pi_l \times d\Pi_m \times \cdots , \tag{3.45}$$

$$d\Pi_j \equiv g_j \frac{1}{(2\pi)^3} \frac{d^3 p_j}{2E_j} . \tag{3.46}$$

Here, P_i is the four momentum and f_i is the phase space distribution of ith particle. $|\mathcal{M}|^2_{(l+m+\cdots \to X+j+\cdots)}$ and $|\mathcal{M}|^2_{(X+j+\cdots \to l+m+\cdots)}$ are the matrix element squared for the processes $l + m + \cdots \to X + j + \cdots$ and $X + j + \cdots \to l + m + \cdots$, which are averaged over initial and final spins, respectively. The summation $\sum_{j,l,m,\cdots}$ is taken over all interactions involving X particle. Physically, the left-hand side of the Boltzmann equation represents dilution of the number density by the cosmic expansion, while the right-hand side represent

the change of the number density by interactions with other particles. The above Boltzmann equations are a coupled set of integral differential equations for the phase space distributions of all the species present, which is in general impossible to solve these.

Fortunately, we can significantly simplify the complicated Boltzmann equation in the following way. Firstly, let assume that the interactions are CP (or T) invariants.[3] Under this assumption, the matrix element squared has following relation

$$|\mathcal{M}|^2_{(l+m+\cdots\to X+j+\cdots)} = |\mathcal{M}|^2_{(X+j+\cdots\to l+m+\cdots)} \equiv |\mathcal{M}|^2 . \tag{3.47}$$

Secondly, we assume that the kinetic equilibrium is maintained, and the distribution functions are approximated by the Maxwell-Boltzmann distribution. Thus, $f_j \simeq \exp(-(E_j - \mu_j)/T)$, and hence, $1 \pm f_j \simeq 1$. Under these approximations, the Boltzmann equations Eq. (3.44) can be rewritten as

$$\frac{dn_X}{dt} + 3\mathrm{H}n_X = \sum_{j,l,m,\cdots} \int d\Pi (2\pi)^4 |\mathcal{M}|^2 \delta^{(4)} \left(\sum_i P_i \right) [f_l f_m \cdots - f_X f_j \cdots] . \tag{3.48}$$

As an illustrate example, let us consider the following $2 \to 2$ process

$$X + \bar{X} \leftrightarrow j + \bar{j}. \tag{3.49}$$

Here, $\bar{X}$ and $\bar{j}$ are the anti-particles of X and j. j and $\bar{j}$ are relativistic ($T \gg m_j$) and are assumed to be in the thermal equilibrium. We also assume that this interaction is CP (or T) invariant and distribution function of j and $\bar{j}$ are approximated by the Maxwell-Boltzmann distribution function with zero chemical potential. Then the Boltzmann equation is given by

$$\frac{dn_X}{dt} + 3Hn_X = -\int d\Pi \, (2\pi)^4 \, \delta^{(4)} \left(P_X + P_{\bar{X}} + P_j + P_{\bar{j}} \right) |\mathcal{M}|^2_{X+\bar{X}\leftrightarrow j+\bar{j}} \left[f_X f_{\bar{X}} - f_j f_{\bar{j}} \right] . \tag{3.50}$$

From the energy conservation inside the delta function $E_X + E_{\bar{X}} = E_j + E_{\bar{j}}$, one obtains

$$f_j f_{\bar{j}} = e^{-(E_j + E_{\bar{j}})/T} = e^{-(E_X + E_{\bar{X}})/T} = f_X^{\mathrm{EQ}} f_{\bar{X}}^{\mathrm{EQ}}, \tag{3.51}$$

[3] In reality, CP symmetry is explicitly broken by the Cabbibo-Kobayashi-Masukawa matrix in the quark sector and PMNS matrix in the lepton sector, but these effects are very small. Hence it is sufficient to our purpose to assume this assumption.

since $f^{\rm EQ}_{X,\bar{X}} \equiv e^{-E_{X,\bar{X}}/T}$. By introducing a thermally-averaged cross section times velocity of the process given by Eq. (3.49) defined by

$$\langle \sigma_{X+\bar{X}\to j+\bar{j}}|v|\rangle \equiv \frac{1}{(n^{\rm eq}_X)^2}\int d\Pi\, |\mathcal{M}|^2_{X+\bar{X}\to j+\bar{j}}\,(2\pi)^4\delta^{(4)}(P_X+P_{\bar{X}}+P_j+P_{\bar{j}})f^{\rm eq}_X f^{\rm eq}_{\bar{X}}, \tag{3.52}$$

the Boltzmann equation Eq. (3.50) can be then rearranged as following simple form

$$\frac{dn_X}{dt}+3{\rm H}n_X = -\langle \sigma_{X+\bar{X}\to j+\bar{j}}|v|\rangle\left[n_X^2-(n^{\rm eq}_X)^2\right]. \tag{3.53}$$

From this expression, the reaction rate Γ_X (or the characteristic time scale defined by Eq. (3.43)) can be expressed as

$$\Gamma_X = \frac{1}{\tau_X} \simeq \langle \sigma_{X+\bar{X}\to j+\bar{j}}|v|\rangle n^{\rm eq}_X. \tag{3.54}$$

At $\Gamma_X > {\rm H}$, the particle number changing process by annihilation corresponding to the right-hand side of the Eq. (3.53), is dominant compared to its dilution by the cosmic expansion, and thus, n_X eventually reach to its equilibrium value $n_X \simeq n^{\rm eq}_X$. On the other hand, at $\Gamma_X < {\rm H}$, the right-hand side of Eq. (3.53) becomes negligible compared to its second term and is decoupled with the thermal plasma. Thus, the number density in co-moving volume (expanding volume), $n_X a^3$, becomes effectively constant at $\Gamma_X = {\rm H}$. The temperature, T_f, which satisfies $\Gamma_X(T_f) = {\rm H}(T_f)$ is therefore called freeze-out temperature.

Chemical potentials in the early Universe

Before closing this subsection, let us confirm the validity of the assumption of vanishing chemical potential for several species $\mu_i \simeq 0$. When the reaction Eq. (3.42) is in thermal equilibrium, chemical potentials obey following equation:

$$\mu_X + \mu_j + \cdots = \mu_l + \mu_m + \cdots . \tag{3.55}$$

Here, μ_J is the chemical potential of particle species of $J = X, j, l, m \cdots$. The photon interact with the electron via the inelastic scattering such as

$$e + \gamma \leftrightarrow e + \gamma + \gamma. \tag{3.56}$$

This leads to zero photon chemical potential, $\mu_\gamma = 0$. Then, annihilations into photons $X + \bar{X} \leftrightarrow 2\gamma$ gives $\mu_X + \mu_{\bar{X}} = 0$. Here, X can be charged leptons and quarks. This implies

chemical potentials of particles and these anti-particles are same magnitude but opposite sign. By using this fact, a number density difference between X particle and $\bar{X}$ can be expressed as

$$n_X - n_{\bar{X}} \simeq \begin{cases} \mu_X T^2/3 \text{ (Bosons)} \\ \mu_X T^2/6 \text{ (Fermions)} \end{cases} . \tag{3.57}$$

To derive above expressions, we have assumed $T \gg m_X, \mu_X$ and used Eq (3.18) and Eq. (3.21). The above expression tell us that the chemical potential parameterizes the number density difference between particle and its anti-particle.

Hence if there is a large amount of the particle asymmetry in the early Universe, effects of chemical potentials are important. It is widely known that a success of the Big Bang Nucleosynthesis requires the tiny baryon asymmetry $n_B - n_{\bar{B}}/s \sim 10^{-10}$ (n_B and $n_{\bar{B}}$: baryon and anti-baryon number densities), and hence, there exists non-zero chemical potential for baryons, but its value is many order magnitude below of the temperature and is negligible amount. Since the Universe is electromagnetically neutral, a lepton asymmetry is same order magnitude of baryon asymmetry. Therefore, the chemical potential of the lepton is also vanishingly small. For this reason, chemical potentials are safely neglected in the standard cosmology.

3.2 Thermal Production of the Dark Matter in Scotogenic Model

It was discussed in Sec. 2.4 that there are DM candidates in minimal scotogenic model, which is the lightest Z_2 odd particle. In this section, we give a basic formalism to calculate the relic abundance of the DM.

We here assume that the temperature of the early Universe is high enough to these Z_2 odd particles are in thermal equilibrium with the SM particles.[4] Then the number density

[4]Since ν_{1R} is a gauge singlet, there exists the possibility of non-thermal fermion DM also in this model, as discussed by the authors of Ref. [45]. While the scalar DM can not be a purely non-thermal DM due to its gauge interactions, it can receive a non-thermal contribution from right handed neutrino decay at late epochs. This possibility was discussed by [42]. We do not discuss such possibilities in this thesis, as it is unlikely to give new insights into the correlation between DM parameter space and that of strong first-order

of the DM particle is given by thermal equilibrium value before the decoupling. As the temperature of the Universe cools down due to the cosmic expansion, the local thermal equilibrium condition is not satisfied when $\Gamma_{\rm DM} = {\rm H}$, where $\Gamma_{\rm DM}$ is the reaction rate of the DM annihilation into SM particles, ${\rm DM} + {\rm DM} \leftrightarrow {\rm SM} + {\rm SM}$. Then, as stated in the previous section around Eq. (3.54), the DM number density becomes constant in co-moving volume and its thermal relic contributes to the DM energy density of the present Universe. In the present setup, we can discuss the conditions (iii) and (iv) listed in Sec. 2.2.3. The condition (iii) is satisfied in this production mechanism because the DM will be decoupled when it is non-relativistic. To satisfy condition (iv), we need to carefully calculate the relic abundance of the DM number density by solving Boltzmann equation for given coupling constants $\lambda_{1,2}$ and λ_3, which were defined in the Lagrangian density of minimal scotogenic model defined in Sec. 2.4.

The Boltzmann equation of this reaction can be written as

$$\frac{dn_{\rm DM}}{dt} + 3Hn_{\rm DM} \;=\; -\langle\sigma v\rangle \left[n_{\rm DM}^2 - (n_{\rm DM}^{\rm eq})^2\right], \tag{3.58}$$

where $n_{\rm DM}$ and $n_{\rm DM}^{\rm eq}$ are the number density and the thermal equilibrium number density of DM, respectively. $\langle\sigma v\rangle$ is the thermally averaged annihilation cross section, which is explicitly given by [112]

$$\langle\sigma v\rangle \;=\; \frac{1}{8m_{\rm DM}^4 T K_2^2\left(\frac{m_{\rm DM}}{T}\right)} \int_{4m_{\rm DM}^2}^{\infty} \sigma(s - 4m_{\rm DM}^2)\sqrt{s}\, K_1\left(\frac{\sqrt{s}}{T}\right) ds\,, \tag{3.59}$$

where $K_i(x)$'s are modified Bessel functions of order i and $m_{\rm DM}$ is the DM mass.

In the presence of coannihilations, the effective cross section at freeze-out can be expressed as [113]

$$\sigma_{\rm eff} \;=\; \sum_{i,j} \langle\sigma_{ij} v\rangle \frac{g_i g_j}{g_{\rm eff}^2} (1+\Delta_i)^{3/2} (1+\Delta_j)^{3/2} e^{-z_f(\Delta_i+\Delta_j)}\,, \tag{3.60}$$

where $\Delta_i = \frac{m_i - m_{\rm DM}}{m_{\rm DM}}$ is the relative mass difference between the heavier component $i = (H, A, \pm, \nu_{1R})$ of the inert Higgs doublet and the DM.

$$g_{\rm eff} \;=\; \sum_i g_i (1+\Delta_i)^{3/2} e^{-z_f \Delta_i}, \tag{3.61}$$

phase transition.

is the total effective degrees of freedom, and

$$\langle \sigma_{ij} v \rangle = \frac{z_f}{8 m_i^2 m_j^2 m_{\rm DM} K_2\left(\frac{m_i z_f}{m_{\rm DM}}\right) K_2\left(\frac{m_j z_f}{m_{\rm DM}}\right)} \times \int_{(m_i+m_j)^2}^{\infty} ds\, \sigma_{ij} \left(s - 2(m_i^2 + m_j^2)\right) \sqrt{s}\, K_1\left(\frac{\sqrt{s}\, z_f}{m_{\rm DM}}\right), \tag{3.62}$$

is the modified thermally averaged cross section, compared to equation (3.59). In the above expressions

$$z_f \equiv \frac{m_{\rm DM}}{T_f} = \ln\left(0.038 \frac{g}{\sqrt{g_*}} M_{\rm Pl} m_{\rm DM} \langle \sigma v \rangle_f\right), \tag{3.63}$$

with g being the number of internal degrees of freedom of the DM and the subscript f on $\langle \sigma v \rangle_f$ means that the quantity is evaluated at the freeze-out temperature T_f. For solving the Boltzmann equations relevant to DM, `micrOMEGAs` package [114] is used.

3.3 The Effective Potential

We have discussed the local equilibrium condition and decoupling of particles in the early Universe. In this section, we discuss thermal effects on the generic scalar potential. Then the idea of the thermal effective potential plays the key role, and hence we briefly review them at first. We refer papers Refs. [115, 116, 117] for more details. Detailed computations of one-loop effective potential are summarized in Appendix. 7.1.

3.3.1 Definition of the Thermal Effective Potential

At sufficiently high temperature, the radiation dominated Universe is surrounding by the thermal plasma. Hence when we compute a scalar potential at that epoch, effects of thermal fluctuations should be taken into account. The main purpose of this section to introduce field theory on the thermal background, which is called *imaginary time formalism* or *Matsubara formalism* [118].

On the thermal background, an expectation value of a generic operator $\hat{\mathcal{O}}$ is described by the canonical ensemble:

$$\langle \hat{\mathcal{O}} \rangle \equiv \frac{{\rm Tr}[\hat{\rho}\hat{\mathcal{O}}]}{{\rm Tr}\hat{\rho}}, \tag{3.64}$$

where $\hat{\rho}$ is the canonical density operator given by

$$\hat{\rho} \equiv \exp^{-\hat{H}/T} . \tag{3.65}$$

In this expression, $\hat{H}$ is a Hamiltonian of a system. We neglect a contribution from chemical potential since it was discussed in Sec. 3.1.3 that it is vanishingly small in our Universe.

We shall next derive the potential of given scalar field $\varphi(x)$:

$$\varphi(x) = e^{i\hat{H}t}\varphi(0,\mathbf{x})e^{-i\hat{H}t}. \tag{3.66}$$

In this expression, the time $t \equiv x^0$ is analytically continued to the complex-plane. In particular, throughout this thesis, we consider the "imaginary time" $t = -i\tau$, where τ is the real valued, and hence, the time t becomes purely imaginary number. The thermal Green function is defined as the canonical average of the ordered product of the n field operators:

$$G^{(c)}(x_1, \ \cdots, \ x_n) = \langle \mathrm{T_c}\varphi(x_1), \ \cdots \varphi(x_n)\rangle, \tag{3.67}$$

In this expression, $\mathrm{T_c}$ ordering. Its definition is explicitly given by

$$\mathrm{T_c}\varphi(x)\varphi(y) = \theta_c(x^0 - y^0)\varphi(x)\varphi(y) + \theta_c(y^0 - x^0)\varphi(y)\varphi(x). \tag{3.68}$$

where $\theta_c(t) = \theta(\tau)$. ($\theta(x)$: step function and τ is a real number.) Then, the generating functional $Z^\beta[J]$ in the presence of the exteral source $J(x)$ can be defined as

$$Z^\beta[J] = \left\langle \mathrm{T_c} \exp\left(i\int_c d^4x J(x)\varphi(x)\right)\right\rangle \tag{3.69}$$

$$= \sum_{n=0}^{\infty} \frac{i^n}{n!}\int_c d^4x_1 \cdots d^4x_n J(x_1)\cdots J(x_n)G^{(c)}(x_1 \cdots x_n). \tag{3.70}$$

The connected green function $W^\beta[J]$ is given by

$$Z^\beta[J] = \exp(iW^\beta[J]). \tag{3.71}$$

Then the effective action is obtained by the Legendre transformation with respect to W^β:

$$\Gamma^\beta[\phi] = W^\beta[J] - \int d^4x \frac{\delta W^\beta[J]}{\delta J(x)} J(x). \tag{3.72}$$

The effective action $\Gamma^\beta[\phi]$ can be explicitly calculated by computing one particle irreducible diagrams [119]. Here, ϕ is given by

$$\phi(x) \equiv \frac{\delta W^\beta}{\delta J(x)}. \tag{3.73}$$

It follows that

$$\frac{\delta\Gamma^{\beta}}{\delta\phi(x)} = J(x), \tag{3.74}$$

and hence, $\Gamma^{\beta}[\varphi]$ can be identified with the action on the thermal background in the absence of the external source. When $\varphi(x)$ possesses a translational invariance, $\phi(x) = \phi$, $\Gamma^{\beta}[\phi]$ can be expressed as

$$\Gamma^{\beta}[\phi] = -\int d^4x V^{\rm tot}_{\rm thermal}(\phi). \tag{3.75}$$

where $V^{\rm tot}_{\rm thermal}$ is called *thermal effective potential*. Then, an expectation value of ϕ is described by the condition

$$\frac{\partial V^{\rm tot}_{\rm thermal}}{\partial\phi} = 0. \tag{3.76}$$

This implies that the effective potential characterizes locations of vacua for a given theory (Lagrangian density) including quantum and thermal effects.

Explicit calculations of the thermal effective potential at one-loop order involving scalar, fermion and gauge bosons are summarized in Appendix. 7.1. In any case, we will see that the thermal effective potential is characterized by a field dependent mass $m_i(\phi)$ where suffix i represent the particle species, which couples to ϕ. The precise form of $m_i(\phi)$ is calculated by given Lagrangian density, but it is usually given by $m_i^2(\phi) = c_i\phi^2 + M_i^2$ where c_i and M_i is the ϕ-independent constants. In the following discussion, to discuss general features of the thermal effective potential for given field dependent masses, we do not specify the concrete Lagrangian density.

A contribution from bosonic particles can be expressed as

$$\begin{aligned} V^{\rm B}_{\rm thermal}(\phi) &= \sum_i n_{{\rm B}_i}\frac{T}{2}\sum_{n_{\rm b}=-\infty}^{+\infty}\int\frac{d^3p}{(2\pi)^3}\log(\omega_{n_{\rm b}}^2 + \omega_i^2(\phi)),\ \omega_{n_{\rm b}} = 2\pi n_{\rm b}T, \\ \omega_i^2(\phi) &= \boldsymbol{p}^2 + m_i^2(\phi), \end{aligned} \tag{3.77}$$

where $n_{{\rm B}_i}$ and $\mathbf{p}$ are the number of degrees of freedom of a bosonic particle species i and three dimensional momentum, respectively. By using

$$f(y) \equiv \sum_{n=0}^{\infty}\frac{y}{y^2+n^2} = -\frac{1}{2y} + \frac{\pi}{2} + \pi\frac{e^{-2\pi y}}{1-e^{-2\pi y}},\ (y:\text{constant}). \tag{3.78}$$

we obtain

$$\sum_{n_{\rm b}=-\infty}^{\infty} \log\left(\omega_{n_{\rm b}}^2 + \omega_i^2(\phi)\right) = \frac{2}{T}\left(\frac{\omega_i(\phi)}{2} + T\log\left(1 - e^{-\omega_i(\phi)/T}\right)\right). \tag{3.79}$$

Therefore, $V_{\rm thermal}^{\rm B}$ can be expressed as

$$V_{\rm thermal}^{\rm B}(\phi) = \sum_i n_{{\rm B}_i} \int \frac{d^3p}{(2\pi)^3}\left(\frac{\omega_i(\phi)}{2} + T\log\left(1 - e^{-\omega_i(\phi)/T}\right)\right). \tag{3.80}$$

A contribution from fermionic particles is given by

$$V_{\rm thermal}^{\rm F}(\phi) = -\sum_i n_{{\rm F}_i}\frac{T}{2}\sum_{n_{\rm f}=-\infty}^{\infty}\int\frac{d^3p}{(2\pi)^3}\log\left(\omega_n^2 + \omega_i^2(\phi)\right),\ \omega_{n_{\rm f}} = (2n_{\rm f}+1)\pi T,$$
$$\omega_i^2(\phi) = \boldsymbol{p}^2 + m_i^2(\phi), \tag{3.81}$$

where $n_{{\rm F}_i}$ is the number of degrees of freedom of a fermionic particle species i. By using

$$\sum_{m=2,4,\cdots}^{\infty}\frac{y}{y^2+m^2} = \sum_{n=1,2,\cdots}^{\infty}\frac{y}{y^2+4n^2} = \frac{1}{2}f\left(\frac{y}{2}\right), \tag{3.82}$$

$$\sum_{m=1,3,\cdots}^{\infty}\frac{y}{y^2+m^2} = f(y) - \frac{1}{2}f\left(\frac{y}{2}\right), \tag{3.83}$$

we obtain

$$\sum_{n_{\rm f}=-\infty}^{\infty}\log\left(\omega_{n_{\rm f}}^2 + \omega_i^2(\phi)\right) = \frac{2}{T}\left(\frac{\omega_i(\phi)}{2} + \log\left(1 + e^{-\omega_i(\phi)/T}\right)\right). \tag{3.84}$$

Therefore, $V_{\rm thermal}^{\rm F}$ can be expressed as

$$V_{\rm thermal}^{\rm F} = -\sum_i n_{{\rm F}_i}\int\frac{d^3p}{(2\pi)^3}\left(\frac{\omega_i(\phi)}{2} + T\log\left(1 + e^{-\omega_i(\phi)/T}\right)\right). \tag{3.85}$$

The one-loop total thermal effective potential is then given by $V_{\rm thermal}^{\rm total} = V_{\rm tree} + V_{\rm thermal}^{\rm B} + V_{\rm thermal}^{\rm F}$, where $V_{\rm tree}$ is the tree-level potential of given Lagrangian density. One should note that the first terms of Eqs. (3.80) and (3.85) correspond to the zero-temperature corrections, while the second terms correspond to the finite-temprature corrections. For zero-temperature corrections, the momentum integration leads to the UV divergence, which is regulated by imposing suitable renormalization conditions. For thermal corrections corresponding to the second terms of Eqs. (3.80) and (3.85), the momentum integration larger than the ambient temperature is exponentially suppressed by the Boltzmann factor, and hence, there is no UV divergence. Since two contributions are totally different, we will separately consider these contributions in different subsections.

3.3.2 The effective potential at zero-temperature

In this subsection, we calculate the zero-temperature contribution of the effective potential by imposing renormalization conditions. In the following discussion, we consider generic field dependent mass of particle species i and do not specify the concrete form of the Lagrangian density.

The zero-temperature effective potential from bosonic and fermionic particles, $V_{\rm zero}(\phi)$, can be rearranged as follows.

$$V_{\rm zero}(\phi) = \sum_i (-)^i \frac{n_i}{2} \int \frac{d^4p}{(2\pi)^4} \log\left(\boldsymbol{p}^2 + m_i(\phi)^2\right), \tag{3.86}$$

In this expression, n_i is the number of degrees of freedom of a particle i, and $(-)^i$ gives 1 for bosons and -1 for fermions.

Let us first insert a hard cut-off $\Lambda_{\rm UV}$ in the momentum integration to regularize it. The result is given by

$$V_{\rm zero}^{\rm cut-off}(\phi) = \sum_i (-)^i n_i \left[\frac{1}{32\pi^2}\Lambda_{\rm UV}^2 m_i^2(\phi) + \frac{m_i^4(\phi)}{64\pi^2}\left(\log\left(\frac{m_i^2(\phi)}{\Lambda_{\rm UV}^2}\right) - \frac{1}{2}\right)\right]. \tag{3.87}$$

Divergences caused by $\Lambda_{\rm UV} \to \infty$ should be subtracted by counterterms. This expression is useful when we consider the cut-off dependence for the scalar field ϕ. For example, quadratic divergent mass corrections to the SM Higgs mass parameter Eq. (2.34) can be easily computed when we use the above expression.

Let us next adopt the $\overline{\rm DR}$ regularization method. In this regularization scheme, the momentum integration is defined in spacetime dimension, $D \equiv 4-2\epsilon$, where ϵ is the infinitesimal parameter. Then, Eq. (3.86), can be rewritten as

$$V_{\rm zero}^{\rm dim}(\phi) = \sum_i (-)^i \frac{n_i}{2} \mu^\epsilon \int \frac{d^Dp}{(2\pi)^D} \log\left(\boldsymbol{p}^2 + m_i^2(\phi)\right). \tag{3.88}$$

In this expression, we introduce renormalization scale μ to maintain the mass dimension of effective potential, $\dim[V_{\rm zero}] = 4$. By doing the integration of eq. (3.88), we obtain

$$V_{\rm zero}^{\rm dim}(\phi) = \sum_i (-)^i n_i \frac{m_i(\phi)}{64\pi^2}\left(C_{\rm UV} + \log\left(\frac{m^2(\phi)}{\mu^2}\right) - \frac{3}{2} + \mathcal{O}(\epsilon)\right), \tag{3.89}$$

$$C_{\rm UV} = \frac{1}{\epsilon} - \gamma_E + \log(4\pi), \tag{3.90}$$

where γ_E is the Euler constant. At $\epsilon \to 0$, the first term in the above expression contains divergence, which should be subtracted by the counterterm. By subtracting the UV divergent part $C_{\rm UV}$, the zero-temperature effective potential is given by

$$V_{\rm zero}^{\overline{\rm DR}}(\phi) = \sum_i (-)^{F_i} \frac{n_i}{64\pi^2} m_i^4(\phi) \left(\log \left(\frac{m_i^2(\phi)}{\mu^2} \right) - \frac{3}{2} \right). \tag{3.91}$$

Note that in the above expression all coupling constants should be evaluated at the scale μ, otherwise one-loop expansion cannot be justified.

In another famous renormalization scheme with dimensional regularization so-called $\overline{\rm MS}$ scheme, Then the zero-temperature effective potential is given by

$$V_{\rm zero}^{\overline{\rm MS}}(\phi) = \sum_i (-)^{F_i} \frac{n_i}{64\pi^2} m_i^4(\phi) \left(\log \left(\frac{m_i^2(\phi)}{\mu^2} \right) - C_i \right). \tag{3.92}$$

In this expression, C_i is given by

$$C_i = \begin{cases} \frac{3}{2}, & \text{(for bosons and fermions)}, \\ \frac{5}{6}, & \text{(gauge bosons)}. \end{cases} \tag{3.93}$$

3.3.3 The thermal effective potential

In this subsection, we shall calculate the thermal effective potential for given field dependent masses. We also discuss validity of the one-loop approximation and explain resummation presriptions, which are important in the finite temperature field theory.

Thermal contributions to the effective potential at one-loop order are given by the second terms of Eqs. (3.80) and (3.85), which can be rewritten as

$$V_{\rm thermal} = \sum_i \left(\frac{n_{{\rm B}i} T^4}{2\pi^2} J_B \left[\frac{m_{Bi}^2(\phi)}{T^2} \right] - \frac{n_{{\rm F}i} T^4}{2\pi^2} J_F \left[\frac{m_{Fi}^2(\phi)}{T^2} \right] \right), \tag{3.94}$$

$$J_B(x) = \int_0^\infty dz z^2 \log \left(1 - e^{-\sqrt{z^2+x}} \right), \tag{3.95}$$

$$J_F(x) = \int_0^\infty dz z^2 \log \left(1 + e^{-\sqrt{z^2+x}} \right), \tag{3.96}$$

where i runs the particle species and the suffixes B and F represent Boson and Fermion contributions, respectively.

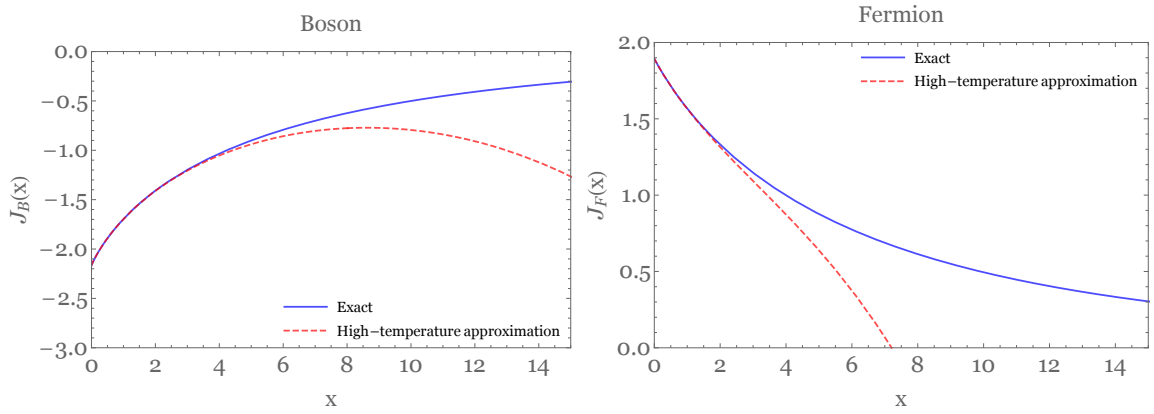

Figure 3.1: $J_B(x)$ (the right panel) and $J_F(x)$ (the right panel) functions with (the red dotted curve) and without (the blue curve) using high-temperature approximations are shown.

At $x < 1$ corresponding to the high-temperature regime $m_{B_i,F_i}(\phi)/T < 1$, $J_{B,F}(x)$-functions can be approximated by

$$J_B(x) \simeq -\frac{\pi^4}{45} + \frac{\pi^2}{12}x - \frac{\pi}{6}x^{\frac{3}{2}} - \frac{x^2}{32}\log\left(\frac{x}{a_b}\right), \tag{3.97}$$

$$J_F(x) \simeq \frac{7\pi^4}{360} - \frac{\pi^2}{24}x - \frac{x^2}{32}\log\left(\frac{x}{a_f}\right), \tag{3.98}$$

where

$$a_b = 16\pi^2 \exp\left[\frac{3}{2} - 2\gamma_E\right], \quad a_f = \pi^2 \exp\left[\frac{3}{2} - 2\gamma_E\right]. \tag{3.99}$$

In this expression, $\gamma_E \simeq 0.5772$ is the Euler constant.

Fig. 3.1 shows the $J_{B,F}(x)$-functions with and without using high-temperature approximations. It is obvious from this figure that the high-temperature approximation can be justified for $x \lesssim 4$ for $J_B(x)$ and $x \lesssim 1.5$ for $J_F(x)$. For larger x, both functions are exponentially suppressed by the Boltzmann factor $\sim e^{-\sqrt{x}}$, and hence, the high-temperature approximation cannot be justified.

Here, we qualitatively discuss general features of $J_{B,F}$-functions. Concretely, let us consider a following Lagrangian density:

$$\mathcal{L}^{\text{example}} = \frac{1}{2}\partial_\mu\phi\partial^\mu\phi + \frac{1}{2}\partial_\mu\chi\partial^\mu\chi - \frac{M^2}{2}\chi^2 - \frac{\kappa}{2}\phi^2\chi^2, \tag{3.100}$$

where ϕ and χ are scalar fields and M^2, κ are the mass of χ fields and the coupling constant of these particles, respectively. A field dependent mass for ϕ field is then given by $m^2(\phi) =$

$\kappa\phi^2 + M^2$. First of all, if $\kappa \ll 1$, this particle very weakly couple to ϕ, and thus, thermal corrections as well as the quantum corrections give negligible effect. For $M > T$, this contribution is suppressed by the exponential suppression and is negligible amount even if κ is large. Furthermore, the thermal correction is also suppressed at a large field value $\kappa\phi^2 > T^2$ for $M^2 = 0$. These facts imply that thermal corrections are important only when ϕ strongly couples to the fields whose masses are not larger than the temperature. This statement plays an important role when we qualitatively discuss a strength of a phase transition. For example, if we consider the electroweak scale or TeV scale cosmic temperature, contributions from particles having masses order of Planck scale or the grand unification scale can be safely neglected.

Let us next discuss a difference between thermal contributions from bosons and fermions. It is apparent that the third term of Eq. (3.97) is absent in Eq. (3.98). To consider the origin of this difference, let us back to the original expressions of $V^{\rm B}_{\rm thermal}$ and $V^{\rm F}_{\rm thermal}$ given by Eq. (3.85) and Eq. (3.80), respectively. We can easily see that bosonic particles contain Matsubara zero-mode, $n_{\rm b} = 0$, while fermionic particles do not, due to the different boundary conditions. The bosonic zero-mode contribution is given by

$$V^{\rm B}_{\rm zero-mode} = \sum_i n_{{\rm B}_i} \frac{T}{2} \int \frac{d^3p}{(2\pi)^3} \log\left(\boldsymbol{p}^2 + m_i^2(\phi)\right). \tag{3.101}$$

By taking the derivative with respect to ϕ, we obtain

$$\begin{aligned}\frac{dV^{\rm B}_{\rm zero-mode}}{d\phi} &= \sum_i n_{{\rm B}_i} T m_i(\phi) \frac{dm_i(\phi)}{d\phi} \int \frac{d^3p}{(2\pi)^3} \frac{1}{\mathbf{p}^2 + m_i^2(\phi)} \\ &= \sum_i n_{\rm B_i} T m_i(\phi) \frac{dm_i(\phi)}{d\phi} \frac{1}{2\pi^2} \left(\Lambda_{\rm UV} - m_i(\phi) \arctan\left(\frac{\Lambda_{\rm UV}}{m_i(\phi)}\right)\right). \end{aligned} \tag{3.102}$$

for $m_i(\phi) > 0$. In this calculation, we have regularized the divergent integral by setting a hard cut-off $\Lambda_{\rm UV}$. At $\Lambda_{\rm UV} \to \infty$, the first term is UV-divergent, which is subtracted by the zero-temperature counterterm, while second term is UV-finite. By dropping the UV-divergent part and integrating with respect to ϕ, we obtain

$$V^{\rm B}_{\rm zero-mode} = -\sum_i n_{\rm B_i} \frac{T}{12\pi} m_i^3(\phi). \tag{3.103}$$

This is exactly same to the third term of Eq. (3.97). We therefore find that the third term Eq. (3.97) comes from the bosonic Matsubara zero-mode, which is absent in the fermion contribution. Note that this statement is independent from the form of $m_i(\phi)$.

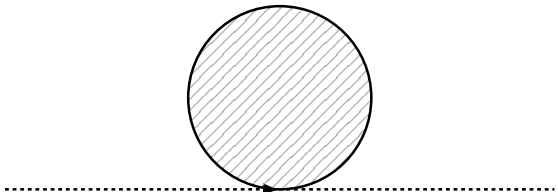

Figure 3.2: The Feynman diagram of one-loop thermal self-energy is schematically shown. External lines correspond to the ith particle which couples to background field ϕ. In the blob circle, particles which couple to ith particles must be included.

3.3.4 Higher-order effects and IR-divergence

In this subsection, we consider higher-order effects which are not taken into account in the previous computation and discuss the validity of the perturbative expansion at finite-temperature field theory.

In the zero-temperature field theory, higher-loop contributions to the effective potential are smaller than that of one-loop as long as the coupling constants are sufficiently small. On the other hand, in the finite-temperature field theory, higher-order corrections are subtle issues because there is an additional dimensionful parameter, which is the ambient temperature, T. It is non-trivial whether higher-order corrections are suppressed, or not, even when coupling constants are small because thermal effects can be large by taking very large T.

To see this, let us compare one-loop thermal self-energy of particle species i which gives field dependent mass $m_i(\phi)$ for scalar field ϕ. The Feynman diagram of one-loop thermal self-energy is indicated in Fig. 3.2. At high-temperature $|\boldsymbol{k}|^2 < T^2$, the one-loop thermal self-energy is generally given by $\Pi_i(T, \boldsymbol{k}) \sim a_i T^2$, where $\boldsymbol{k}$ and a_i are an external spatial (3D) momentum and a numerical value depending on coupling constants.[5] Then, if the ratio

$$\epsilon_{(i)} \equiv \left(\frac{a_i T^2}{m_i^2(\phi)} \right), \tag{3.104}$$

is larger than unity, we should include higher-order corrections otherwise the effective potential, which is evaluated with the one-loop approximation is not reliable.

Let us more quantitatively discuss above discussion here. Since we know that higher-order corrections shown in Fig. 3.2 gives the dominant contribution to the mass term, the

[5] At low-temperature $|\boldsymbol{k}|^2 > T^2$, the thermal contribution is suppressed by the Boltzmann factor which becomes unimportant.

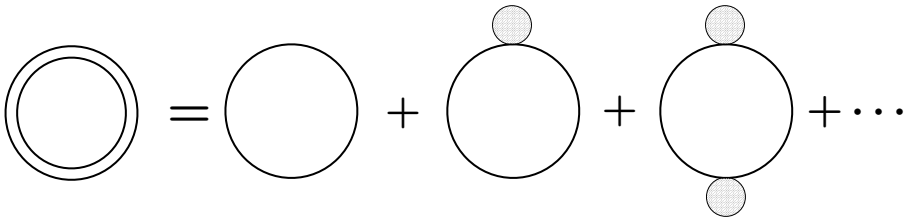

Figure 3.3: The ring diagram, which gives dominant contribution to the effective potential at high-temperature, is schematically shown. Here, external legs corresponding to the background field ϕ are omitted.

Feynman diagram shown in Fig. 3.3, which is obtained by the insertion of thermal mass correction, is important. For bosonic contribution, this diagram can be evaluated as [120]

$$\delta V^{\rm B}_{\rm thermal}(\phi) = \sum_i n_{{\rm B}_i} \frac{T}{2} \sum_{n_{\rm b}=-\infty}^{+\infty} \int \frac{d^3p}{(2\pi)^3} \sum_{N=1}^{\infty} \frac{1}{N} \left(\frac{-\Pi_i(T, \boldsymbol{k}=0)}{\omega_{n_{\rm b}}^2 + \omega_i^2(\phi)} \right)^N , \tag{3.105}$$

If the factor $\Pi_i(T, \boldsymbol{k}=0)/(\omega_{n_{\rm b}}^2 + \omega_i^2(\phi))$ is smaller than the unity, infinite series with respect to N is convergent and gives small corrections. The denominator of this factor is explicitly given by $(2\pi n_{\rm b})^2 + \boldsymbol{p}^2 + m_i^2(\phi)$. The numerical factor a_i is usually smaller than π in weakly coupled theory such as electroweak theory. This implies that ring diagram contribution is dominant only when $n_{\rm b} = 0$ and $|\boldsymbol{p}|^2 + m_i^2(\phi) < a_i T^2$, corresponding to the IR regime. The naive expansion parameter $\epsilon_{(i)}$ defined in Eq. (3.104) is obtained by setting $n_{\rm b} = 0$ and $\boldsymbol{p} = 0$. For fermionic contributions, there is no Matsubara zero-mode and hence ring diagram contribution is not divergent.

We have seen that $\epsilon_{(i)} > 1$ can occur only for Matsubara zero-mode of bosonic particles. One can possible to relax this perturbative condition $\epsilon_{(i)} > 1$ by *resumming* the ring diagrams. By computing the summation with respect to N in Eq. (3.105) for $n_{\rm b} = 0$, we obtain

$$V_{\rm ring} = -\sum_i \frac{n_{Bi} T}{12\pi} \left(\left(\overline{m}_i^2(\phi,\ T) \right)^{\frac{3}{2}} - \left(m_i^2(\phi) \right)^{\frac{3}{2}} \right), \tag{3.106}$$

where

$$\overline{m}_i^2(\phi, T) \equiv m_i^2(\phi) + a_i T^2. \tag{3.107}$$

This is equivalent to calculate the thermal effective potential by using the dressed propagator, whose mass is given by $\overline{m}_i(\phi, T)$ rather than $m_i(\phi)$, for $n_{\rm b} = 0$. This resummation prescription was proposed by the authors of Ref. [121] (Arnold-Espinosa method).

An alternative resummation prescription was proposed in Ref. [122] (Parwani method). In this prescription, the thermal effective potential as well as the zero-temperature effective potential for bosonic particles are calculated by using $\overline{m}(\phi, T)$. The difference of these resummation prescriptions was investigated in Ref. [123].

When non-Abelian gauge fields are involved, we need to take into account another subtle issue called "Linde" problem [124]. The longitudinal modes of the gauge bosons receive the so-called Debye mass $m_{\rm D} \sim gT$, where g is the gauge coupling, which can be computed by perturbative calculation. Therefore, corrections from a ring diagram involving the longitudinal modes of gauge bosons can be relaxed by the resummation technique outlined above. However, it was shown in Ref. [124] that the transverse modes of the gauge bosons receive the so-called magnetic mass $m_{\rm mag} \sim g^2 T$, which cannot be computed by perturbative calculation.

Then, with a similar discussion given above, the higher loop of non-Abelian gauge bosons will give the contributions with the powers of $g^2 T/m(\phi)$ [124, 125] and the perturbation breaks down at high temperature [126],

$$g^2 \frac{T}{m(\phi)} > 1. \tag{3.108}$$

In this case, even the resummed effective potential is not reliable and the dynamics of phase transition should be analyzed by a non-perturbative way such as the lattice simulation Since we expect the parameter a given above is at most unity, we conclude that the resummed effective potential is valid for

$$g^2 T/m(\phi) \simeq gT/\phi < 1, \tag{3.109}$$

when $m(\phi) \simeq g\phi$. Therefore, the potential shape is not reliable at around $\phi \lesssim gT$. Unfortunately, there is no perturbative approach to calculate the effective potential at that regime. As we will see in sec. 3.4.3, this fact makes us difficult to analyze the order of the phase transition such as the ordinary electeoweak phase transition in the SM. In particular, in this thesis, we will consider the case where ϕ couples to the non-Abelian SU(2) gauge fields.

3.4 Cosmological Phase Transitions and Gravitational wave Production

In this section, we discuss order of a phase transition in a simple model. We will see that if the background field ϕ couples to the bosonic particles, a potential barrier between a local and global minima are generated by thermal corrections. A calculation method of a decay rate of metastable state and formulae of GW signals generated by first order phase transition are also presented.

3.4.1 Order of phase transitions

In this subsection, we analyze a phase transition dynamics of a simple model including the electroweak theory.

As a simple example, we start from the background field ϕ, whose tree-level potential is given by

$$V_{\rm tree} = \frac{\lambda}{4}(\phi^2 - v^2)^2. \tag{3.110}$$

This potential describes a spontaneous (local or global) symmetry breaking with ϕ being the order parameter. If we regard above potential as the one of the SM Higgs field $H_{\rm SM} = (0, \phi/\sqrt{2})^t$ with $\phi \equiv h_{\rm SM}$, the vacuum expectation value and the quartic coupling are fixed and are given by $v \equiv v_{\rm SM} \simeq 246\,{\rm GeV}$ and $\lambda \equiv \lambda_{\rm SM} \simeq 0.13$, respectively.

Also, in the following discussion, we assume that field dependent masses are given by $m_i(\phi) \simeq c_i\phi$ and do not specify concrete form of the Lagrangian density. At the one-loop order without resummation, by using the high-temperature expansion Eqs. (3.97) and (3.98), we obtain an approximate expression of the total effective potential as follows.

$$\begin{aligned} V_{\rm tot}(\phi, T) &\simeq \frac{1}{2}M^2(T)\phi^2 - ET\phi^3 + \frac{\lambda}{4}\phi^4, \\ M^2(T) &= D(T^2 - T_0^2). \end{aligned} \tag{3.111}$$

where numerical constants D, T_0, and E depend on c_i and number of degrees of freedoms, which couple to ϕ. For example, in the electroweak theory where ϕ becomes the SM Higgs boson, the field dependent masses will be explicitly given by Eq. (3.125). Here, we have neglected the zero-temperature correction for simplicity. This simplification does not change

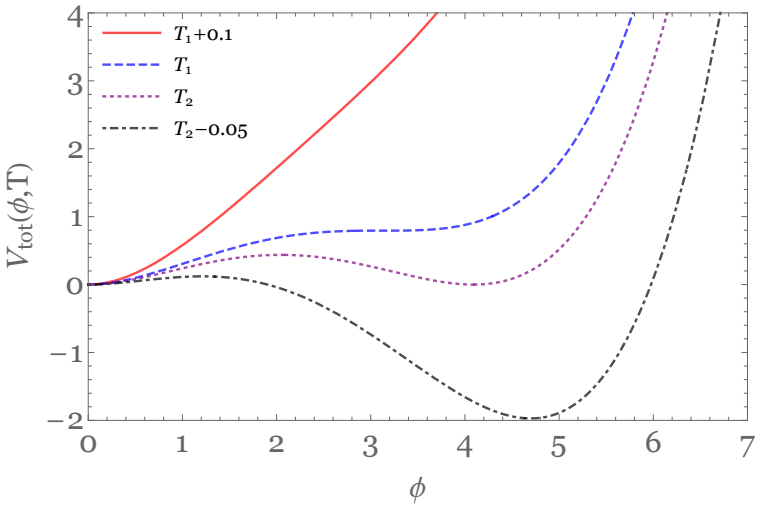

Figure 3.4: The thermal effective potential given by Eq. (3.111) is indicated for different temperatures with $D = 1,\ T_0 = 1.2,\ E = 0.15$ and $\lambda = 0.1$. Definitions of T_1 and T_2 can be found in the main text.

following discussion significantly as long as λ is not largely affected against radiative corrections. To capture general features of the shape of the total effective potential, we plot $V_{\rm tot}(\phi, T)$ for different temperatures in Fig. 3.4. The value of constants D, T_0, E and λ depend on the underlying physics, but we here treat as fixed parameters to study the shape of the potential Eq. (3.111) in the figure.

At very high-temperature $T > T_1 = T_0/(1-9E^2/8\lambda D)^{1/2}$ (the red curve), there is only the unique minimum at $\phi = 0$ corresponding to the symmetric phase. Therefore, the Universe is in symmetric phase at this temperature. As the temperature decreases due to the cosmic expansion, an extra minimum appears at $T = T_1$ (the blue dashed curve), which is separated by the potential barrier. At $T_C = T_0/(1 - E^2/\lambda D)^{1/2} < T_1$ (the purple dotted curve), the two minima are degenerated, where the position of the extra minimum can be expressed as

$$\frac{\langle\phi(T_C)\rangle}{T_C} = \frac{2E}{\lambda}. \tag{3.112}$$

For slightly low-temperature $T_0 < T \lesssim T_C$, there exists the potential barrier between these vacua since the curvature of the potential at the origin is positive $M^2(T) > 0$, but the extra minimum is energetically favored. The potential barrier eventually disappears at $T = T_0$, and hence, there is only unique minimaum different from the origin. Note that constant E comes from third term of J_B-function defined in Eq. (3.97), which is the origin of the

potential barrier.

We shall now discuss the order of the phase transition based on the potnetial Eq. (3.111). In the presence of the potential barrier $E \neq 0$, the expectation value, $\langle\phi(T)\rangle$, is discontinuously changed at the nucleation temperature $T_{\rm n}$ when the tunneling takes place, and hence, a first-order phase transition takes place. The precise definition and the evaluation of the nucleation temperature $T_{\rm n}$ will be given in the next subsection. (See Eq. (3.121).) On the other hand, in the absence of the potential barrier $E = 0$ in Eq. (3.111), $\langle\phi(T)\rangle$ can be expressed as

$$\langle\phi(T)\rangle = \begin{cases} 0 & (T > T_0) \\ \sqrt{-\frac{2M^2(T)}{\lambda}} & (T < T_0) \end{cases}. \tag{3.113}$$

Since the first derivative of the order parameter is discontinuously changed at temperature at $T = T_0$, this phase transition is of second order.

We have discussed the order of the phase transition based on Eq. (3.111), which is evaluated at one-loop order with high-temperature expansions. Even if we take account effect of a resummation, above qualitative discussion does not change. However, as we discussed in the sec. 3.3.4, the thermal effective potential is suffered from corrections from non-Abelian gauge field at $\phi \lesssim gT$. Since perturbative computation cannot be reliable, above discussion cannot be trusted at that regime. We will consider this issue and how to determine the order of phase transition with perturbative computation in the next subsection.

3.4.2 Cosmological first-order phase transitions

In this subsection, we give a basic method to calculate the reaction rate of the false vacuum decay and clarify the nucleation temperature at which bubbles are nucleated.

A first order phase transition occurs as a result of true vacuum bubble nucleations. This is understood as quantum or thermal tunneling from a false vacuum to a true vacuum that is separated by a potential barrier. The tunneling rate or the bubble nucleation rate $\Gamma(T)$ per unit volume and unit time can be expressed as

$$\Gamma(T) = \mathcal{A}(T)e^{-\mathcal{B}}, \tag{3.114}$$

where $\mathcal{B}$ is the bounce action and pre-factor $\mathcal{A}(T)$ is obtained by evaluating the fluctuation around the bounce solution [127], respectively. The bounce action including the finite-

temperature effect, is given by [128, 129]

$$\mathcal{B} = \frac{S_3}{T}, \tag{3.115}$$

where $S_3(T)$ is the bounce action in $D = 3$ dimension:

$$\frac{S_3}{T} = \int_0^\infty dr 4\pi r^2 \left(\frac{1}{2} \left(\frac{d\phi(r)}{dr} \right)^2 + V_{\rm tot}(\phi(r),\ T) \right). \tag{3.116}$$

In this expression, $V_{\rm tot}(\phi, T)$ and r are the total effective potential and the radial coordinate in the three dimensional polar coordinate system, respectively. The total effective potential depends on concrete form of the Lagrangian density, but we here do not assume its specific form. By dimensional analysis, $\mathcal{A}(T)$ is roughly given by $\mathcal{A}(T) \approx T^4$. We keep this rough estimate in this thesis because it will turn out that important physical quantities such as nucleation temperature is less sensitive to $\mathcal{A}(T)$.

S_3 can be obtained by constructing $O(3)$ symmetric *bounce solution* governed by the following differential equation:

$$\frac{d^2\phi}{dr^2} + \frac{2}{r}\frac{d\phi}{dr} - \frac{\partial V_{\rm tot}(\phi,\ T)}{\partial \phi} = 0, \tag{3.117}$$

with boundary conditions

$$\phi(r \to \infty) = \phi_{\rm False}, \quad \left.\frac{d\phi}{dr}\right|_{r=0} = 0. \tag{3.118}$$

Here, $\phi_{\rm false}$ is the field value of the false vacuum.

The time or the temperature of the phase transition is characterized by the nucleation time $t_{\rm n}$ or the temperature $T_{\rm n}$, defined as a temperature when the nucleation probability inside one Hubble volume $\mathrm{H}^{-3}(T)$, where $\mathrm{H}(T)$ is the Hubble parameter, becomes unity,

$$\int_0^{t_n} \frac{\Gamma(T)}{\mathrm{H}^3(T)} dt = \int_{T_n}^\infty \frac{dT}{T} \frac{\Gamma(T)}{\mathrm{H}^4(T)} = 1. \tag{3.119}$$

Since the dominant contribution in the integral (3.121) comes from that around $t \sim t_{\rm n}$ or $T \sim T_{\rm n}$, it can be approximated as

$$\frac{\Gamma(T_n)}{\mathrm{H}^4(T_n)} = 1, \tag{3.120}$$

which can be used to determine $T_{\rm n}$. When we consider the electroweak phase transition since the electroweak symmetry breaking takes place at $T_{\rm n} \sim \mathcal{O}(100)$ GeV, the bounce action at the time of bubble nucleation is roughly given by

$$\frac{S_3}{T_{\rm n}} = 4 \log \left(\frac{T_{\rm n}}{\mathrm{H}} \right) \sim 140. \tag{3.121}$$

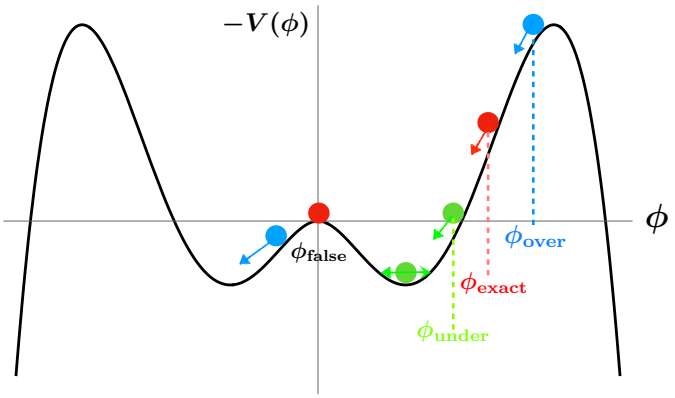

Figure 3.5: The algorithm of the under/over-shooting method is schematically depicted. $\phi_{\rm over}$, $\phi_{\rm exact}$ and $\phi_{\rm over}$ are positions of the initial field values corresponding to under-shooting, exact and over-shooting solutions, respectively. See main text for detailed discussions.

In this calculation, we have used the Hubble parameter during the radiation domination era given by Eq. (3.40) with $g_* = \mathcal{O}(10^2)$. In order to determine the nucleation temperature as well as the bubble profile accurately, we need to solve the equation of motion (3.117) with the boundary condition (3.118) numerically.

Let us explain how to solve the bounce equation Eq. (3.117) here. First of all, the differential equation Eq. (3.117) can be regarded as the equation of motion of the scalar field $\phi(r)$ with r being the *time* and with the *inverted potential* $-V_{\rm tot}(\phi, T)$. Then, the boundary condition Eq. (3.118) implies that the *velocity*, $d\phi/dr$, is zero at the initial position $\phi(r = 0)$, and ϕ must stop for $r = \infty$ at $\phi_{\rm false}$. Therefore, if we can find the initial position $\phi_{\rm exact}$, which leads to $\phi(r \to \infty) = \phi_{\rm false}$, we obtain the bounce solution. However, since the potential is inverted, $\phi_{\rm false}$ becomes a saddle point, which implies that the bounce solution is unstable under a small fluctuation around it. How do we find $\phi_{\rm exact}$?

Fortunately, $\phi_{\rm exact}$ can be numerically obtained by the following algorithm so-called *over/under-shooting method*. The basic idea is schematically depicted in Fig. 3.5. From Eq. (3.117), we can find that there is a friction term, which is proportional to $2/r$. Hence if we take the initial value at $\phi_{\rm under} < \phi_{\rm exact}$ (corresponding to the green colored circle in Fig. 3.5), ϕ rolls towards the $\phi_{\rm false}$, but it cannot reach $\phi_{\rm false}$ due to the friction term. This solution is called under-shooting solution. On the other hand, if we choose the initial value as $\phi_{\rm over} > \phi_{\rm exact}$ (corresponding to the blue colored circle), $\phi(r)$ overcomes $\phi_{\rm false}$ and it even-

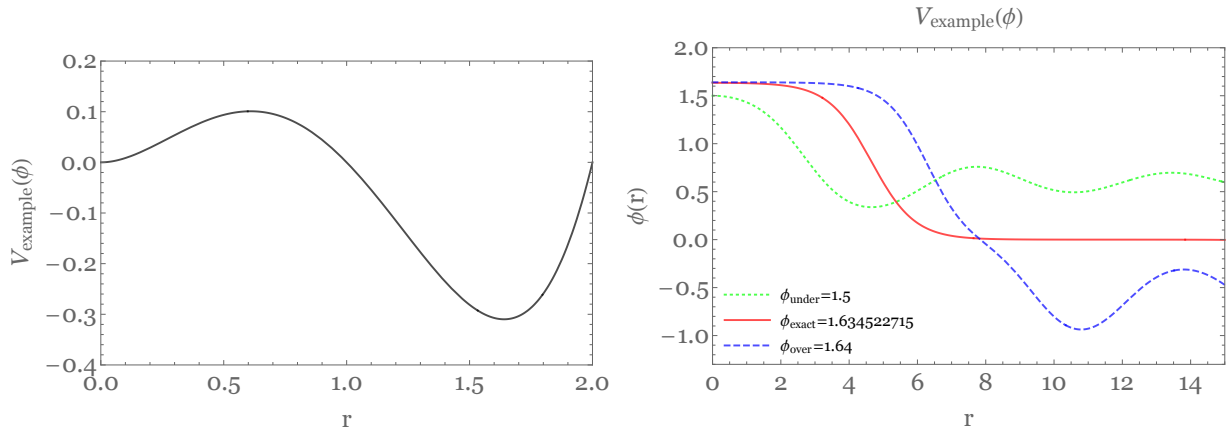

Figure 3.6: **The left panel**: The shape of the potential barrier $V_{\text{example}}(\phi)$ is shown. **The right panel**: Solutions of the differential equation Eq. (3.117) with boundary conditions $\phi_{\text{under}} = 1.5$, (the green dotted curve) $\phi_{\text{exact}} = 1.634522715$ (the red solid curve) and $\phi_{\text{over}} = 1.64$ (the blue dashed curve) are shown.

tually oscillates around $-\phi_{\text{false}}$. This solution is called over-shooting solution. As a initial condition, we choose $\phi^{i=0}_{\text{under}}$ in such a way that $V(\phi_{\text{false}}) = V(\phi^{i=0}_{\text{under}})$, $\phi_{\text{false}} < \phi^{i=0}_{\text{under}} < \phi_{\text{true}}$ is satisfied. By increasing the value of $\phi^{i=0}_{\text{under}}$ with finite difference $\delta\phi^{i=0}$ and solving the differential equation Eq. (3.117), we will find the threshold field value leading to the over-shooting, $\phi^{i=0}_{\text{over}} \approx \phi_{\text{exact}}$. Here, index i labels the trial number. The precision of the bounce solution can be improved by doing same procedure with initial condition $\phi^{i=1}_{\text{under}} = \phi^{i=0}_{\text{over}} - \delta\phi^{i=0}$ and with finite small difference $\delta\phi^{i=1} < \delta\phi^{i=0}$. Constructing a loop calculation with respect to the trial number i, we can control the precision of the bounce solution.

As an simple example, we consider the scalar potential given by

$$V_{\text{example}}(\phi) = \phi^2 - \frac{3}{2}\phi^3 + \frac{1}{2}\phi^4, \ \phi > 0. \tag{3.122}$$

As can be seen from the left panel of Fig. 3.6, this potential has a local and global minima at $\phi_{\text{false}} = 0$ and $\phi_{\text{true}} \approx 1.604$, respectively. The behavior of under-shooting, exact and over-shooting solutions are shown in the right panel of Fig. 3.6. For $\phi_{\text{under}} = 1.5$ and $\phi_{\text{over}} = 1.64$, ϕ oscillates around true minima ϕ_{true} and $-\phi_{\text{true}}$ at $r \to 15$, respectively. (Here, we take $r = 15$ as a cut-off of $r \to \infty$.) For $\phi_{\text{exact}} \approx 1.634522715$, $\phi(r \to 15) \simeq 0$ is realized corresponding to the bounce solution.

We shall now consider the validity of perturbative computation of the thermal effective potential. As we discussed in sec. 3.3.4, at the small field values, including the origin, the

resummed effective potential or its approximated one (3.111) is not reliable at $\phi \lesssim gT$ due to the non-perturbative corrections from non-Abelian gauge fields. However, since the bounce action is mainly determined by the information of the potential around the broken phase ($\phi \neq 0$) rather than the symmetric phase ($\phi = 0$), the non-perturbative corrections can be neglected if $\langle\phi(T_{\rm n})\rangle \gtrsim gT_{\rm n}$ is satisfied. Here, $\langle\phi(T_{\rm n})\rangle$ denotes the position of the global minimum at $T_{\rm n}$. Thus, if

$$\frac{\langle\phi(T_{\rm n})\rangle}{T_{\rm n}} \gtrsim g, \tag{3.123}$$

is satisfied, we can safely state that the phase transition is of first order. This condition should be regarded as the order estimation because it depends on the potential height in reality.

Moreover, we define the phase transition as *strong* first order if

$$\frac{\langle\phi(T_{\rm n})\rangle}{T_{\rm n}} > 1, \tag{3.124}$$

is satisfied. The difference between first order phase transition ($gT_{\rm n}/\langle\phi(T_{\rm n})\rangle < 1$) and strong first order phase transition ($T_{\rm n}/\langle\phi(T_{\rm n})\rangle < 1$) is important when we consider electroweak baryogenesis because the sphaleron decoupling condition is given by Eq. (3.124). On the other hand, this difference is not important when we discuss the gravitational wave background generated by first order phase transition. Since a first order phase transition proceeds through bubble nucleation, the production of gravitational wave background requires a first order phase transition, not a strong first order phase transition as we will see in sec. 3.4.5

3.4.3 The electroweak phase transition in the SM

In this subsection, we explicitly compute the thermal effective potential within the SM framework and discuss the validity of the perturbative expansion during the phase transition.

Since the SM Higgs couples to the $\mathrm{SU(2)_W} \times \mathrm{U(1)_Y}$ gauge bosons and top quark, these loop corrections must be taken into account. Other quarks, leptons and Higgs self-coupling of course contribute to the effective potential, but it is negligible amount, and hence, we can safely neglect it. Field dependent masses and degrees of freedoms of these particles are listed

below:

$$\begin{aligned}
&\text{W gauge bosons}: \quad n_W = 6, \quad m_W^2 = \frac{g_2^2 h_{\rm SM}^2}{4}, \\
&\text{Z gauge bosons}: n_Z = 3, \quad m_Z^2 = (g_1^2 + g_2^2)\frac{h_{\rm SM}^2}{4}, \\
&\text{Top quarks}: n_t = 12, \quad m_t^2 = \frac{y_t^2 h_{\rm SM}^2}{2},
\end{aligned} \tag{3.125}$$

Here, n_W, n_Z and n_t are the internal degrees of freedoms of W, Z boson and the top quark, respectively, while m_W, m_Z and m_t are the field dependent masses for these particles. We have parameterized the SM Higgs field as

$$H_{\rm SM} = \begin{pmatrix} 0 \\ h_{\rm SM}/\sqrt{2} \end{pmatrix}. \tag{3.126}$$

At one-loop order with the high-temperature approximation, the shape of the Higgs field can be approximated by Eq. (3.111), where constants D, T_0 and E are explicitly given by

$$D = D_{\rm SM} \equiv \left(\frac{y_t^2}{4} + \frac{3g_2^2 + g_1^2}{32} \right) T^2, \tag{3.127}$$

$$T_0^2 = T_{0\rm SM}^2 \equiv \lambda_{\rm SM} v_{\rm SM}^2 / D_{\rm SM}, \tag{3.128}$$

$$E_{\rm SM} = \frac{2g_2^3 + (g_2^2 + g_1^2)^{\frac{3}{2}}}{16\pi}. \tag{3.129}$$

It is obvious that this potential shape indicates the (weakly) first-order electroweak phase transition in the perturbative analysis since the potential barrier $E_{\rm SM} \neq 0$ is generated by the $\mathrm{SU(2)_W} \times \mathrm{U(1)_Y}$ gauge bosons. (See Fig. 3.4.) To clarify the order of the phase transition, let us here consider the perturbative condition $\langle h_{\rm SM}(T_{\rm n}) \rangle \gtrsim g_2 T_{\rm n}$. We can obtain an approximate expression of $\langle h_{\rm SM}(T_{\rm n}) \rangle / T_{\rm n}$ by identifying it with $\langle h_{\rm SM}(T_{\rm C}) \rangle / T_{\rm C}$, where T_C is the critical temperature at which the two vacua are degenerated with each other. Under this approximation, as discussed in sec. 3.4.1, we obtain very simple expression:

$$\frac{\langle h_{\rm SM}(T_C) \rangle}{T_C} = \frac{2E_{\rm SM}}{\lambda_{\rm SM}} \simeq 0.15 \ll g_2. \tag{3.130}$$

In this calculation, we have used $g_2 = 0.65$, $g_1 = 0.36$ and $\lambda_{\rm SM} = 0.131$. This result implies that we cannot reliably estimate the potential shape at around the true vacuum, and thus, we cannot determine the order of the phase transition by the perturbative calculation.

From (3.130), we can see that a first-order phase transition takes place if the self-coupling $\lambda_{\rm SM}$ is small enough and the cubic pre-factor $E_{\rm SM}$ is large enough (although these values are

fixed in the SM). This is because the parameter $E_{\rm SM}$ determines the height of the barrier between the origin and the other minimum. Indeed, lattice studies [1, 2, 3] confirmed that it is actually a crossover transition rather than the first-order phase transition with the observed Higgs mass $m_{\rm Higgs} = \sqrt{2\lambda_{\rm SM}} v_{\rm SM} \simeq 125\,{\rm GeV}$, but it becomes first order in the light Higgs mass regime $m_{\rm Higgs} \lesssim 80\,{\rm GeV}$ (corresponding to small $\lambda_{\rm SM}$).

3.4.4 First-order phase transitions in physics beyond the Standard Model

When we consider extensions of the SM motivated by several problems such as the electroweak hierarchy problem, dark matter and so on, the electroweak phase transition can be of first order because additional particles, which couple to the SM-like Higgs, can change the shape of the effective potential. Then the natural question arises: *What kind of models realize first-order phase transitions*? To answer this question, let us consider the method to make $\langle h_{\rm SM}(T_C)\rangle/T_C$ large (because if this quantity is large enough, the electroweak phase transition becomes first order).

Since E defined in Eq. (3.111) comes from the bosonic loop contribution discussed in sec. 3.3.3, new bosons strongly coupled to $h_{\rm SM}$ are needed for a strong first order phase transition. Such new bosons mass must be small compared to the temperature, otherwise its thermal contribution is Boltzmann suppressed and is negligible amount discussed in sec. 3.4.1. Indeed, in Chapter 5, we will find that the electroweak phase transition is of (strong first-order) in the scotogenic model thanks to the additional couplings between the SM-like Higgs and an additional scalar doublet.

We have focused on the ordinary electroweak phase transition in the beyond standard model. In such theories, there often exists additional (global or local) spontaneous symmetry breaking, and hence, there are addition phase transitions associated with these. (For example, in twin Higgs models, which will be discussed in Chapter 4, has spontaneous symmetry breaking of $\mathrm{U}(4) \to \mathrm{U}(3)$.) Assuming the tree-level potential is given by Eq. (4.11), we can have a similar discussion above. Then, we can increase $\langle\phi(T_{\rm n})\rangle$ by making small λ, which is the quartic coupling of ϕ with ϕ being the new Higgs field different from the ordinary SM Higgs field.

We finally comment on the effect of the ring diagram on the strength of the phase transi-

tion. In the expression of the ring diagram contribution (3.106), the thermal field dependent mass $\overline{m}_i(\phi,\ T)$ is given by Eq. (3.107). After the resummation, if the thermal mass is much larger than the zero-temperature part, that is, $m_i^2(\phi) \ll \Pi$ at $T = T_C$, $(\overline{m}_i^2)^{\frac{3}{2}}$ behaves like a constant term $\simeq \Pi^{\frac{3}{2}}(T_C)$ which does not give the potential barrier. This effect makes $\langle\phi(T_C)\rangle$ small hence the resummation generally makes the phase transition weaker. For the same reason, if we consider the case where the field dependent masses of bosonic particles are given by $m_i^2(\phi) \simeq c_i\phi^2 + M^2$, where c_i and M^2 are a ϕ-independent constants. The phase transition strength becomes weaker. These facts imply that new bosonic particles coupled to the SM Higgs should not have ϕ-independent mass squared term to enhance the strength of the phase transition.

3.4.5 Gravitational wave signals generated by first-order phase transitions

The first-order cosmological phase transition proceeds via bubble nucleations. Nucleated bubbles expand due to the free energy (pressure) difference between the symmetric and broken phases. They eventually coalesce with each other until they fill the Universe.

Now let us give the expressions of the spectrum of the gravitational background from the first order phase transition. Since the broken phase is energetically favored, the nucleated bubbles expand, and collide each other, and finally the whole Universe settles down to the true vacuum. Since the bubble collisions as well as the plasma bulk motion induced by the bubble dynamics are highly inhomogeneous and violent process, gravitational waves are emitted through such processes.

The spectrum of the gravitational wave is determined by the (initial) kinetic energies of the bubbles and the duration of the phase transition. The former is parameterized by bag parameter ϵ in the so-called bag model [130], defined by

$$\epsilon = \Delta V_{\rm tot} - \frac{T}{4}\frac{\partial \Delta V_{\rm tot}}{\partial V}. \tag{3.131}$$

In the above expression, $\Delta V_{\rm tot}$ is the total effective potential difference between the false vacuum and the true vacuum. We parameterize the kinetic energy of bubbles by a dimensionless parameter α representing the ratio between the latent heat density and the radiation

energy density,

$$\alpha = \left.\frac{\epsilon}{\rho_{\rm rad}}\right|_{T=T_{\rm n}}, \tag{3.132}$$

where $\rho_{\rm rad} = g_*\pi^2 T_{\rm n}^4/30$ is defined by Eq. (3.31). The duration of the phase transition is characterized by the parameter β, defined by

$$\Gamma(t) \simeq \Gamma_0 e^{\beta t}, \tag{3.133}$$

with Γ_0 being a constant. Here, Γ is defined by Eq. (3.114). β is expressed in terms of the bounce action as

$$\frac{\beta}{{\rm H}(T_{\rm n})} = T\frac{d}{dT}\left(\frac{S_3}{T}\right)\bigg|_{T=T_{\rm n}}. \tag{3.134}$$

It has been argued that not only the bubble collision or the scalar field dynamics, but also the plasma dynamics caused by the bubble dynamics source the GW signals [4, 5, 6, 7, 8]. It is indeed found to be the dominant contribution to the GW signals since due to the interaction between the scalar field bubble wall and the plasma, the energy originally carried by bubble walls is quickly taken away to the plasma bulk motion. According to the popular convention, we further classify it into the sound waves in the plasma described in the linear regime, which are generated by the bubble motion and generate gravitational waves around the bubble collision, and the turbulence of plasma bulk motion further developed in the non-linear regime after the bubble collision. Then the total contribution can be schematically written as

$$\Omega_{\rm GW}h^2 = \Omega_{\rm bubble}h^2 + \Omega_{\rm sw}h^2 + \Omega_{\rm tur}h^2 \simeq \Omega_{\rm sw}h^2 + \Omega_{\rm tur}h^2, \tag{3.135}$$

where $\Omega_{\rm bubble}$, $\Omega_{\rm sw}$ and $\Omega_{\rm tur}$ denote the contributions from the bubble collisions, sound waves and turbulence of the plasma, respectively. More precisely, $\Omega_A \equiv \rho_{A,0}/\rho_c$ ($A =$ bubble, sw, tur) and $\rho_{A,0}$ is the present energy density of A-component. The critical density ρ_c is defined by Eq. (3.12). The value of h was defined by Eq. (3.6).

The contribution coming from sound wave of the plasma is estimated in Refs. [15, 131, 11, 132] as

$$\Omega_{\rm sound}h^2 = 2.65\times10^{-6}\times{\rm H}\tau_{\rm sound}\left(\frac{{\rm H}(T_{\rm n})}{\beta}\right)\left(\frac{\kappa_{\rm sound}\alpha}{1+\alpha}\right)^2\left(\frac{100}{g_*}\right)^{\frac{1}{3}}v_w\left(\frac{\rm f}{\rm f_{sound}}\right)^3\left[\frac{7}{4+3\left(\frac{\rm f}{\rm f_{sound}}\right)^2}\right]^{\frac{7}{2}}, \tag{3.136}$$

where $\kappa_{\rm sound}$ and v_w are the efficiency factor and the bubble wall velocity, respectively. The factor $\mathrm{H}(T_{\rm n})\tau_{\rm sound}$ represents a suppression factor coming from the short-lasting sound wave as originally pointed out in Ref. [133] (Also, See e.g. Refs. [134, 135].) and is given by

$$\mathrm{H}(T_{\rm n})\tau_{\rm sound} = \min\left\{1,\ (8\pi)^{\frac{1}{3}}\left(\frac{\max\{c_s,\ v_w\}}{\beta/\mathrm{H}(T_{\rm n})}\right)\left(\frac{4}{3}\frac{1+\alpha}{\kappa_{\rm sound}\alpha}\right)^{\frac{1}{2}}\right\}. \tag{3.137}$$

Here c_s is the speed of sound wave in the plasma and $\mathrm{f}_{\rm sound}$ is the peak frequency of the GW signals given by

$$\mathrm{f}_{\rm sound} = 1.9\times10^{-2}\mathrm{mHz}\times\frac{1}{v_w}\left(\frac{\beta}{\mathrm{H}(T_{\rm n})}\right)\left(\frac{T_n}{100\mathrm{GeV}}\right)\left(\frac{g_*}{100}\right)^{\frac{1}{6}}. \tag{3.138}$$

We here simply estimate the bubble wall velocity by adopting following formula [136][6]:

$$v_w = \frac{1/\sqrt{3}+\sqrt{\alpha^2+2\alpha/3}}{1+\alpha}. \tag{3.139}$$

With above bubble wall velocity called Jouguet detonations, the efficiency factor, $\kappa_{\rm sound}$, is fitted by following formula as found in Ref. [130]:

$$\kappa_{\rm sound} = \frac{\sqrt{\alpha}}{0.135+\sqrt{0.98+\alpha}}. \tag{3.140}$$

The contribution from turbulence plasma is estimated in Refs. [15, 131] as

$$\Omega_{\rm tur}h^2 = 3.35\times10^{-4}\left(\frac{\mathrm{H}(T_{\rm n})}{\beta}\right)\left(\frac{\kappa_{\rm tur}\alpha}{1+\alpha}\right)^{\frac{3}{2}}\left(\frac{100}{g_*}\right)^{\frac{1}{3}}v_w\frac{\left(\frac{\mathrm{f}}{\mathrm{f}_{\rm tur}}\right)^3}{\left(1+\left(\frac{\mathrm{f}}{\mathrm{f}_{\rm tur}}\right)\right)^{\frac{11}{3}}\left(1+\frac{8\pi\mathrm{f}}{\mathrm{H}_*}\right)}, \tag{3.141}$$

where $\kappa_{\rm tur}$ is the efficiency factor of the turbulence. $\kappa_{\rm tur}$, H_0 and the peak frequency, $\mathrm{f}_{\rm tur}$, are given by

$$\kappa_{\rm tur} \simeq 0.1\kappa_{\rm sound}, \tag{3.142}$$

$$\mathrm{H}_* \simeq 1.65\times10^{-4}\mathrm{mHz}\times\left(\frac{T_{\rm n}}{100\mathrm{GeV}}\right)\left(\frac{g_*}{100}\right)^{\frac{1}{6}}, \tag{3.143}$$

$$\mathrm{f}_{\rm tur} = 2.7\times10^{-2}\mathrm{mHz}\left(\frac{1}{v_w}\right)\left(\frac{T_{\rm n}}{100\mathrm{GeV}}\right)\left(\frac{\beta}{H(T_{\rm n})}\right)\left(\frac{g_*}{100}\right)^{\frac{1}{6}}. \tag{3.144}$$

Note that by adopting the formula with the envelope approximation in Ref. [141] the contributions from bubble collisions turned out to be subdominant in our setup.[7] Thus we safely omitted the contributions from the bubble collisions in our analysis.

[6] See Refs. [137, 138, 139, 140], however, for the discussion of the bubble wall velocity v_w.

[7] Recently it is claimed that there might be another contribution from "fluid bubble" in Refs. [142, 143, 144], but it gives a subdominant contribution compared to the sound waves [9, 10, 11].

Chapter 4

Phase Transitions in Twin Higgs Models

In this chapter, we investigate how the electroweak symmetry breaking and the global symmetry breaking $\mathcal{G} \to \mathcal{H}$ (typically, U(4) $\to$ U(3)) proceed in thermal history of the Universe realized in twin Higgs models. In particular, we address the question whether these phase transitions can be first order in that framework, or not. If phase transitions are of first order, we calculate the GW signals and discuss its detectability. This chapter is based on my original work [63].

4.1 Motivation and Outline

In this section, we explain basic setup and outline to clarify the phase transition dynamics as well as a calculation method of the GW signals generated by cosmological first-order phase transition.

Motivation

It was discussed in Sec. 2.3.1 that all new particles in addition to the SM particles introduced in twin Higgs models are singlet under the SM gauge group. Hence it is difficult to produce these particles by LHC experiments and this is the essential reason why these models can provide the solution to the little hierarchy problem. However, this fact implies that these models are very difficult to be tested or constrained by collider experiments Thus, it is

interesting if we have other method to test or constrain parameter space of these models. We have seen in Sec. 3.4.5 that first-order cosmological phase transition produce GW signals, which will be tested by the future planned experiments. The main purpose of this chapter is to clarify the dynamics of cosmological phase transitions occurred in these models. Moreover, if a cosmological phase transition is of first order, we explicitly calculate GW signals and extract the important information of these models.

Outline

Before going to have a detailed analysis and discussions, we here explain how to analyze the order of phase transitions and how to calculate the GW signals generated by first-order phase transition in the twin Higgs models. First of all, the Lagrangian densities of the Mirror and the Fraternal twin Higgs models are summarized in Sec. 2.3.2. Based on this Lagrangian densities, one can compute the thermal effective potential of both H_A and H_B fields by using the calculation method outlined in Sec. 3.3. Secondly, by studying the shape of the thermal effective potential for different cosmic temperatures T, we can determine the order of phase transitions occurred in these models. Concretely, if the computed thermal effective potential has potential barrier between the symmetric phase and the broken phase, we can calculate the tunneling rate $\Gamma(T)$, which was defined by Eq. (3.114) by solving the bounce equation as explained in Sec. 3.4.2. Hence we can evaluate the nucleation temperature $T_{\rm n}$ given by Eq. (3.121) at which a phase transition takes place. Thirdly, we confirm the validity of the perturbative calculation of the thermal effective potential given by Eq. (3.123) at $T_{\rm n}$. If this condition is satisfied, the phase transition is of first order, and hence, we expect the production of the GW signals. Finally, GW signals are derived by using formulae summarized in Sec. 3.4.5 and then discuss its detectability. It should be emphasized that we can clarify the dynamics of the phase transition and GW signals produced by a first order phase transition from the Lagrangian densities summarized in Sec. 2.3.2.

4.2 The Thermal History in Twin Higgs models

The twin Higgs models generally accommodate breakings of the two symmetries as we have seen in the previous subsection. One of them is the standard electroweak symmetry breaking and another is the breaking of the U(4) symmetry to the U(3) one, through which the SM

Higgs field is identified with one of the pNGBs. Let us call the phase transition corresponding to the latter breaking the U(4)-breaking phase transition. In this chapter, we analyze not only the electroweak phase transition but also this U(4)-breaking phase transition in cosmology for completeness. In this section, we study the order of the electroweak phase transition in twin Higgs models, with and without supersymmetric UV completion.

Here, we would like to discuss the thermal history in the early Universe. Since we take account of not only the H_A field but also the H_B field, we consider the following background fields,

$$H_A = \begin{pmatrix} 0 \\ \dfrac{\phi_A}{\sqrt{2}} \end{pmatrix}, \ H_B = \begin{pmatrix} 0 \\ \dfrac{\phi_B}{\sqrt{2}} \end{pmatrix}. \tag{4.1}$$

Note that H_A is identified with the SM Higgs $H_A \equiv H_{\rm SM}$. At high-temperature, both of ϕ_A and ϕ_B fields are trapped at the origin of the potential due to the thermal mass terms (See red colored curve of Fig. 3.4). When the temperature cools down, another minimum different from the origin appears. Below the critical temperature, ϕ_A and ϕ_B fields eventually roll down or tunnel to the true vacuum, and the U(4) symmetry and its subgroup, the SM electroweak symmetry, finally break down. However, we do not know how these two phase transitions proceed. Let us denote the temperatures when ϕ_A and ϕ_B fields acquire their VEVs by T_A and T_B, respectively. In general, there are three possible trajectories of these two phase transitions, which are schematically described in Fig. 4.1. The red line (1) shows the trajectory of a two-step phase transition with $T_B \gg T_A$, in which ϕ_B field acquires its VEV first and ϕ_A field does later. The blue solid line (2) shows the trajectory of a one-step phase transition with $T_A \sim T_B$, in which the Higgs field rolls (or tunnels) to the true vacuum directly. The green dotted line (3) shows the trajectory of another two-step phase transition with $T_A \ll T_B$, in which ϕ_A field acquires its VEV first and ϕ_B field does later. In our analysis, we consider the case with $T_B \gg T_A$ and we call the phase transition at which ϕ_B field acquires its VEV, the U(4)-breaking phase transition. Let us consider the condition under which this case happens. The thermal mass terms for ϕ_A and ϕ_B fields are given by

$$m_A^2(H_A,\ T)) = (\zeta_A T^2 - (\lambda - \sigma_1) f^2)|H_A|^2, \tag{4.2}$$

$$m_B^2(H_B,\ T) = (\zeta_B T^2 - \lambda f^2)|H_B|^2, \tag{4.3}$$

where ζ_A and ζ_B represent the numerical coefficients depending on the coupling constants. The critical temperatures T_A and T_B are evaluated by the condition $m_A(T_A) = m_B(T_B) = 0$,

which yields

$$\frac{T_A}{T_B} = \sqrt{\frac{\zeta_B}{\zeta_A}}\sqrt{1-\frac{\sigma_1}{\lambda}}. \tag{4.4}$$

Taking into account the twin $\mathbf{Z_2}$ symmetry $\zeta_A \simeq \zeta_B$, we obtain $T_A/T_B \simeq \sqrt{1-\sigma_1/\lambda}$. Therefore, $\sigma_1 > 0$ is a necessary condition to realize $T_A \ll T_B$. The region with $\sigma_1 > 0$ is also shown in Fig. 2.3 for this purpose.

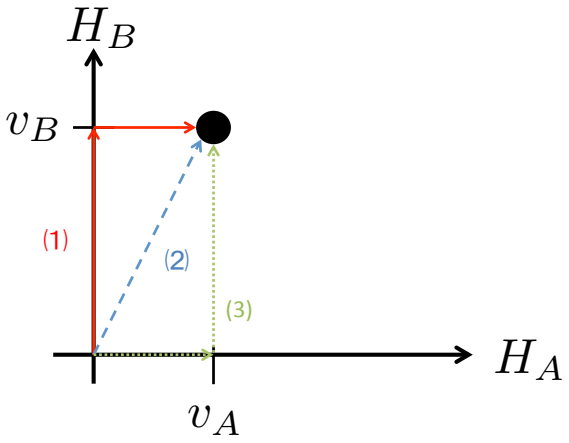

Figure 4.1: This figure shows three possible trajectories of the phase transitions. In this figure, v_A and v_B are the vacuum expectation values of the H_A and H_B fields at the zero temperature. The black point represents the true vacuum at the zero temperature. We consider only the path (1).

4.3 The electroweak phase transition

In this section, we shall study the strength of the electroweak phase transition. The thermal resummed effective potential for both of H_A and H_B Higgs fields are calculated at the one-loop order in the same way as Ref. [145], where Arnold-Espinosa prescription was used for the calculation of ring diagram. We take account of the top, twin top quarks, $\mathrm{SU(2)_W} \times \mathrm{U(1)_Y}$ gauge bosons, and $\mathrm{SU(2)_{\widehat{W}}}$ gauge bosons, respectively, because they give dominant contributions to the effective potential. The general expression of the thermal effective potential is summarized in sec. 3.3.3.

Let us calculate the thermal one-loop resummed effective potential for H_A and H_B in the non-supersymmetric case starting from the effective potential (2.51). The number of degrees

of freedom (d.o.f) and the field dependent masses of $\mathrm{SU}(2)_{\mathrm{W}} \times \mathrm{U}(1)_{\mathrm{Y}}$ gauge bosons, $\mathrm{SU}(2)_{\widehat{\mathrm{W}}}$ gauge bosons, top quark and twin top quark are given by respectively

$$n_W = 6, \quad m_W^2 = \frac{g_2^2 \phi_A^2}{4}, \tag{4.5}$$

$$n_Z = 3, \quad m_Z^2 = (g_1^2 + g_2^2)\frac{\phi_A^2}{4}, \tag{4.6}$$

$$n_{\widehat{W}} = 9, \quad m_{\widehat{W}}^2 = \frac{\widehat{g}_2^2 \phi_B^2}{4}, \tag{4.7}$$

$$n_t = 12, \quad m_t^2 = \frac{y_t^2 \phi_A^2}{2}, \tag{4.8}$$

$$n_{\widehat{t}} = 12, \quad m_{\widehat{t}}^2 = \frac{\widehat{y}_t^2 \phi_B^2}{2}. \tag{4.9}$$

Note that here we considered the Fraternal model where the mirror U(1) gauge fields are absent, but that we expect that the basic results are unchanged even if we include them since the U(1) gauge coupling is tiny. With the supersymmetric completions visible and mirror stops might also contribute, but we do not take account of them by assuming they are sufficiently heavy through the Higgs ϕ_B's VEV and are suppressed by the Boltzmann factor. With this assumption, our conclusion is applicable also to the case with the supersymmetric UV completions as long as new particle masses are not light during the electroweak phase transition.

The one-loop total effective potential V_{tot} with $\overline{\mathrm{DR}}$ regularization is explicitly given by

$$V_{\mathrm{tot}} = V_{\mathrm{tree}} + V_{\mathrm{zero}} + V_{\mathrm{thermal}}, \tag{4.10}$$

$$V_0(\phi_A,\ \phi_B) = \frac{\lambda}{4}(\phi_A^2 + \phi_B^2 - f^2)^2 + \frac{\kappa}{4}(\phi_A^4 + \phi_B^4) + \frac{\rho}{4}\phi_A^4 + \frac{\sigma}{2} f^2 \phi_A^2, \tag{4.11}$$

$$\begin{aligned} V_{\mathrm{zero}}(\phi_A,\ \phi_B) = &-\frac{3}{16\pi^2} m_t^4(\phi_A)\left(\log\left(\frac{m_t^2(\phi_A)}{\mu^2}\right) - \frac{3}{2}\right) - \frac{3}{16\pi^2} m_{\widehat{t}}^4(\phi_B)\left(\log\left(\frac{m_{\widehat{t}}^2(\phi_B)}{\mu^2}\right) - \frac{3}{2}\right) \\ &+ \frac{3}{32\pi^2} m_W^4(\phi_A)\left(\log\left(\frac{m_W^2(\phi_A)}{\mu^2}\right) - \frac{3}{2}\right) + \frac{3}{64\pi^2} m_Z^4(\phi_A)\left(\log\left(\frac{m_Z^2(\phi_A)}{\mu^2}\right) - \frac{3}{2}\right) \\ &+ \frac{9}{64\pi^2} m_{\widehat{W}}^4(\phi_B)\left(\log\left(\frac{m_{\widehat{W}}^2(\phi_B)}{\mu^2}\right) - \frac{3}{2}\right), \end{aligned} \tag{4.12}$$

$$\begin{aligned} V_{\mathrm{thermal}}(\phi_A,\ \phi_B,\ T) = &-\frac{6}{\pi^2} T^4 J_F\left[\frac{m_t^2(\phi_A)}{T^2}\right] - \frac{6}{\pi^2} T^4 J_F\left[\frac{m_{\widehat{t}}^2(\phi_B)}{T^2}\right] \\ &+ \frac{3}{\pi^2} T^4 J_B\left[\frac{m_W^2(\phi_A)}{T^2}\right] + \frac{3}{2\pi^2} T^4 J_B\left[\frac{m_Z^2(\phi_A)}{T^2}\right] + \frac{9}{2\pi^2} T^4 J_B\left[\frac{m_{\widehat{W}}^2(\phi_B)}{T^2}\right]. \end{aligned} \tag{4.13}$$

See the sec. 3.3.3 for the definition of $J_{B,F}$-function. Here, κ, ρ and σ are the tree-level couplings and do not include the contribution of the one-loop zero-temperature corrections. In addition, we consider the ring diagram contributions denoted by $V_{\rm ring}$ discussed in sec. 3.3.3 to improve the perturbativity. Since the masses of the $\mathrm{SU(2)}_{\widehat{\mathrm{W}}}$ gauge bosons originating from the VEV of the H_B field are much larger than thermal corrections to the masses around the critical temperature, the $\mathrm{SU(2)}_{\widehat{\mathrm{W}}}$ ring diagram contributions can be neglected. On the other hand, the ring diagram contributions coming from $\mathrm{SU(2)_W \times U(1)_Y}$ gauge bosons are not negligible and we need to take them into account. $V_{\rm ring}$ was computed in Ref. [146] and is given by

$$V_{\rm ring} = T \sum_{i=W_L,\ Z_L,\ \gamma_L} -\frac{n_i}{12\pi^2}\left((\overline{m}_i^2(\phi_A,\ T))^{\frac{3}{2}} - (m_i^2(\phi_A))^{\frac{3}{2}} \right), \tag{4.14}$$

with

$$n_{W_L} = 2, \quad \overline{m}_{W_L}^2(\phi_A,\ T) = m_W^2(\phi_A) + \frac{11}{6} g_2^2 T^2, \tag{4.15}$$

$$n_{Z_L} = 1, \quad \overline{m}_{Z_L}^2(\phi_A,\ T) = \frac{1}{2}\left[m_Z^2(\phi_A) + \frac{11}{6}(g_2^2+g_1^2)T^2 + \Delta(\phi_A, T) \right], \tag{4.16}$$

$$n_{\gamma_L} = 1, \quad \overline{m}_{\gamma_L}^2(\phi_A,\ T) = \frac{1}{2}\left[m_Z^2(\phi_A) + \frac{11}{6}(g_2^2+g_1^2)T^2 - \Delta(\phi_A, T) \right], \tag{4.17}$$

$$\Delta = \sqrt{m_Z^4(\phi_A) + \frac{11}{3}\frac{(g_2^2-g_1^2)^2}{g_2^2+g_1^2}\left[m_Z^2 + \frac{11}{12}(g_2^2+g_1^2)T^2 \right] T^2}. \tag{4.18}$$

The explict calculation of field dependent masses of longitudinal mode for Z-boson and photon are summerized in Appendix. 7.2. Here, n_i represents the number of d.o.f. for each longitudinal mode. We do not take account of transverse modes of the $\mathrm{SU(2)_W \times U(1)_Y}$ gauge bosons because if it gives the dramatic effect, the perturbative computation of the thermal effective potential is suffered from Linde problem as discussed in sec. 3.3.4.

In our case, the electroweak phase transition occurs after the U(4)-breaking phase transition. Therefore, during the electroweak phase transition, ϕ_B already obtains a non-zero VEV, $\phi_B(T) \neq 0$. Then, in the same way as Eq. (2.59), we integrate out the $\phi_B(T)$ field by setting

$$\phi_A^2(T) = f^2 - \phi_B^2(T). \tag{4.19}$$

Here, $\phi_{A(B)}(T)$ represent the temperature dependent VEVs, respectively. It should be noticed that, when we take the $T = 0$ limit, Eq. (4.19) is reduced to Eq. (2.59). The one-loop

resummed effective potential for h can be written as

$$V(\phi_A,\ T) = V_0(\phi_A,\ f^2-\phi_A^2) + V_{\rm CW}(\phi_A,\ f^2-\phi_A^2) + V_{\rm thermal}(\phi_A,\ f^2-\phi_A^2,\ T) + V_{\rm ring}(\phi_A,\ T), \tag{4.20}$$

where V_0, $V_{\rm CW}$, $V_{\rm thermal}$, and $V_{\rm ring}$ are given by Eq. (4.11), (4.12), (4.13), and (4.14), respectively. For the zero temperature part $V_0 + V_{\rm CW}$, we set the renormalization conditions given by

$$\left.\frac{d}{d\phi}(V_0+V_{\rm CW})\right|_{\phi=v_A} = 0, \tag{4.21}$$

$$\left.\frac{d^2}{d\phi^2}(V_0+V_{\rm CW})\right|_{\phi=v_A} = 2\lambda_{SM}v_A^2. \tag{4.22}$$

Neglecting $\mathcal{O}(\phi_A^6)$ terms, we obtain the following expression,

$$\begin{aligned} V_0 + V_{\rm CW} = &-\frac{\lambda_{SM}}{2}v_A^2\phi_A^2 + \frac{\lambda_{SM}}{4}\phi_A^4 \\ &+ \frac{n_i}{64\pi^2}\sum_i \left(m_i^4(\phi_A)\left(\log\left(\frac{m_i^2(\phi_A)}{m_i^2(v_A)}\right) - \frac{3}{2}\right) + 2m_i^2(v_A)m_i^2(\phi_A)\right), \end{aligned} \tag{4.23}$$

where the suffix i represents only the SM contribution. Now the system is parameterized only by the $U(4)$-breaking scale f since the condition (4.19) and renormalization condition Eqs. (4.21) and (4.22) completely fix the other model parameters, $\kappa_1, \sigma_1, \rho_1$, and λ.

In Ref. [145], it was shown that the one-loop effective potential obtained by use of the relation Eq. (4.19) exhibits the restoration of the electroweak symmetry at high temperature, which guarantees the presence of the electroweak phase transition. Here, we try to clarify the order of the electroweak phase transition. For this purpose, we will first check the validity of perturbative expansion near the critical temperature. As is seen in sec. 3.3.4, the perturbative expansion is valid only when the following condition is satisfied,

$$g_2^2\frac{T_C}{m_W(\phi_A(T_C))} \sim g_2\frac{T_C}{\phi_A(T_C)} < 1, \tag{4.24}$$

where T_C is the critical temperature of the EWSB. Here the critical temperature T_C is defined so that the electroweak symmetry preserving and breaking vacua are degenerate. $\phi_A(T_C)$ represents the expectation value of ϕ_A for a breaking phase at T_C.

In Fig. 4.2, the ratio $\phi_A(T_C)/T_C$ is plotted for each $U(4)$ symmetry breaking scale f. We have evaluated the one-loop resummed effective potential given in Eq. (4.20) without resort to the high temperature expansions given by Eqs. (3.97) and (3.98). It is easily seen that the

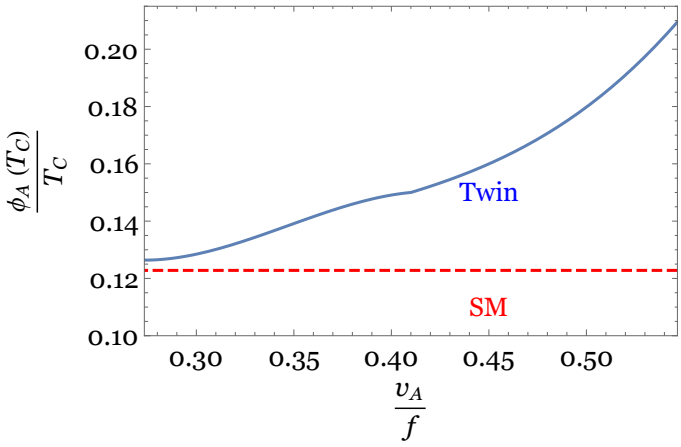

Figure 4.2: The ratio $\phi_A(T_C)/T_C$ for each $U(4)$ symmetry breaking scale f. The blue curve represents $\phi_A(T_C)/T_C$ evaluated by use of Eq. (4.20). The dashed red line represents the same ratio but with only the Standard Model contributions being taken into account.

larger a breaking scale f is, the smaller $\phi_A(T_C)/T_C$ is. This fact can be easily understood as follows. The thermal contributions from the twin particles could strengthen the first order nature of the electroweak symmetry breaking. However, the twin partners acquire masses proportional to $\phi_B(T)$ through the Higgs mechanism. Thus, a larger breaking scale f leads to larger masses of the twin particles, which easily induces thermal decoupling of twin particles during the electroweak phase transition. This decoupling makes $\phi_A(T_C)/T_C$ in our case approach the value in the standard model case. Hence a larger v_A/f indeed increases $\phi_A(T_C)/T_C$.

However, the largest value of $\phi_A(T_C)/T_C$ for $f > 2v_A$ required by the constraint of the Higgs coupling measurement is at most 0.2, which is not large enough to satisfy the criteria (4.24). Therefore, we conclude that the non-perturbative corrections from $\mathrm{SU(2)_W}$ cannot be neglected and the perturbative expansion is not valid near T_C. For the correct analysis, lattice simulations are required. This result has an important implication for the electroweak baryogenesis because it requires the sphaleron decoupling condition $\phi_A(T_C)/T_C > 1$ around the critical temperature. Our results strongly suggest that this condition is hardly satisfied in the Fraternal twin Higgs model as long as the condition (4.19) is valid, and we cannot expect for the implementation of the electroweak baryogenesis. This conclusion remains unchanged even if we go beyond the Fraternal model, as long as the condition (4.19) and the assumption of the trajectory of two-step phase transition are adopted. We do not exclude

the possibility to have the strong first order electroweak phase transition once we relax one of these assumptions, which is beyond the scope of the present study.

Finally let us comment on some issues on UV completions. We here do not assume concrete UV physics (SUSY and composite Higgs) in our analysis and analyze the electroweak phase transition by use of effective field theory for the ϕ_A field. As long as its usage is valid, our result is still robust in supersymmetric and composite twin Higgs models. However, it was shown in Refs. [147, 148] that the electroweak phase transition can be the strong first order in the composite Higgs scenario. In the setup adopted in Refs. [147, 148], the electroweak phase transition and the confinement phase transition, which corresponds to the U(4)-breaking phase transition in twin Higgs models, occurred simultaneously. In addition, the SM-like Higgs field couples with an additional scalar field. Thus this approach does not apply to our consideration.

4.4 The U(4)-breaking phase transition

In this section, we explore the U(4)-breaking phase transition in twin Higgs models with and without supersymmetric UV completion. For the concrete calculation, we adopt the Fraternal model, but general features would apply to other models. (See Ref. [149] for general discussions of gravitational wave productions from a first order phase transition associated with SU(N) breaking into SU(N − 1) in a hidden sector.) As discussed in Sec. 4.3, we assume that the U(4)-breaking phase transition occurs first and the electroweak phase transition does next in the following discussion.

4.4.1 The case of the twin Higgs model without UV completion

Let us first consider the twin Higgs model without any UV completions, in the sense that no new particles other than the mirror particles to the SM are involved. The U(4)-breaking phase transition generally depends on UV physics such as SUSY and composite Higgs. However, if new particles in the UV completion are sufficiently heavy during the phase transition, we can safely neglect the effect of these particles. We shall study the strength of the U(4)-breaking phase transition by using the potential (2.51) with this assumption.

In our set up, the Higgs field H_A is trapped at the origin of the potential $H_A = 0$ due to the thermal mass term during the U(4)-breaking phase transition. Thus, we take the

background fields as

$$H_A = \begin{pmatrix} 0 \\ 0 \end{pmatrix}, \qquad H_B = \begin{pmatrix} 0 \\ \dfrac{\phi_B}{\sqrt{2}} \end{pmatrix}. \tag{4.25}$$

and calculate the resummed one-loop potential given by Eq. (3.106) for the field H_B. We take account of the twin top and $\mathrm{SU}(2)_{\widehat{\mathrm{W}}}$ gauge bosons which give dominant contributions to the effective potential. On the other hand, a larger quartic coupling $\lambda > \widehat{g}_2^2$ makes the U(4)-breaking phase transition weaker $\phi_B(T_C)/T_C < \widehat{g}_2$, and hence, we consider a small quartic coupling $\lambda < \widehat{g}_2^2$. Since the quartic coupling $\lambda < \widehat{g}_2^2$ is smaller than $\widehat{g}_2$ and $y_{\widehat{t}}$, we neglect the H_A and H_B loop contributions to the effective potential in the following discussion.

With the field dependent masses of the twin top and $\mathrm{SU}(2)_{\widehat{\mathrm{W}}}$ gauge bosons given by Eqs. (4.7) and (4.9), The one-loop effective potential V_{eff} is expressed as

$$V_{\mathrm{eff}} = V_0 + V_{\mathrm{zero}} + V_{\mathrm{thermal}}, \tag{4.26}$$

$$V_0(\phi_B) = \frac{\lambda}{4}(\phi_B^2 - f^2)^2 + \frac{\kappa}{4}\phi_B^4 = -\frac{\lambda}{2}f^2\phi_B^2 + \frac{\lambda+\kappa}{4}\phi_B^4 + \frac{\lambda}{4}f^4, \tag{4.27}$$

$$V_{\mathrm{zero}}(\phi_B) = -\frac{3}{16\pi^2}m_{\widehat{t}}^4(\phi_B)\left(\log\left(\frac{m_{\widehat{t}}^2(\phi_B)}{\mu^2}\right) - \frac{3}{2}\right) + \frac{9}{64\pi^2}m_{\widehat{W}}^4(\phi_B)\left(\log\left(\frac{m_{\widehat{W}}^2(\phi_B)}{\mu^2}\right) - \frac{3}{2}\right), \tag{4.28}$$

$$V_{\mathrm{thermal}}(\phi_B,\ T) = -\frac{6}{\pi^2}T^4 J_F\left[\frac{m_{\widehat{t}}^2(\phi_B)}{T^2}\right] + \frac{9}{2\pi^2}T^4 J_B\left[\frac{m_{\widehat{W}}^2(\phi_B)}{T^2}\right]. \tag{4.29}$$

In order to find the ring diagram contribution V_{ring}, we need to evaluate the thermal masses of the $\mathrm{SU}(2)_{\widehat{\mathrm{W}}}$ gauge bosons. We here take account of the one-loop self-energy of longitudinal modes [150]

$$\Pi_{\widehat{W}_L} = \frac{7}{6}\widehat{g}_2^2 T^2, \tag{4.30}$$

in which only one generation (third generation) is included for the Fraternal model. The transverse modes receive the magnetic masses, but we omit them as is the case of the electroweak phase transition. We then obtain the ring diagram contribution V_{ring} given by

$$V_{\mathrm{ring}} = -\frac{T}{4\pi}\left(\left(\overline{m}_{\widehat{W}_L}^2(\phi_B,\ T)\right)^{\frac{3}{2}} - \left(m_{\widehat{W}}^2(\phi_B)\right)^{\frac{3}{2}}\right), \tag{4.31}$$

$$\overline{m}_{\widehat{W}_L}^2 = m_{\widehat{W}}^2(\phi_B) + \Pi_{\widehat{W}_L}. \tag{4.32}$$

When we use the high-temperature expansions given by Eq. (3.97) and Eq. (3.98), the resummed one-loop effective potential takes the following form:

$$\begin{aligned} V &= V_0 + V_{\rm CW} + V_{\rm Thermal} + V_{\rm ring} \\ &= \frac{1}{2}M^2(T)\phi_B^2 - \frac{T}{2\pi}\left(\frac{\widehat{g}_2^2\phi_B^2}{4}\right)^{3/2} - \frac{T}{4\pi}\left(\frac{\widehat{g}_2^2\phi_B^2}{4} + \Pi_{\widehat{W}_L}\right)^{\frac{3}{2}} + \frac{\lambda+\kappa_1(T)}{4}\phi_B^4, \end{aligned} \tag{4.33}$$

where

$$M^2(T) = -\lambda f^2 + \frac{\widehat{y}_t^2}{4}T^2 + \frac{3\widehat{g}_2^2}{16}T^2, \tag{4.34}$$

$$\kappa_1(T) = \kappa - \frac{3\widehat{y}_t^4}{16\pi^2}\left(\log\left(\frac{a_f T^2}{\mu^2}\right) - \frac{3}{2}\right) + \frac{9\widehat{g}_2^4}{256\pi^2}\log\left(\left(\frac{a_b T^2}{\mu^2}\right) - \frac{3}{2}\right). \tag{4.35}$$

We here analyze the order of the phase transition by using the approach, which is different from the one explained in Sec. 4.1. Thanks to the twin $\mathbf{Z_2}$ symmetry, $y_t \simeq \widehat{y}_t$ and $g_2 \simeq \widehat{g}_2$, the U(4)-breaking phase transition described by the potential (4.33) is similar to the electroweak phase transition in the SM studied in sec. 3.4.3. As discussed in that section, lattice simulations indicate that the electroweak phase transition in the SM is of the first order when $m_H \lesssim 70 - 80$ GeV (or $\lambda_{\rm SM} \lesssim 0.04$) is satisfied.

Here, let us derive the condition of first-order U(4)-breaking phase transition by utilizing the lattice results of the electroweak phase transition within the SM framework, in which the the quartic coupling $\lambda_{\rm SM}$ is treated as a free parameter. One might wonder if the difference between U(4)-breaking sector and the SM sector prevents us from adopting the results of the SM to the U(4)-breaking case. But these differences are negligible for our purpose in the following reasons. First of all, the breaking scale of the U(4)-breaking phase transition, f, is different from that of the electroweak phase transition, v_A. However, the order of the electroweak phase transition in the SM depends on the parameter $\lambda_{\rm SM}/g_2^2$ [151], but not v_A. Thus, we have only to identify $\lambda + \kappa_1$ in our model with $\lambda_{\rm SM}$ in the SM electroweak phase transition. Second, there is no $\mathrm{U}(1)_{\widehat{\rm Y}}$ gauge boson in the Fraternal twin Higgs model. Since the $\mathrm{U}(1)_{\widehat{\rm Y}}$ gauge coupling $\widehat{g}_1$ is tiny compared to the $\mathrm{SU}(2)_{\widehat{\rm W}}$ gauge coupling $\widehat{g}_2$, we can neglect this effect safely. Indeed, the original paper [151] also does not include $\mathrm{U}(1)_{\rm Y}$ and they concluded that the error due to this assumption is small enough. Finally, the coefficient of the thermal mass (4.30) for the Fraternal model[1] differs from that of the $\mathrm{SU}(2)_{\rm W}$ gauge bosons in the SM. In the lattice simulation [151], they use the three-dimensional effective

[1] In the Mirror twin Higgs models the coefficient of the thermal mass is the same to the SM.

Lagrangian obtained by integrating out all fermions and the longitudinal modes of $SU(2)_W$ gauge bosons [152, 153, 154], which affects the values of the parameters λ_{SM} and g_2. We confirmed that this difference gives only 10 percent changes in the parameters of three-dimensional effective Lagrangian, and hence we can safely neglect it. Therefore, the order of the U(4)-breaking phase transition can be analyzed by use of the result of the electroweak phase transition in the SM. We conclude that the U(4)-breaking phase transition is the first order when $\lambda + \kappa_1 \lesssim 0.04$ is satisfied, thanks to $y_t \simeq y_{\widehat{t}}$ and $g_2 \simeq \widehat{g}_2$.

As discussed in Sec. 2.3.2, the parameters κ_1 and λ are bounded below, $\lambda + \kappa_1 \gtrsim 0.1$, due to the EWSB conditions and the conditions $\lambda > \sigma_1,\ \kappa_1,\ \rho_1$ as we can see from Fig. 2.3. Therefore, it cannot satisfy the condition for the first order U(4)-breaking phase transition, $\lambda + \kappa_1 \lesssim 0.04$. We also expect no gravitational wave production because of the absence of a first order phase transition in the case of twin Higgs models without any UV completions. The differences in the Fraternal and Mirror models give minor effects and are within the uncertainties in our estimate. More generally, our conclusion is robust in any models as long as the tree-level potential is given by Eq. (2.51) and there are no additional light degrees of freedom so that the thermal masses for twin $SU(2)_{\widehat{W}}$ gauge bosons do not differ so much.

4.4.2 The case of supersymmetric twin Higgs models

In the previous subsection, we do not consider effects of UV physics such as composite Higgs and SUSY on the U(4)-breaking phase transition. If other fields strongly couple to the Higgs field H_B, we cannot apply the argument in the previous subsection. Let us now consider supersymmetric twin Higgs models and explore the order of the U(4)-breaking phase transition. Especially, since any such models contain twin stops, which are strongly coupled to the Higgs field H_B and possibly light at the restored phase in the absence of the Higgs VEV, we focus on the effect of light twin stops. This is because, as we discussed in Sec. 3.4.4, when the H_B field strongly couples to the light bosonic particles, the strength of U(4)-breaking phase transition can be enhanced. Hereafter, we take the decoupling limit, simply assuming that every supersymmetric partner except for twin stops acquires a large soft mass and decouples with thermal plasma during the U(4)-breaking phase transition. We will show that there is some parameter space where the U(4)-breaking phase transition is of the first order and estimate the gravitational wave amplitude generated through this phase transition.

Let us calculate the one-loop resummed effective potential. Since we take the decoupling limit as explained in section 2.3.3, the background fields are given by

$$H_u^A = \begin{pmatrix} 0 \\ 0 \end{pmatrix}, \quad H_d^A = \begin{pmatrix} 0 \\ 0 \end{pmatrix}, \quad H_u^B = \begin{pmatrix} 0 \\ \frac{\phi_B}{\sqrt{2}} \sin\beta \end{pmatrix}, \quad H_d^B = \begin{pmatrix} \frac{\phi_B}{\sqrt{2}} \cos\beta \\ 0 \end{pmatrix}. \tag{4.36}$$

We take account of the left and right-handed twin stops, the twin top quarks and the $\mathrm{SU}(2)_{\widehat{\mathrm{W}}}$ gauge bosons, which give dominant contributions to the effective potential. We neglect the Higgs loop correction as is the non-supersymmetric case. The tree level potential V_0 can be concretely written as

$$V_0 = \frac{\lambda}{4}(\phi_B^2 - f^2)^2 + \frac{\kappa}{4}\phi_B^4, \tag{4.37}$$

where the second term includes the D-term contribution, $\kappa \supset \widehat{g}_2^2 \cos^2 2\beta/8$. The thermal one-loop corrections V_{zero} and V_{thermal} are evaluated as follows. The field dependent masses of twin top quarks and $\mathrm{SU}(2)_{\widehat{\mathrm{W}}}$ gauge bosons are given by Eqs. (4.9) and (4.7). Those of the left and right-handed twin stops can be written as

$$\mathcal{M}^2_{\widehat{\mathrm{stop}}} = \begin{pmatrix} \widetilde{m}^2_{\widehat{Q}} + m^2_{\widehat{t}}(\phi_B) + \frac{\widehat{g}_2^2}{8}\phi_B^2 \cos 2\beta & m_{\widehat{t}}(\phi_B) X_{\widehat{t}} \\ m_{\widehat{t}}(\phi_B) X_{\widehat{t}} & \widetilde{m}^2_{\widehat{t}_R} + m^2_{\widehat{t}}(\phi_B) \end{pmatrix}, \quad X_{\widehat{t}} \equiv A_{\widehat{t}} - \mu \cot\beta, \tag{4.38}$$

where $\widetilde{m}^2_{\widehat{Q}}$, $\widetilde{m}^2_{\widehat{t}_R}$ and $A_{\widehat{t}}$ are the twin left, right-handed stop soft mass-squared and the twin A-term, respectively. The diagonalized masses are given by

$$n_{\widetilde{t}}^{1(2)} = 6, \tag{4.39}$$

$$m^2_{\widetilde{t}^B_{1,2}}(\phi_B) = \frac{(\mathcal{M}^2_{\widehat{\mathrm{stop}}})_{11} + (\mathcal{M}^2_{\widehat{\mathrm{stop}}})_{22}}{2} \pm \sqrt{\left(\frac{(\mathcal{M}^2_{\widehat{\mathrm{stop}}})_{11} - (\mathcal{M}^2_{\widehat{\mathrm{stop}}})_{22}}{2}\right)^2 + \left((\mathcal{M}^2_{\widehat{\mathrm{stop}}})_{12}\right)^2}, \tag{4.40}$$

where $n_{\widetilde{t}}^{1(2)}$ and the superscript of $\mathcal{M}^2_{\widehat{\mathrm{stop}}}$ represent the number of d.o.f for the left (or right)-handed twin stop and the component of $\mathcal{M}^2_{\widehat{\mathrm{stop}}}$ matrix, respectively. The one-loop effective

potential is then written as

$$V_{\rm zero}(\phi_B) = -\frac{3}{16\pi^2} m_{\widehat{t}}^4(\phi_B)\left(\log\left(\frac{m_{\widehat{t}}^2(\phi_B)}{\mu^2}\right) - \frac{3}{2}\right) + \frac{9}{64\pi^2} m_{\widehat{W}}^4(\phi_B)\left(\log\left(\frac{m_{\widehat{W}}^2(\phi_B)}{\mu^2}\right) - \frac{3}{2}\right)$$
$$+ \frac{3}{32\pi^2} m_{\tilde{t}_1^B}^4(\phi_B)\left(\log\left(\frac{m_{\tilde{t}_1^B}^2(\phi_B)}{\mu^2}\right) - \frac{3}{2}\right) + \frac{3}{32\pi^2} m_{\tilde{t}_2^B}^4(\phi_B)\left(\log\left(\frac{m_{\tilde{t}_2^B}^2(\phi_B)}{\mu^2}\right) - \frac{3}{2}\right), \tag{4.41}$$

$$V_{\rm thermal}(\phi_B,\ T) = -\frac{6}{\pi^2} T^4 J_F\left[\frac{m_{\widehat{t}}^2(\phi_B)}{T^2}\right] + \frac{9}{2\pi^2} T^4 J_B\left[\frac{m_{\widehat{W}}^2(\phi_B)}{T^2}\right]$$
$$+ \frac{3}{\pi^2} T^4 J_B\left[\frac{m_{\tilde{t}_1^B}^2(\phi_B)}{T^2}\right] + \frac{3}{\pi^2} T^4 J_B\left[\frac{m_{\tilde{t}_2^B}^2(\phi_B)}{T^2}\right]. \tag{4.42}$$

In order to calculate the ring diagram contribution $V_{\rm ring}$, we need to evaluate thermal masses of the longitudinal mode of the $\mathrm{SU}(2)_{\widehat{\mathrm{W}}}$ gauge bosons. As a result of the twin $\mathbf{Z}_2$ symmetry, thermal masses of the $\mathrm{SU}(2)_{\widehat{\mathrm{W}}}$ gauge bosons can be calculated in the same way as the case of the minimal supersymmetric standard model [150]. The thermal masses of the longitudinal mode of the $\mathrm{SU}(2)_{\widehat{\mathrm{W}}}$ gauge bosons, the left and right-handed twin stops are given by

$$\Pi_{\widehat{W}_L} = \frac{5\widehat{g}_2^2}{3} T^2, \tag{4.43}$$
$$\Pi_{\widehat{t}_R} = \frac{4}{9}\widehat{g}_3^2 T^2 + \frac{\widehat{y}_t^2}{6}\left(1 + \frac{1}{\sin^2\beta}\right) T^2, \tag{4.44}$$
$$\Pi_{\widehat{Q}} = \frac{4}{9}\widehat{g}_3^2 T^2 + \frac{\widehat{y}_t^2}{12}\left(1 + \frac{1}{\sin^2\beta}\right) T^2 + \frac{\widehat{g}_2^2}{4} T^2. \tag{4.45}$$

Then the temperature dependent mass matrix is given by

$$\overline{\mathcal{M}}_{\widehat{\rm stop}}^2 = \begin{pmatrix} \widetilde{m}_{\widehat{Q}}^2 + m_{\widehat{t}}^2(\phi_B) + \frac{\widehat{g}_2^2}{8}\phi_B^2 \cos 2\beta + \Pi_{\widehat{Q}} & m_{\widehat{t}}(\phi_B) X_{\widehat{t}} \\ m_{\widehat{t}}(\phi_B) X_{\widehat{t}} & \widetilde{m}_{\widehat{t}_R}^2 + m_{\widehat{t}}^2(\phi_B) + \Pi_{\widehat{t}_R} \end{pmatrix}, \tag{4.46}$$
$$n_{\widetilde{t}}^{1(2)} = 6, \tag{4.47}$$

where $n_{\widetilde{t}}^{1(2)}$ represents the number of d.o.f for the left (or right)-handed twin stop. From this

expression, the ring diagram contributions are calculated as follows.

$$V_{\rm ring} = -\frac{T}{4\pi}\left((\overline{m}^2_{\widehat{W}_L}(\phi_B,\ T))^{\frac{3}{2}} - (m^2_{\widehat{W}}(\phi_B))^{\frac{3}{2}}\right) - \frac{T}{2\pi}\left((\overline{m}^2_{\tilde{t}^B_1}(\phi_B))^{\frac{3}{2}} - (m^2_{\tilde{t}^B_1}(\phi_B))^{\frac{3}{2}} + ((\overline{m}^2_{\tilde{t}^B_2}(\phi_B))^{\frac{3}{2}} - (m^2_{\tilde{t}^B_2}(\phi_B))^{\frac{3}{2}}\right), \tag{4.48}$$

$$\overline{m}^2_{\tilde{t}^B_{1,2}}(\phi_B) = \frac{(\overline{\mathcal{M}}^2_{\widehat{\rm stop}})_{11} + (\overline{\mathcal{M}}^2_{\widehat{\rm stop}})_{22}}{2} \pm \sqrt{\left(\frac{(\overline{\mathcal{M}}^2_{\widehat{\rm stop}})_{11} - (\overline{\mathcal{M}}^2_{\widehat{\rm stop}})_{22}}{2}\right)^2 + \left((\overline{\mathcal{M}}^2_{\widehat{\rm stop}})_{12}\right)^2}. \tag{4.49}$$

Moreover, in our set up, the twin QCD two-loop contribution is non-negligible compared to the resummed one-loop effective potential because the large strong coupling $\widehat{g}_3$ and the top Yukawa coupling $\widehat{y}_t$ are large compared to the other matter couplings.[2] In the MSSM, the sunset diagram, which gives the dominant contribution, is evaluated in Ref. [155]. We adopt it and calculate the two-loop twin QCD contribution as

$$V^{(2)}_{\rm thermal} = -\frac{\widehat{g}_3^2}{2\pi^2}T^2\left((\overline{m}^2_{\tilde{t}^B_1}(\phi_B))^2\log\left(\frac{2\overline{m}^2_{\tilde{t}^B_1}(\phi_B)}{3T}\right) + (\overline{m}^2_{\tilde{t}^B_2}(\phi_B))^2\log\left(\frac{2\overline{m}^2_{\tilde{t}^B_2}(\phi_B)}{3T}\right)\right). \tag{4.50}$$

In this expression, the high-temperature expansion [122] and mass-averaging approximation [121] are used. According to the discussions in Refs. [156, 157], their usage is justified for our purpose. It should be noticed that this negative logarithmic dependence of ϕ_B in Eq. (4.50) gives an additional contribution to the potential barrier between the origin and another minimum. Without taking this contribution into account, we would underestimate $\phi_B(T_C)/T_C$.

As discussed in Sec. 3.4.2, in order to realize the first order phase transition at the perturbative calculation and gravitational wave production, $\phi_B(T_C)/T_C \gtrsim \widehat{g}_2$ is required. This ratio becomes larger for a smaller $\lambda + \kappa_1$ (See discussion in Sec. 3.4.4.). As discussed in Sec. 2.3.2 (see Fig. 2.3), we have the conditions $\lambda > 0.05$ and $\kappa_1 > 0.05$, from the requirements $\lambda > \rho_1, \kappa_1$ and $m_h \simeq 125$ GeV. Thus hereafter we take $\lambda \simeq 0.05$ and $\kappa_1 \simeq 0.05$ as the benchmark point. For simplicity we require the quartic coupling κ_1 is dominated by the D-term, $\kappa \simeq (\widehat{g}_2^2/8)\cos^2 2\beta$, so that $\tan\beta \simeq 10$. The value of the twin QCD coupling

[2] You may wonder that this contribution is sufficiently suppressed by the loop factor. However, since the twin gluon belongs to the adjoint representation of $\mathrm{SU}(3)_{\widehat{\mathrm{C}}}$, degrees of freedoms of it is $n_{\widehat{\mathrm{g}}} = 8$, which is comparable to the loop suppression.

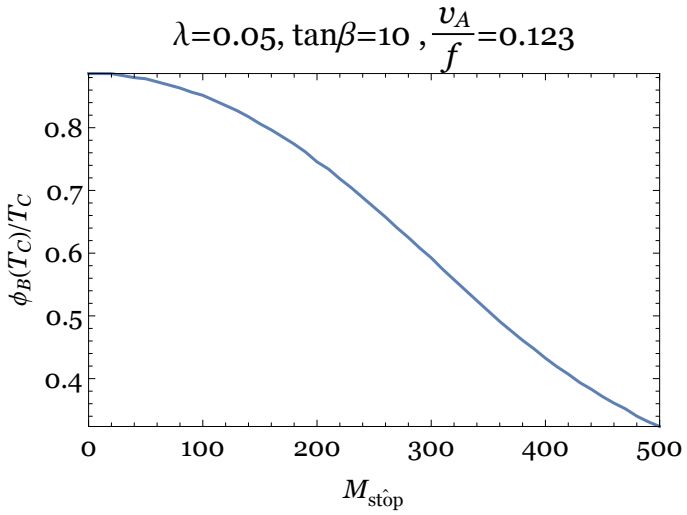

Figure 4.3: This graph shows $\phi_B(T_C)/T_C$ and common left, right-handed twin stop soft masses. We set some physical parameters as $\lambda = 0.05$, $\widehat{g}_3 = 1$, $\tan\beta = 10$, $X_{\widehat{t}} = 0$ and $v_A/f = 0.123$.

constant $\widehat{g}_3$ can be somewhat different from the value of the visible QCD coupling constant g_3 because the exact $\mathbf{Z_2}$ symmetry is not necessary from the view point of naturalness [78, 158]. Here we simply set the twin QCD coupling to be $\widehat{g}_3 = 1$. The change of the value of $\widehat{g}_3$ allowed by naturalness leads to a 10% effect for $\phi_B(T_C)/T_C$. In addition, we take $X_{\widehat{t}} = 0$ in our evaluation for the following reason. A non-zero $X_{\widehat{t}}$ tends to induce unwanted color-breaking vacua. In order to avoid the appearance of such vacua, larger soft masses are required, which reduces the ratio between the effective mass and the cubic term. Thus, with a non-zero $X_{\widehat{t}}$, $\phi_B(T_C)/T_C$ will be smaller compared to the case with a vanishing $X_{\widehat{t}}$.

Now the ratio $\phi_B(T_C)/T_C$ is determined by the twin stop soft parameters and the U(4)-breaking scale f. Figure 4.3 shows the ratio $\phi_B(T_C)/T_C$ as the function of the left and right-handed twin stop (common) soft masses $|\widetilde{m}^2_{\widehat{Q}}| = |\widetilde{m}^2_{\widehat{t}_R}| \equiv M^2_{\widehat{\text{stop}}}$ for $v_A/f = 0.123$. The renormalization scale is set to be $\mu = T$. We can see that the ratio $\phi_B(T_C)/T_C$ takes the maximal value for the massless limit of the light twin stop $M_{\widehat{\text{stop}}} \simeq 0$, which is roughly 0.9. For other choices of the ratio $v_A/f \gtrsim 0.1$, required from the point of view of naturalness, we confirmed that $\phi_B(T_C)/T_C \simeq 0.9 > \widehat{g}_2$ for $M_{\widehat{\text{stop}}} \simeq 0$. Thus, for this parameter choice, the phase transition is of the first order, which leads to the generation of the gravitational wave. Note that here we admit the strong violation of the $\mathbf{Z}_2$ symmetry in the soft stop mass, but we assume that the $\mathbf{Z}_2$ symmetry is hold for $\tan\beta$ otherwise we cannot have the

$T_{\rm n}$ [GeV]	$\phi_B(T_{\rm n})/T_{\rm n}$	α	$\beta/{\rm H}(T_{\rm n})$
682	1	7×10^{-3}	7×10^{4}

Table 4.1: Parameters $T_{\rm n}$, $\phi_B(T_{\rm n})/T_{\rm n}$, α and $\beta/{\rm H}(T_{\rm n})$ for the evaluation of the spectrum of gravitational wave background with the benchmark point $\lambda = 0.05$, $\widehat{g}_3 = 1$, $\kappa_1 = 0.05$, $M_{\widehat{\rm stop}} = 0$, $X_{\widehat{t}} = 0$, $v_A/f = 0.123$ and $\tan\beta = 10$.

Mexican-hat type U(4)-breaking potential.

Now let us evaluate the GW signals generated in this model. For this purpose, we need to estimate the nucleation temperature $T_{\rm n}$, α parameter and the duration of the phase transition β (See Sec. 3.4.5 for the detailed definitions of these parameters). They can be obtained by solving the bounce equations for the thermal resummed effective potential $V(\phi_B,\ T) = V_0 + V_{\rm zero} + V_{\rm thermal} + V_{\rm ring} + V^{(2)}_{\rm thermal}$. Table 4.1 shows the values of these parameters for our benchmark points, $\lambda = 0.05$, $\kappa_1 = 0.05$, $\widehat{g}_3 = 1$, $\tan\beta = 10$, $X_{\widehat{t}} = 0$, and $v_A/f = 0.123$.

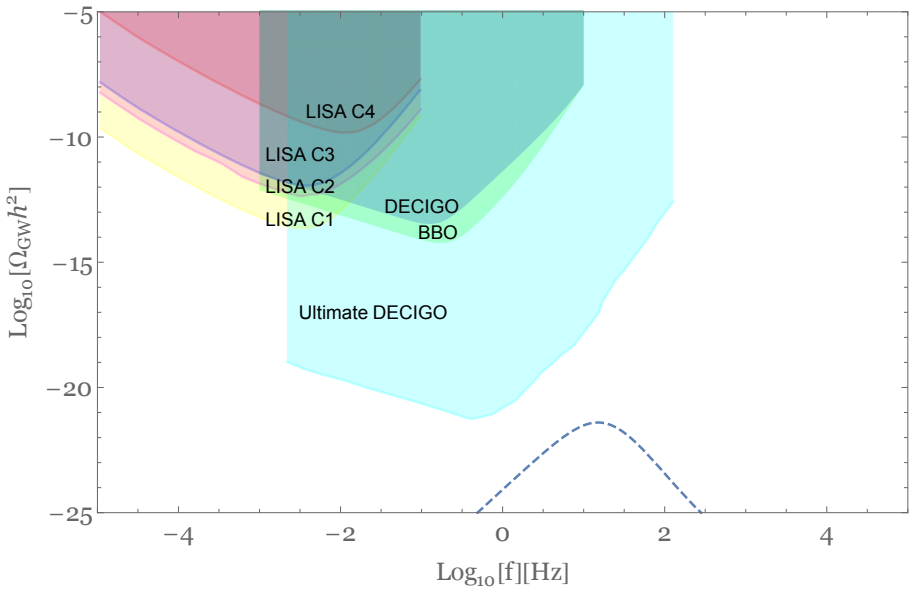

Figure 4.4: The maximal gravitational wave amplitude realized in the twin Higgs model with light twin stop is shown. Sensitivity curves of future-palned experiments such as LISA, BBO, DECIGO and ultimate-DECIGO are also shown.

Figure 4.4 shows the GW signal for our benchmark point (see sec. 3.4.5 for the formalism to calculate it). The most dominant source of the gravitational wave for our benchmark

point is found to be the sound wave of the plasma bulk motion after the bubble collision, $\Omega_{\rm gw}h^2 \simeq \Omega_{\rm sw}h^2$ given by (3.136). The peak frequency is around $\mathcal{O}(10)$Hz and the peak amplitude of gravitational wave is around $\mathcal{O}(10^{-19})$ due to the large $\beta/\mathrm{H}(T_{\rm n}) \simeq 7\times 10^4$ and small $\alpha \simeq 7\times 10^{-3}$. We can easily see that it is well below the sensitivities of LISA, DECIGO, BBO and ultimate-DECIGO.

Note that the Fig. 4.4 is different from the figure found in the original work in Ref. [63]. After the publication of this paper, the suppression on gravitational wave amplitude from sound waves given by Eq. (3.137), which was *not* included in our original analysis, was pointed out. Therefore, in this thesis, we include this suppression factor to improve our original result although our conclusion is unchanged.

It is nontrivial whether our benchmark point, which gives the maximal ratio $\phi_B(T_C)/T_C$, gives the maximal amplitude of the GW signals. We numerically confirmed that it is approximately maximal for our benchmark point. Concretely,

- For λ, κ_1 and $M_{\widehat{\rm stop}}$, we confirmed that smaller $\lambda+\kappa_1$ and $M_{\widehat{\rm stop}}$ give larger gravitational wave amplitude. Since we restrict them as $\lambda > 0.05, \kappa_1 > 0.05$, and $M_{\widehat{\rm stop}} > 0$,[3] our benchmark point gives the maximal amplitude.

- The peak amplitude of GW signals, $\Omega_{\rm GW}^{\rm peak}h^2$, does not depend on the breaking scale f. We can write the effective potential as $V(\phi_B,\ T,\ f,\ M_{\widehat{\rm stop}}) = T^4\mu(\widetilde{\phi},\ \widetilde{f},\ \widetilde{M}_{\widehat{\rm stop}})$, where $\widetilde{\phi},\ \widetilde{f}$ and $\widetilde{M}_{\widehat{\rm stop}}$ are parameters normalized by the temperature, $\widetilde{\phi} \equiv \phi/T,\ \widetilde{f} \equiv f/T$ and $\widetilde{M}_{\widehat{\rm stop}} \equiv M_{\widehat{\rm stop}}/T$. One can show that the bounce action S_3/T given by (3.116) is $S_3/T = S_3/T(\widetilde{\phi},\ \widetilde{f},\ \widetilde{M}_{\widehat{\rm stop}})$, after rescaling the radial coordinate as $r' = r/T$. Then by definitions of α and β parameters given by (3.132) and (3.133), we obtain $\alpha = \alpha(\widetilde{\phi},\ \widetilde{f},\ \widetilde{M}_{\widehat{\rm stop}})$ and $\beta/H = \beta/H(\widetilde{\phi},\ \widetilde{f},\ \widetilde{M}_{\widehat{\rm stop}})$. The peak amplitude of gravitational wave, $\Omega_{\rm GW}^{\rm peak}h^2$, only depends on the α and β/H parameters at $T = T_{\rm n}$ hence we obtain $\Omega_{\rm GW}^{\rm peak}h^2 = \Omega_{\rm GW}^{\rm peak}h^2(\widetilde{\phi},\ \widetilde{f},\ \widetilde{M}_{\widehat{\rm stop}})|_{T=T_{\rm n}}$. The nucleation temperature is roughly given by $T_n \simeq T_B \simeq T_C$, where T_B and T_C are given in Sec. 4.3 and App. 3.3.3, respectively. From the expression (4.3), we can easily find $f/T_n \simeq f/T_B = \text{const}$. In addition, from the expression (3.112), the fraction $\phi_B(T_{\rm n})/T_{\rm n} \simeq \phi_B(T_C)/T_C$ does not depend on the

[3] Note that when we allow the negative twin stop soft masses, the gravitational wave amplitude would be larger. In this case, however, we have to take account of the $SU(3)_{\widehat{C}}$ breaking minimum hence we do not consider such a scenario in our analysis.

breaking scale f (the quartic coupling ξ is less sensitive to the change of $T_{\rm n}$). Thus, when we vary the breaking scale f with $M_{\widehat{\rm stop}} = 0$, the peak amplitude of gravitational wave does not change. On the other hand, the peak frequency $f_{\rm sound}$ is proportional to the nucleation temperature, $T_{\rm n}$, hence a smaller f leads to a lower peak frequency due to the lower nucleation temperature. We numerically confirm this behavior.

- We numerically confirm that a smaller $\tan\beta$ makes the gravitational wave amplitude larger. However, a smaller $\tan\beta$ leads to a larger up-type Higgs-top Yukawa coupling, $Y_{\hat{t}} = y_{\hat{t}}/\sin\beta$. Here we impose the perturbative condition of the Yukawa coupling $Y_{\hat{t}}^2/(4\pi) \lesssim 1$ at the electroweak scale. This condition gives $\tan\beta \gtrsim 0.28$. For $\tan\beta = 0.28$, the peak amplitude of gravitational wave is larger than that of $\tan\beta = 10$ by merely around factor 10.

Note also that the change of the value of the twin QCD coupling constant allowed by naturalness affects the amplitude of gravitational wave by around factor 10 at most, and hence this effect does not change our result significantly. Thus, we conclude that, even if we take the effect of a light twin stop into account, it is almost impossible to generate gravitational wave background detectable by DECIGO, BBO or ultimate-DECIGO.

Finally, we would like to give some comments. We have assumed that ϕ_B acquires the VEV first and ϕ_A does later. In order to verify this assumption, we have calculated the thermal resummed effective potential $V(\phi_A,\ \phi_B,\ T_{\rm n})$ for both of the Higgs fields ϕ_A and ϕ_B when ϕ_B obtains the VEV at $T = T_{\rm n}$. We numerically confirmed that the potential minimum appears only in the ϕ_B direction at $T_{\rm n}$ given in TABLE. 4.1. Therefore, the assumption of two-step phase transition is validated.

4.5 Summary and Discussion

In this section, we give a summary of results obtained in this chapter and discussions related to the twin Higgs models.

We have investigated the dynamics of the electroweak phase transition and the phase transition associated with global U(4) breaking in twin Higgs models with and without supersymmetric completion. In Sec. 4.3, we found that the electroweak phase transition in twin Higgs models cannot be analyzed perturbatively as long as the effective potential is

given by (2.51) and (4.19). It does not satisfy the condition of a strong first order phase transition, and hence we cannot expect for the realization of the electroweak baryogenesis as well as the generation of gravitational wave background. In Sec. 4.4.1, we considered the U(4)-breaking phase transition in twin Higgs models without any UV completions such as composite Higgs and SUSY. We confirmed that the U(4)-breaking phase transition is the first order only when $\lambda + \kappa_1 \lesssim 0.04$ is satisfied. However, as discussed in Sec. 2.3.3, we obtained the relation $\lambda + \kappa_1 > 0.1$ in order to realize the adequate EWSB and the conditions $\lambda > \sigma_1,\ \kappa_1,\ \rho_1$. Thus, the U(4)-breaking phase transition cannot be the first order, and we expect that there is no gravitational wave production. In Sec. 4.4.2, we considered the U(4)-breaking phase transition with supersymmetric UV completions in the decoupling limit where only the effect of light twin stops is taken into account. We calculated the resummed effective potential including the dominant two-loop twin QCD contribution. Then, we confirmed that the U(4)-breaking phase transition can be analyzed perturbatively only when the light twin stop masses with $M_{\widehat{\text{soft}}} \simeq 0$ are realized. We calculated the largest possible gravitational wave amplitude within the parameters for which the electroweak symmetry breaking conditions and the conditions $\lambda > \sigma_1,\ \kappa_1,\ \rho_1$ are satisfied. However, we found that the gravitational wave amplitude cannot reach the detectable regions by LISA, DECIGO, BBO and ultimate-DECIGO. We conclude that it is impossible to produce large enough amplitude of gravitational wave to be detected by DECIGO or BBO in twin Higgs models, under our assumptions such as taking the decoupling limit, the perturbative conditions $\lambda > \sigma_1,\ \kappa_1,\ \rho_1$ and the trajectory of two-step phase transition.

If there is an additional field strongly coupled to the Higgs fields H_A and H_B, the dynamics of the electroweak phase transition and the $U(4)$-breaking phase transition will be changed due to the additional contribution to the effective potential. For example, as mentioned in Sec. 2.3.3, there is a singlet scalar field coupled to the Higgs field H_A and H_B in F-term twin Higgs models. If such a singlet scalar field is sufficiently light during the $U(4)$-breaking phase transition, the situation might be dramatically changed. We do not consider such specific cases because we are mostly interested in giving model independent predictions.

Finally, we would like to comment on cosmological phenomena apart from phase transitions here. In the Mirror twin Higgs models, there are light elements such as a twin photon and twin neutrinos. (See the left panel of Fig. 2.2.) They give sizable contributions to the radiation energy density, which is strongly disfavored by measurements of Cosmic Mi-

crowave Background [159] and Big Bang Nucleosynthesis [160]. This issue was studied in [158, 161, 162, 163]. The effects of twin baryons on the large scale structure and CMB are also investigated in Ref. [164]. On the contrary, there is a candidate of dark matter in the Mirror twin Higgs model, which has been investigated in Ref. [165]. The Fraternal twin Higgs model does not lead to an extra dark radiation component but still accommodates a dark matter candidate [166, 167, 168, 169].

Chapter 5

The Electroweak Phase Transition in the Minimal Scotogenic Model

In this chapter, we study minimal scotogenic model at finite-temperature and clarify the dynamics of the electroweak phase transition. We also calculate relic abundances of the scalar and fermion DM and discuss its connection to the GW signals generated by first-order electroweak phase transition. It will turn out that the electroweak phase transition can be of strong first-order and produced GW signals can be detected by ultimate-DECIGO.

5.1 Motivation and Outline

Motivation

As explained in Sec. 2.4, the additional $\mathrm{SU}(2)_{\mathrm{W}}$ scalar doublet and three right-handed neutrinos are introduced into minimal scotogenic model. In this model, depending on the size of masses of these new particles, H or ν_{1R} particles can be DM candidate. A lot of previous studies [29, 30, 31, 32, 33, 34, 35, 36, 37, 38, 39, 40, 41, 42, 43] showed that this model can produce the correct DM relic abundance both the scalar and the fermion DM scenarios. Furthermore, the left-handed neutrino masses are generated radiatively and thus this model can simultaneously explain origins of the DM and neutrino masses. Of course, this fact does not imply that minimal scotogenic model is really realized in nature. To confirm its existence, we need to test or constrain the model by various observations. The simplest method is to use collider searches including precision tests. Indeed, as summarized in Sec. 2.4.3 and

Sec. 2.4.4, there are several collider and precision constraints on this model. In addition to these constraints, similar to the previous chapter, it is interesting to pursue the possibility of the detection of GW signals generated by first-order cosmological phase transitions because it may bring us new information of the model.

A remarkable point of this work is that the phase transition dynamics and resultant GW signals generated by first-order phase transition are strongly related to the mass spectra of new particles and the DM relic abundance in the scalar DM scenario and to the charged flavor violation processes in the fermion DM scenario. Therefore, in future, we can strongly constrain these model by considering the synergy between the observation of GW signals and the collider and precision measurements.

Outline

Here, we shall explain basic calculation method to clarify the order of the phase transition and to estimate the GW signals in minimal scotogenic model. We start with the Lagrangian density of this model, which was summarized in Sec. 2.4. Then, one can compute the thermal effective potential for the SM Higgs field, whose calculation method was outlined in Sec. 3.3. Field dependent masses, needed to compute the thermal effective potential, in this model will be explicitly listed in next section. Similar to the twin Higgs model, we study the thermal effective potential at different temperature and estimate the nucleation temperature $T_{\rm n}$. By calculating the tunneling rate, we can estimate GW signals produced by the first-order phase transition and clarify the parameter space which will be constrained by the future experiments.

In addition to the dynamics of the phase transition, we also compute the relic abundance of DM in both of scalar and fermion DM scenarios. The computation method of relic abundance of the DM was explained in Sec. 3.2. Recall that the Yukawa coupling Y^S_{mn} is chosen to be consistent with the neutrino oscillation data summarized in Sec. 2.2.2 and other parameters are also chosen to be consistent with the collider and precision measurements. In both scalar and fermion DM scenarios, we consider important constraints such as the DM direct detection constraints and charged lepton flavor violation processes in addition to the analysis of the phase transition.

5.2 The First-Order Electroweak Phase Transition in Minimal Scotogenic Model

Before calculating the thermal effective potential and analyzing the order of the electroweak phase transition, we would like to discuss thermal history realized in this model.

We assume that the temperature of the Universe is high enough so that the electroweak symmetry is restored, that is, the SM Higgs VEV is zero at the beginning. In this high-temperature regime, the additional particles such as S scalar and the right-handed neutrinos ν_{nR} are in thermal plasma with the SM particle. The tree level scalar potential of minimal scotogenic model $V_{\rm tree}^{\rm scotogenic}$ Eq. (2.75) consists of two scalar particles, which are the SM Higgs and the inert scalar S. If there is a possibility that S acquires VEV, there is the associated phase transition in addition to the ordinary electroweak phase transition. However, as argued in Sec. 2.4, S does not develop VEV to maintain the Z_2 symmetry (otherwise there is no dark matter candidates in this mode), and hence, we need to only focus on the dynamics of the SM Higgs field. After the electroweak phase transition in this model, the DM is thermally produced as explained in Sec. 2.4.2.

To clarify the dynamics of the electroweak phase transition, we shall now calculate the effective potential of the SM Higgs field. Let us consider contributions coming from inert scalar doublet, $\mathrm{SU(2)_W} \times \mathrm{U(1)_Y}$ gauge bosons and top quarks because those couplings are large compared to other particles. Field dependent masses and degrees of freedoms are then

listed as

$$n_\pm = 2 : m_\pm^2(h_{\rm SM}) = m_1^2 + \frac{\lambda_1}{2}h_{\rm SM}^2 + \Pi_S(T), \tag{5.1}$$

$$n_H = 1 : \ m_H^2(h_{\rm SM}) = m_1^2 + \frac{1}{2}\lambda_H h_{\rm SM}^2 + \Pi_S(T), \tag{5.2}$$

$$n_A = 1 : \ m_A^2(h_{\rm SM}) = m_1^2 + \frac{1}{2}\lambda_A h_{\rm SM}^2 + \Pi_S(T), \tag{5.3}$$

$$n_W = 4 : \ m_W^2(h_{\rm SM}) = \frac{g_2^2}{4}h_{\rm SM}^2, \tag{5.4}$$

$$n_Z = 2 : \ m_Z^2(h_{\rm SM}) = \frac{(g_1^2+g_2^2)}{4}h_{\rm SM}^2, \tag{5.5}$$

$$n_{W_L} = 2 : \ m_{W_L}^2(h_{\rm SM}) = \frac{g_2^2}{4}h_{\rm SM}^2 + \Pi_W(T), \tag{5.6}$$

$$n_{Z_L} = 1 : \ m_{Z_L}^2(h_{\rm SM}) = \frac{1}{2}(m_Z^2(h_{\rm SM}) + \Pi_W(T) + \Pi_Y(T) + \Delta(h_{\rm SM}, T)), \tag{5.7}$$

$$n_{\gamma_L} = 1 : \ m_{\gamma_L}^2(h_{\rm SM}) = \frac{1}{2}(m_Z^2(h_{\rm SM}) + \Pi_W(T) + \Pi_Y(T) - \Delta(h_{\rm SM}, T)), \tag{5.8}$$

$$\Delta^2(h_{\rm SM}, T) \equiv \left(\frac{g_2^2}{4}h_{\rm SM}^2 + \Pi_W(T) - \frac{g_1^2}{4}h_{\rm SM}^2 - \Pi_Y(T)\right)^2 + 4g_1^2 g_1^2 h_{\rm SM}^4. \tag{5.9}$$

where $\lambda_A = \lambda_1 + \lambda_2 - 2\lambda_3$ and $\lambda_H = \lambda_1 + \lambda_2 + 2\lambda_3$. Field dependent masses for longitudinal modes of Z boson and photon can be obtained diagonalizing the matrix given by Eq. (7.75) in Appendix. 7.2. In these expressions, we use Parwani method to include the resummation effects, which was discussed Sec. 3.3.4. The total effective pontential is given by sum of the tree-level Higgs potential, a zero-temperature correction with $\overline{\rm MS}$ regularization and a finite temperature correction, where field dependent masses are listed above.

The thermal mass for the inert scalar doublet, $\Pi_S(T)$, is calculated in Ref. [60] as

$$\Pi_S = \left(\frac{1}{8}g_2^2 + \frac{1}{16}(g_1^2+g_2^2) + \frac{1}{2}\lambda_S + \frac{1}{12}\lambda_1 + \frac{1}{24}\lambda_A + \frac{1}{24}\lambda_H\right)T^2. \tag{5.10}$$

One should note that the Yukawa coupling between the inert doublet and the neutrino given by Eq. (2.76) may give an additional contribution to $\Pi_S(T)$. However, since the right-handed neutrino has Majorana mass comparable to the nucleation temperature, this effect is suppressed due to the Boltzmann suppression in finite-temperature, and hence, we expect that this contribution will not change our result significantly. We therefore neglect this contribution in our analysis. The Debye mass of the $\mathrm{SU(2)_W \times U(1)_Y}$ gauge bosons can be estimated by using SM result [120, 170] with adding an additional $\mathrm{SU(2)_W}$ inert scalar doublet as

$$\Pi_W = 2g_2^2T^2, \ \Pi_Y = 2g_1^2T^2. \tag{5.11}$$

We here qualitatively comment on the strength of the electroweak phase transition. From Eq. (2.75), we can easily find that the tree-level Higgs potential is completely same as the SM one. As we described in Sec. 3.4.3, the electroweak phase transition within the SM framework is of not first order due to the non-perturbative corrections from $SU(2)_W$ gauge bosnos. However, since there is an additional scalar particle, S, which couples to the SM Higgs, the perturbative requirement $\langle h_{SM}(T_n)\rangle/T_n \simeq \langle h_{SM}(T_n)\rangle/T_n > g_2$ can be very easily satisfied when coupling between the inert scalar doublet and the SM Higgs, λ_H, λ_A and λ_1 are sufficiently large. Therefore, in our analysis, we focus on the parameter space leading to the strong first-order electroweak phase transition $\langle h_{SM}(T_n)\rangle/T_n > 1$ to consider the possibility of the electroweak baryogenesis.

Larger m_1 makes the phase transition strength weaker due to the screening effect, which was discussed in Sec. 3.4.4. For the same reason, since a larger λ_S corresponds to larger thermal mass of the inert scalar (See Eq. (5.10)), it makes the phase transition strength weaker. Therefore the strong first-order electroweak phase transition requires larger λ_H, λ_A and λ_1, and smaller m_1 and λ_S. It should be noted that the right-handed neutrinos does not couple to SM Higgs at tree-level. Hence its effect of the electroweak phase transition is irrelevant. Quantitative discussions will be presented in Sec. 5.3 for scalar DM and fermion DM scenarios.

5.3 Results

In this section, we discuss our results obtained after performing a full numerical scan by incorporating all existing constraints and the criteria for a strong first-order phase transition $\langle h_{SM}(T_n)\rangle/T_n > 1$ and the correct DM relic density. In this parameter search, we vary the parameters m_1, λ_1, λ_2, λ_3 and λ_S. While all four parameters are relevant for the electroweak phase transition, the last one does not affect the DM relic abundance. We have also imposed the LEP bounds as well as the perturbative and vacuum stability conditions discussed in Sec. 2.4.3. The constraints coming from light neutrino masses are incorporated by using Casas-Ibarra parametrisation discussed in Sec. 2.4.1.

5.3.1 Scalar dark matter

In this subsection, we show some results in the case of scalar DM scenario. In addition to collider bounds, the perturbative and the vacuum stability conditions, we impose conditions $\lambda_3 < 0$ and $\lambda_2 + 2\lambda_3 < 0$ in order to make CP even component of inert doublet H to be DM candidate.

We show the data points satisfying the conditions $\langle h_{\rm SM}(T_n)\rangle/T_n > 1$ on $(m_\pm,\ m_A)$-plane in upper panels of Fig. 5.1. We confirm that all data points leading to the strong first-order electroweak phase transition is realized by small $m_1 < 50\,\text{GeV}$ and large couplings with the SM-like Higgs boson $\lambda_H,\ \lambda_A,\ \lambda_1 \gtrsim 1$. This result is in agreement with the qualitative discussion presented in Sec. 5.2.

In lower left panel of Fig. 5.1 we show the parameter region on $(m_\pm,\ m_A)$-plane which satisfies $\Omega_{\rm DM}h^2 = 0.120 \pm 0.001$ with varying DM mass shown as color code. This clearly shows the two distinct regions of DM (H particle) mass: $m_H < 80$ GeV (low mass regime) and $m_H > 550$ GeV (high mass regime). While the DM relic satisfying points in low mass regime remain scattered, there is a linear correlation in high mass regime beyond 550 GeV, as can be seen from bottom panel plots of Fig. 5.1. This arises because of the fact that, in order to satisfy correct DM relic in high mass regime $m_{\rm H} > 550$GeV, the mass splitting between inert doublet components is required to be small.

In the lower right panel, we also superimpose the points which satisfy the $\langle h(T_{\rm n})\rangle/T_{\rm n} > 1$, showing overlap with parameter space corresponding to low mass DM. We confirm that there is a parameter regime simultaneously satisfying conditions $\langle h(T_{\rm n})\rangle/T_{\rm n} > 1$ and $\Omega_{\rm DM}h^2 = 0.120 \pm 0.001$, specially for low DM mass $m_H < 80$ GeV.

In the large DM mass regime, $m_{\rm H} > 550$GeV, we need larger values of m_1 making the phase transition strength weaker, and thus, it is impossible to realize $\phi(T_n)/T_n > 1$ with imposing perturbative conditions $|\lambda_i| < 4\pi$ $(i = 1, 2, 3)$. Thus, the low mass DM region $m_H < 80$GeV is only the allowed region from conditions of realizing strong first-order electroweak phase transition and the correct DM relic abundance in the scalar DM scenario of this model. Furthermore, the strong first-order electroweak phase transition requires a cancellation between a large $\lambda_1 \sim \mathcal{O}(1)$ and $\lambda_2 + 2\lambda_3 \sim \mathcal{O}(1)$ to maintain small $\lambda_H = \lambda_1 + \lambda_2 + 2\lambda_3 \sim \mathcal{O}(0.1 \sim 0.01)$ for a low DM mass regime, $m_H < 80$GeV.

We show peak amplitudes of total GW signals with sensitivity curves of U-DECIGO, U-DECIGO-corr, LISA (C1-C4) [132, 171], DECIGO, BBO [172] and Einstein Telescope

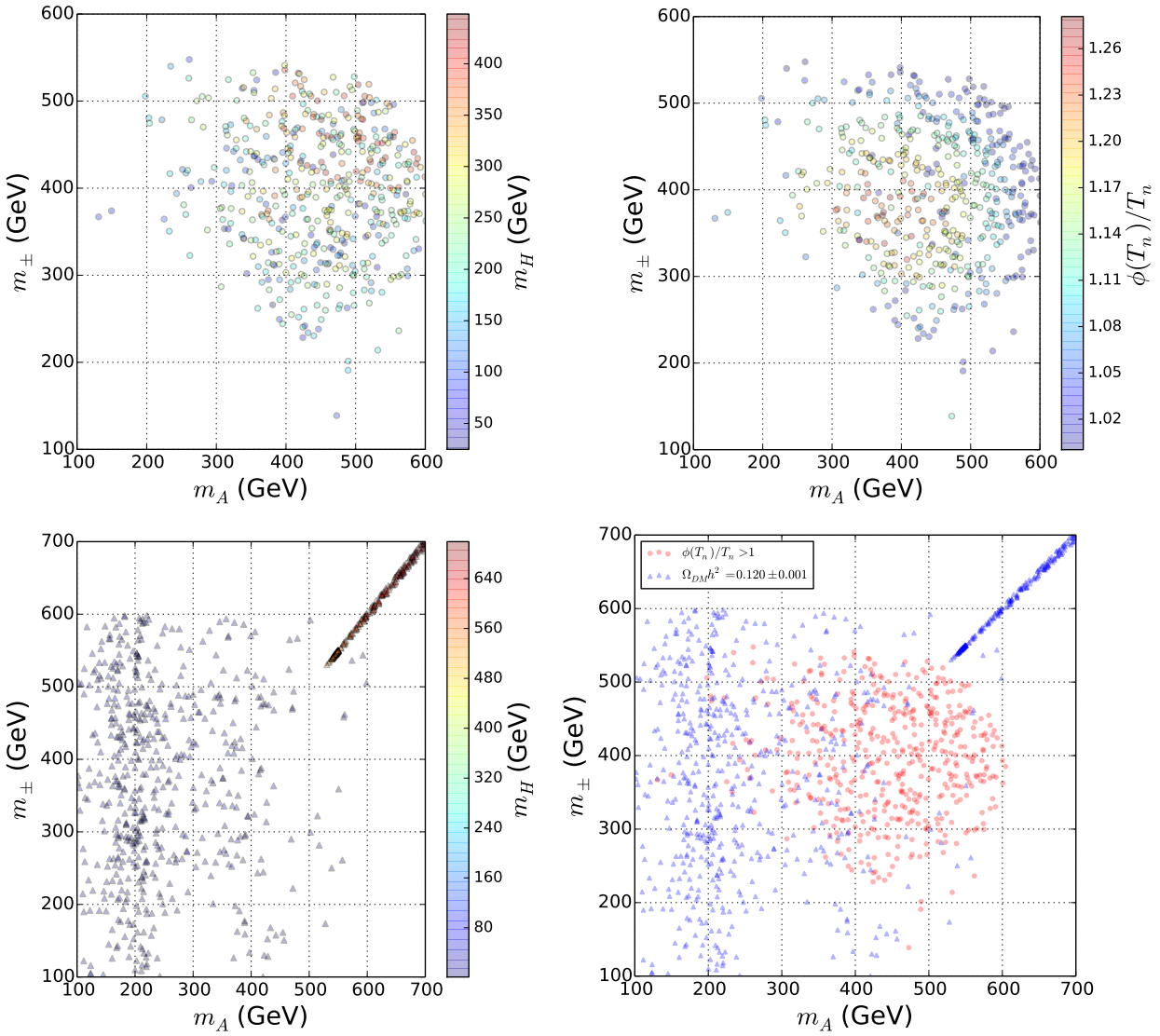

Figure 5.1: Scatter plots on ($m_\pm$, m_A)-plane satisfying $\langle h(T_\mathrm{n})\rangle/T_\mathrm{n} > 1$ for different scalar DM mass, m_H, (upper left) and the strength of the electroweak phase transition $\langle h(T_\mathrm{n})\rangle/T_\mathrm{n}$ (upper right) are shown in the case of scalar DM scenario. A parameter regime satisfying $\Omega_\mathrm{DM}h^2 = 0.120 \pm 0.001$ for different DM mass (lower left) and a combined scatter plot (lower right) for $\langle h_\mathrm{SM}(T_n)\rangle/T_n > 1$ (red circles) and $\Omega_\mathrm{DM}h^2 = 0.120 \pm 0.001$ (blue triangles) are also shown.

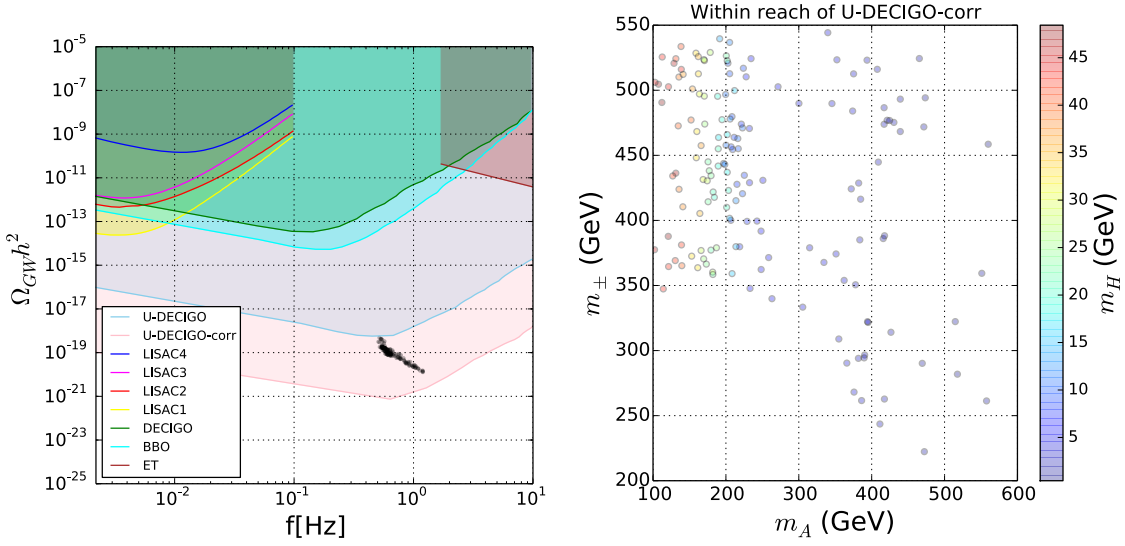

Figure 5.2: Left panel: peak points of GW signals in our model along with sensitivity curves of U-DECIGO, U-DECIGO-corr, LISAC1∼C4 [132, 171], DECIGO, BBO [172] and Einstein Telescope (ET) [173]. Scatter plots on $(m_\pm, m_A)$-plane within reach of U-DECIGO with a correlation analysis (U-DECIGO-corr) [174] for different m_H (right panel) are shown in the case of scalar DM. All data points satisfy correct DM relic density, $\Omega_{\rm DM}h^2 = 0.120 \pm 0.001$.

(ET) [173] in the left panel of Fig. 5.2. It is obvious from the figure that GW signals can only be detected by U-DECIGO-corr. The corresponding mass spectra of S particles are shown in $(m_\pm, m_A)$-plane (right panel of Fig. 5.2). In the figure, we assume that H particle explains 100% of dark matter $\Omega_{\rm DM}h^2 = 0.120 \pm 0.001$. We confirm that all data points satisfying the strong first-order electroweak phase transition give GW signals detected by U-DECIGO.

The low mass DM region, which we have discussed, is also tightly constrained by direct detection as well as other collider searches. To confirm the consistency with DM direct detection constraint, all data points shown is projected into $(\sigma_{\rm SI}, m_{\rm DM})$-plane in Fig. 5.3. Here, $\sigma_{\rm SI}$ is the spin-indepenedent cross section is given by [30]

$$\sigma_{\rm SI} = \frac{\lambda_H^2 f^2}{4\pi} \frac{\mu^2 m_n^2}{m_h^2 m_{\rm DM}^2}, \tag{5.12}$$

where m_n, $\mu = m_n m_{\rm DM}/(m_n + m_{\rm DM})$ and $f \simeq 0.3$ are the nucleon mass, the reduced DM-nucleon mass and the hadronic uncertainties investigated in Refs. [175, 176].

As can be seen from this figure, all data points leading to the first-order electroweak phase

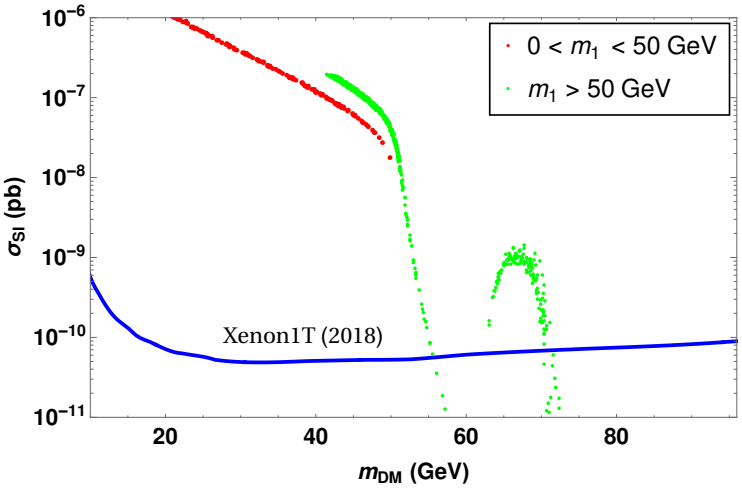

Figure 5.3: Spin independent DM-nucleon cross section for scalar DM. The red coloured points satisfy $\langle h(T_{\rm n})\rangle/T_{\rm n} > 1$.

transition (the red colored points) and GW signals detected by U-DECIGO are ruled out by Xenon1T data. The dark matter mass regime, $m_{\rm DM} = m_H = m_h/2$, is still allowed thanks to the Higgs resonance, which enhances the annihilation cross section. However, these green colored points cannot lead to the first-order electroweak phase transition. This is because, in order to realize $m_H \simeq m_h/2$ with $m_1 < 50\,\text{GeV}$, we need larger λ_H leading to a large $\sigma_{\rm SI}$, which is disfavored by the Xenon1T observation. The stringent direct detection constraints will disappear in the case of the fermion DM scenario as we will see in the next subsection.

5.3.2 Fermion dark matter

In this subsection, we show the results in fermion DM scenario where ν_{1R} is the lightest state of the Z_2-odd particles. Therefore, conditions $\lambda_3 < 0$ and $\lambda_2 + 2\lambda_3 < 0$ imposed in the previous subsection are not necessary in this subsection.

We show the parameter regime satisfying the condition $\langle h_{\rm SM}(T_{\rm n})\rangle/T_{\rm n} > 1$ on $(m_\pm,\ m_A)$-plane in upper panel of Fig. 5.4. Since conditions $\lambda_3 < 0$ and $\lambda_2 + 2\lambda_3 < 0$ imposed in the scalar DM scenario, is evaded in the fermion DM scenario, the lighter mass regime for the charged and the CP-odd component of S can be viable regime. Indeed, compared to the Fig. 5.2, which is obtained in the scalar DM scenario, we can easily find that the strong first-order electroweak phase transition can be realized for small $m_\pm$ and m_A.

In the lower panels of Fig. 5.4, the parameter space on $(m_\pm,\ m_A)$-plane satisfying the

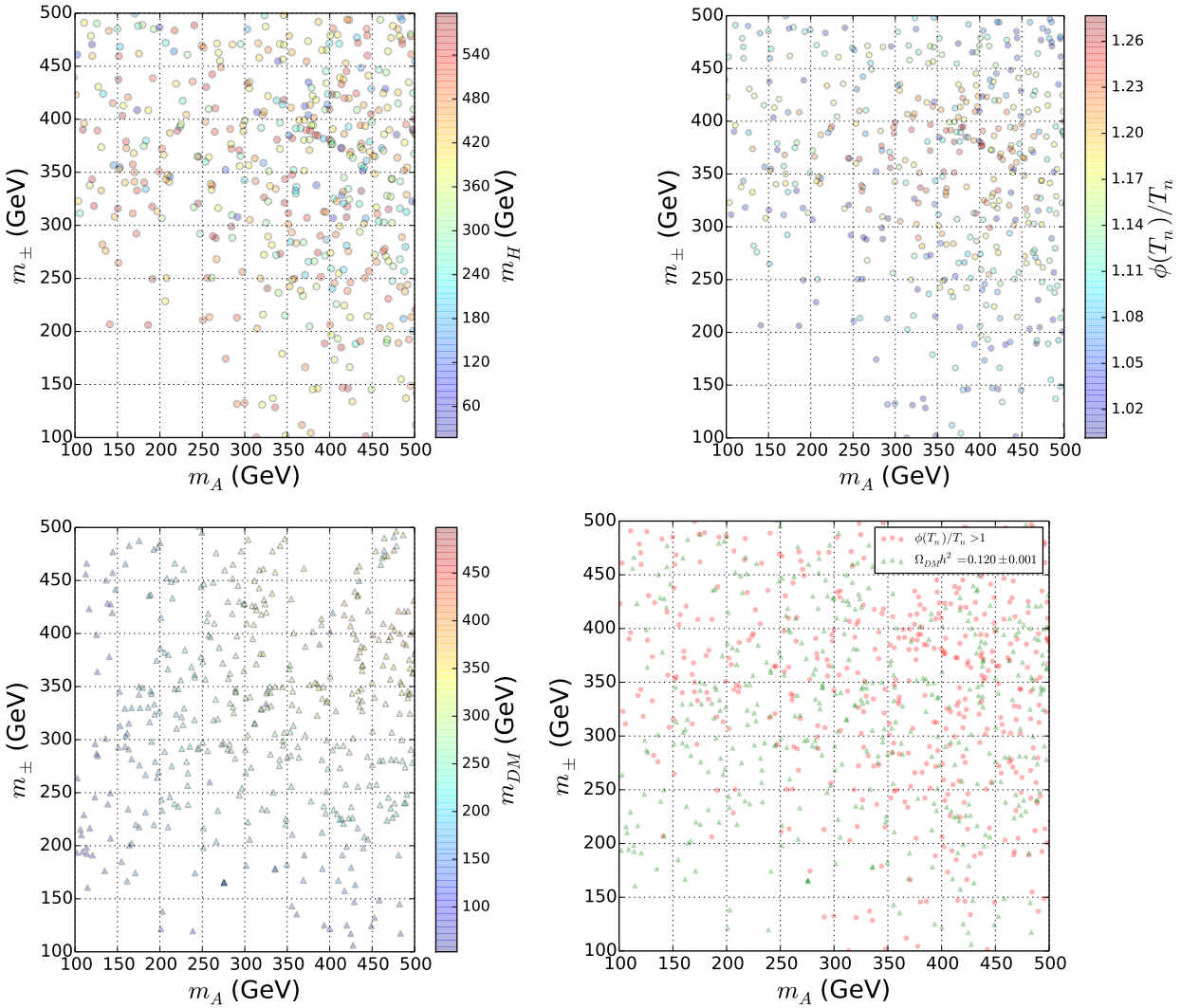

Figure 5.4: Scatter plots on ($m_\pm$, m_A)-plane satisfying $\langle h_{\rm SM}(T_{\rm n})\rangle/T_{\rm n} > 1$ for different m_H, (upper left) and the strength of the electroweak phase transition $\langle h_{\rm SM}(T_{\rm n})\rangle/T_{\rm n}$ (upper right) are shown in the case of fermion DM scenario. A parameter regime satisfying $\Omega_{\rm DM}h^2 = 0.120 \pm 0.001$ for different m_H (lower left) and a combined scatter plot (lower right) for $\langle h_{\rm SM}(T_n)\rangle/T_n > 1$ (red circles) and $\Omega_{\rm DM}h^2 = 0.120 \pm 0.001$ (green triangles) are also shown.

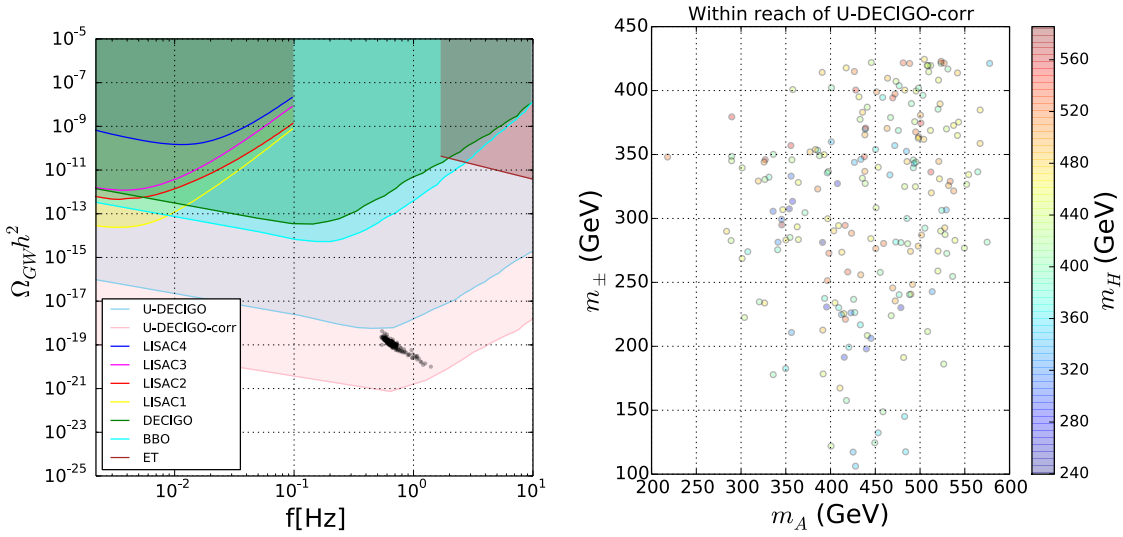

Figure 5.5: Left panel: peak points of GW signals along with sensitivity curves of U-DECIGO, U-DECIGO-corr, LISAC1∼C4, DECIGO, BBO and ET. Scatter plots on $(m_\pm, m_A)$-plane within reach of U-DECIGO-corr for different m_H (right panel) is shown in the case of fermion DM scenario. All data points satisfy correct DM relic density, $\Omega_{\rm DM}h^2 = 0.120 \pm 0.001$.

correct DM relic are shown in which fermion DM mass is shown as a color code. We combine the figures of left upper panel with the left lower panel and show it in the right lower panel. As can be seen from this figure, there exists overlap regime satisfying the strong first-order electroweak phase transition and the correct DM relic.

The points satisfying the fermion DM relic correspond to small λ_3 so that the Yukawa couplings (in $Y^S_{n1}\,\bar{L}_n\tilde{S}\nu_{1R}$) are sizeable enough to enhance fermion DM annihilation and coannihilation channels. This correspondence between small λ_3 and large Yukawa arises through Casas-Ibarra parametrisation discussed in Sec. 2.4.1. We consider lightest neutrino mass 0.1 eV in order to enhance the Yukawa couplings. Small λ_3 gives rise to almost degenerate H, A in this scenario.

We also show peak amplitudes of total GW signals in left panel of Fig. 5.5. The corresponding mass spectra of S particle are shown on $(m_\pm, m_A)$-plane in the right panel of Fig. 5.5. In the figure, we assume that ν_{1R} particle explains 100% of dark mater $\Omega_{\rm DM}h^2 = 0.120 \pm 0.001$. On contrary to the scalar DM scenario, a large λ_H can be allowed because there is no stringent direct detection constraint in the fermion DM scenario. In fact, there is

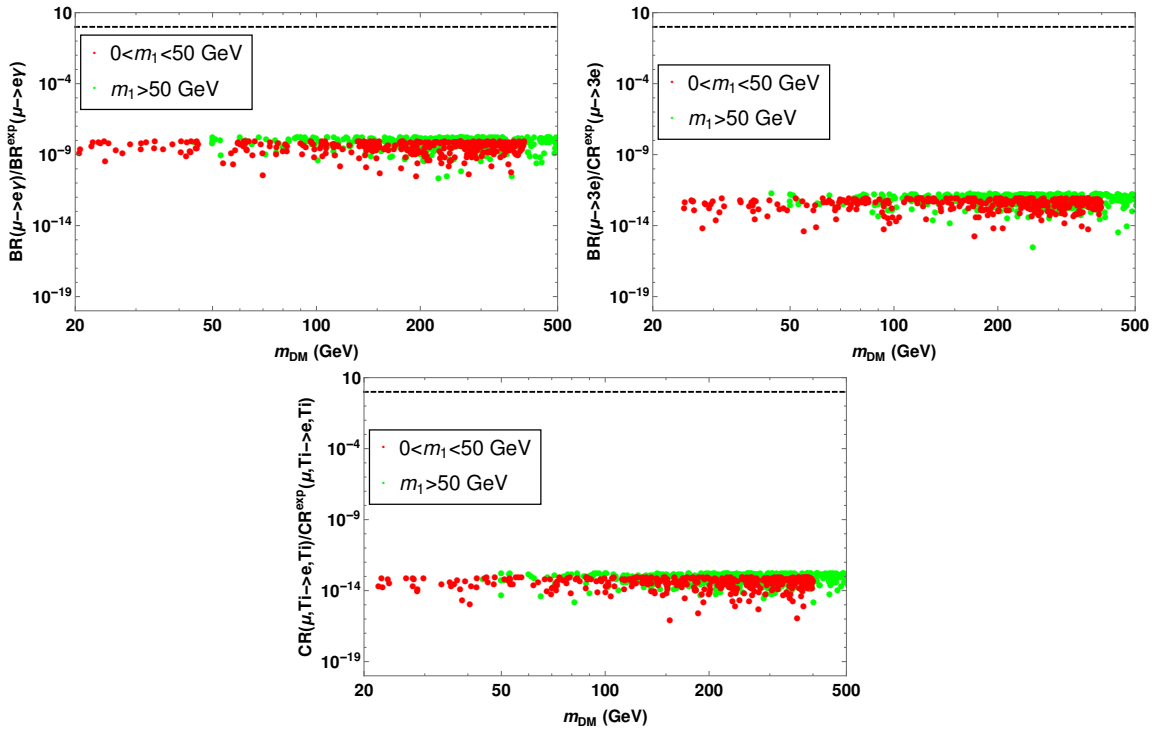

Figure 5.6: Predictions for different charged lepton flavor violation processes for fermion DM scenario. All points satisfy the DM relic criteria while the red colored points realize the strong first-order electroweak phase transition.

no tree level direct detection cross section with ν_{1R} particle because it does not couple to the SM Higgs and SM gauge fields at tree-level. However, such leptophilic fermion DM scenario can be tightly constrained by experimental bounds on charged lepton flavor violation as we discuss in the next subsection. We also confirm that all data points satisfying the strong first-order electroweak phase transition give GW signals detected by U-DECIGO.

We discussed in Sec. 2.4.4 that charged lepton flavor violation processes give stringent constraints on this model. Here, we would like to consider these constraints. Formulae of charged lepton flavor violation processes were already summarized in Sec. 2.4.4 We have used the `SPheno 3.1` interface [177] in order to implement the flavor constraints into the model. For fermion DM model, the predictions for charged lepton flavor violation processes are shown in figure 5.6. As can be seen from this figure, all the predicted points lie way below the current experimental bounds. This is due to the fact that fermion singlet DM relic is mainly governed by its coannihilation with inert doublet components and hence even relatively smaller Yukawa couplings can give rise to the correct relic. This fact was also

noted in earlier works [111].

5.4 Summary and Discussion

In this chapter, we investigated the first-order electroweak phase transition and derived gravitational wave signals realized in minimal scotogenic model, where three right-haded neutrinos and an additional scalar $\mathrm{SU}(2)_{\mathrm{W}}$ doublet so-called the inert scalar doublet are introduced. The new particles are odd under the discrete Z_2 symmetry, and hence, they are stable, which can be (WIMP) DM candidates as long as the lightest particle is electromagnetically neutral. The left-handed neutrino masses are radiatively generated by the Yukawa coupling between SM leptons, the right-handed neutrinos and the inert scalar doublet. With imposing phenomenological and theoretical constraints including the LEP bound, the unitarity and stability of the vacuum condition, we found that the electroweak phase transition can be of strong first-order when couplings between the SM-like Higgs and the inert scalar doublet are sufficiently large, in both of scalar and fermion DM scenarios.

In the scalar DM scenario, one of the electromagnetically neutral components of the inert scalar doublet must be lightest. Under this assumption, we found that generated GW signals can be detected by U-DECIGO with simultaneously realizing the correct DM relic $\Omega_{\mathrm{DM}}h^2 = 0120 \pm 0.001$. However, all parameter points leading to the strong first-order electroweak phase transition and GW signals detected by ultimate-DECIGO, are ruled out by the direct detection constraint from Xenon1T experiment.

In the fermion DM scenario, the DM candidate is the lightest right-handed neutrinos, which is singlet under the SM gauge group. The generated gravitational wave signals can also be detected by U-DECIGO with simultaneously realizing the correct DM relic. In comparison to the scalar DM scenario, the direct detection constraint is unimportant in this scenario because the right-handed neutrinos only couple to SM lepton at tree-level. Although such a coupling induces charged lepton flavor violation processes, which can be the important constraints of this scenario. By the detailed analysis, it turned out that parameter regions, where the strong first-order electroweak phase transition is satisfied and gravitational wave signals can be detected by U-DECIGO, are still consistent with experimental bounds in this model.

Finally, we would like to comment on cosmological phenomena apart from the first-order

electroweak phase transition. Since the lepton number is violated by the Majorana mass term of the right-handed neutrinos, baryogenesis via thermal leptogenesis is a viable scenario to explain the origin of matter anti-matter asymmetry in the early Universe. This scenario is studied in Refs. [46, 43, 47, 48, 49, 45, 50].

Chapter 6

Conclusion and Discussion

We have discussed the dynamics of cosmological phase transitions by calculating the thermal effective potential in several physics beyond the SM. Within the SM framework, the electroweak phase transition is of not first order, but the physics beyond the SM can assist the realization of (strong) first-order electroweak phase transitions. The strong first-order electroweak phase transition not only provide the GW signals but also accommodates the electroweak baryogenesis. Moreover, if cosmological phase transitions associated with additional spontaneous symmetry breaking in beyond the SM physics are of first order, these also provide the GW signals which can be tested by future planned experiments.

In Chapter 2, we review the SM of particle physics. The SM Lagrangian density was constructed based on the gauge principle and allowed by the renormalizability. We reviewed the dynamics of the EWSB within the SM framework and confirmed that it is in agreement with the present collider experiments. However, we saw that the SM contains some difficulties *e.g.* the naturalness of the SM Higgs mass parameter, origins of the DM and non-zero neutrino masses and so on. To address these difficulties, new physics beyond the SM would be needed. In particular, we introduced twin Higgs models and minimal scotogenic model to solve the little hierarchy problem and to explain origins of the DM and neutrino masses. We studied these models at zero-temperature and summarize some conditions such as the correct EWSB as well as collider and precision constraints.

In chapter 3, we reviewed the standard cosmology. We derived Friedmann equation and explain expanding Universe. In the past, the Universe was so dense and filled by the hot thermal plasma, and hence, the standard thermodynamics plays an important role to un-

derstand the dynamics occurred in the early Universe. The local equilibrium condition is derived based on the Boltzmann equation in the expanding Universe. We saw that the expansion of the Universe leads to the out-of-equilibrium processes such as DM production and cosmological phase transitions. The DM is thermally produced, whose precise abundance be rigorously estimated by solving the Boltzmann equation. We also considered the thermal effect on the generic scalar potential and showed that broken symmetry at the zero-temperature is restored by the thermal plasma. We found that phase transitions can be of first-order when a potential barrier, which separates the global and local minima, exists. Since such a potential barrier is naturally generated by bosonic one-loop thermal corrections, bosonic particles, which strongly couple to the order parameter, are needed to realize the first-order phase transitions. Finally, calculation method of the tunneling rate and formulae of GW signals were summarized.

In chapter 4, we have considered the twin Higgs models at finite-temperature and studied cosmological phase transitions realized in these models. In this model, mirror copies of the SM particles are introduced. (See Fig. 2.2 for the detailed matter content and variations of the model.) In these models, since the SM Higgs is identified with the pNGB arising from the spontaneous global symmetry $\mathrm{U}(4) \to \mathrm{U}(3)$, there is a cosmological phase transition associated with it. By the detailed analysis, it was turned out that it is generally difficult to realize first-order phase transitions in this model without any UV completion under the assumption of two-step phase transition. With the supersymmetric UV completion, the twin stop can trigger the first-order phase transition associated with $\mathrm{U}(4) \to \mathrm{U}(3)$ breaking. In this case, GW signals are generated, but it was turned out that it is very small to be detected by future planned experiments including DECIGO, BBO and ultimate-DECIGO.

In chapter 5, we have considered minimal scotogenic model and studied the cosmological electroweak phase transition. In the scotogenic model, three right-handed neutrinos with TeV scale Majorana masses and an additional $\mathrm{SU}(2)_{\mathrm{W}}$ scalar doublet are introduced into SM sector. These new particles possess a discrete Z_2 symmetry, and hence, they can be dark matter candidates. Depending on the DM candidates, the dynamics of the electroweak phase transition has been studied with assuming that new particle comprises 100% of DM. By the detailed analysis, it turned out that the electroweak phase transition can be of strong first-order and provide GW signals, which can be only detected by ultimate-DECIGO. When the DM candidate is a electromagnetically neutral scalar, the DM direct detection constraint

is stringent, which rules out parameter points satisfying the strong first-order electroweak phase transition. When the DM candidate is the lightest right-handed neutrinos, charged flavor violation processes are important, but the parameter regime leading to the strong first-order electroweak phase transition and GW signals detected by ultimate-DECIGO, is still consistent with current experiments on contrary to the scalar DM scenario.

We finally comment on uncertainty on the analysis of the cosmological phase transitions and GW signals. The resummed effective potential at finite temperature depends on a gauge-fixing parameter. In our calculation, we adopted the Landau gauge. The effect of gauge dependence is discussed in, *e.g.*, Ref. [178, 179]. According to Ref. [179], the uncertainty due to gauge choice is roughly one or two order magnitude for $\Omega_{\rm GW}h^2$. The gauge dependence of the thermal effective potential is discussed by many authors. See. e.g. Refs. [178, 180] and references therein.

Acknowledgement

First of all, I would like to thank to my supervisor Masahide Yamaguchi. He have been a tremendous mentor for me. It has been an honor to be his Ph.D. student. Beside my advisor, I would like to thank Nakai Yuichiro for valuable discussion in a wide range of physics. Without discussion with him, I could not have completed researches. I am also grateful to Kohei Kamada, Debasish Borah, Devabrat Mahanta, Sin Kyu Kang and Arnab Dasgupta who are collaborators of researches included in this thesis. I learn a lot from all collaborators, including research methods. I would like to thank my colleagues, Atsuhisa Ota, Daisuke Yoshida, Kensuke Akita and Keigo Shimada for a lot of discussions. On a final note, I thank a lot my parents.

I was supported by JSPS and NRF under the Japan-Korea Basic Scientific Cooperation Program and would like to thank participants attending the JSPS and NRF conference for useful comments. I am also supported by JSPS Grants-in-Aid for Research Fellows No. 20J12415.

Chapter 7

Appendix

In this appendix, we summarize detailed calculations of the thermal field theory.

7.1 Appendix A: Thermal Field Theory

Here, we explicitly show how to compute the thermal effective potential.

From the definitions Eqs. (3.64) and (3.65), we can obtain following relation:

$$G_+(t - i\beta,\ \mathbf{x}) = G_-(t, \mathbf{x}). \tag{7.1}$$

This is known to be Kubo-Martin-Schwinger relation. Let us here consider the free scalar boson. Then the Green function satisifies the following equation

$$[\partial_\mu \partial^\mu + m^2] G^c(x - y) = -i\delta_c(x - y), \tag{7.2}$$

where $\delta_c(x - y) \equiv \delta_c(-i(x^0 - y^0))\delta^{(3)}(\mathbf{x} - \mathbf{y})$. The scalar field $\phi(x)$ can be expanded as follows, which is same to the zero-temperature calculation:

$$\phi(x) = \int \frac{d^3p}{(2\pi)^3\sqrt{2\omega_{\mathbf{p}}}} \left[a(\mathbf{p})e^{-ipx} + a^\dagger(\mathbf{p})e^{ipx}\right], \tag{7.3}$$

$$\omega_{\mathbf{p}} = \sqrt{\mathbf{p}^2 + m^2}. \tag{7.4}$$

The commutation relation at equal time is given by

$$[\phi(\mathbf{x},\ t),\ \dot{\phi}(\mathbf{y},\ t)] = i\delta^{(3)}(\mathbf{x} - \mathbf{y}). \tag{7.5}$$

From above equation, we can find following relation:

$$[a(\mathbf{p}),\ a^\dagger(\mathbf{k})] = \delta^{(3)}(\mathbf{p}-\mathbf{k}). \tag{7.6}$$

The Hamiltonian of the free scalar field system $\hat{H}$ can be expressed as

$$\hat{H} = \int \frac{d^4p}{(2\pi)^3}\omega_{\mathbf{p}} a^\dagger_{\mathbf{p}} a_{\mathbf{p}}. \tag{7.7}$$

The number operator $\hat{N}$ is defined as

$$\hat{N} = \int \frac{d^3p}{(2\pi)^3} a^\dagger_{\mathbf{p}} a_{\mathbf{p}}. \tag{7.8}$$

Then the Hamiltonian Eq. (7.7) can be expressed as follows.

$$\hat{H} \equiv \omega_{\mathbf{p}} \hat{N} \tag{7.9}$$

By introducing the complete set of eigenstate of $\hat{N}$ in such a way that following equation is satisfied.

$$\hat{N}|n\rangle = n|n\rangle, \tag{7.10}$$

$$a|n\rangle = |n-1\rangle, \tag{7.11}$$

$$a^\dagger|n\rangle = |n+1\rangle, \tag{7.12}$$

$$\sum_n |n\rangle\langle n| = 1. \tag{7.13}$$

Then we can obtain

$$\mathrm{Tr}[e^{-\beta\hat{H}}] = \langle n|e^{-\beta\hat{H}}|n\rangle \tag{7.14}$$

$$= \sum_{n=0}^{\infty} e^{-\beta\omega_n} \tag{7.15}$$

$$= \frac{1}{1-e^{-\beta\omega}}. \tag{7.16}$$

and

$$\mathrm{Tr}[e^{-\beta\hat{H}} a^\dagger a] = \sum_{n=0}^{\infty} n e^{-\beta\omega_n} \tag{7.17}$$

$$= \frac{e^{-\beta\omega}}{(1-e^{-\beta\omega})^2}. \tag{7.18}$$

By using these equation, we obtain the number density on the thermal background:

$$\langle n_B(\omega)\rangle \equiv \frac{\mathrm{Tr}[e^{-\beta\hat{H}}a^\dagger_{\mathbf{p}}a_{\mathbf{k}}]}{\mathrm{Tr}[e^{-\beta\hat{H}}]} \tag{7.19}$$

$$= \frac{1}{e^{\beta\omega}-1}\delta^{(3)}(\mathbf{p}-\mathbf{k}). \tag{7.20}$$

This result simply shows that the number density on the thermal background is given by the Boltzmann distribution. By using following equation,

$$\langle a(\mathbf{k})a^\dagger(\mathbf{p})\rangle = [1+n_B(\omega)]\delta^{(3)}(\mathbf{p}-\mathbf{k}), \tag{7.21}$$

the Green function can be expressed as

$$G^{(c)}(x-y) = \int \frac{d^4p}{(2\pi)^4}\rho(p)e^{-ip(x-y)}[\theta_c(x^0-y^0)+n_B(\omega)], \tag{7.22}$$

$$\rho(p) \equiv 2\pi[\theta(p^0)-\theta(-p^0)]\delta(p^2+m^2). \tag{7.23}$$

Let us next consider the free Weyl fermion. The Green function is defined as

$$S^{(c)}_{\alpha\beta}(x-y) \equiv \langle T_c\psi_\alpha(x)\bar{\psi}_\beta(y)\rangle \tag{7.24}$$

$$= \theta_c(x^0-y^0)S^+_{\alpha\beta}(x-y)+\theta_c(y^0-x^0)S^-_{\alpha\beta}(x-y), \tag{7.25}$$

$$S^+_{\alpha\beta} \equiv \langle\psi_\alpha(x)\bar{\psi}_\beta(y)\rangle, \tag{7.26}$$

$$S^-_{\alpha\beta}(x-y) = S^+(y-x). \tag{7.27}$$

where α and $\beta = 1,2$ are the index of SU(2) spinor. The Kubo-Martin-Schwinger relation of the fermion is given by

$$S^+_{\alpha\beta}(t-i\beta,\ \mathbf{x}) = -S^-_{\alpha\beta}(t,\ \mathbf{x}). \tag{7.28}$$

Compared to the corresponce boson expression Eq. (7.1), there is a negative sign which comes from the spin static of the fermion. The Green function satisfies the following equation

$$S^{(c)}_{\alpha\beta}(x-y) = (i\partial\!\!\!/+m)_{\alpha\beta}G^{(c)}(x-y) \tag{7.29}$$

where $G^{(c)}(x-y)$ is given by Eq. (7.2). The Hamiltonian and the number operators are given by

$$\hat{H} = \omega\hat{N}, \tag{7.30}$$

$$\hat{N} = b^\dagger b\ \langle\hat{N}\rangle = 0 \text{ or } 1. \tag{7.31}$$

This is same to the zero-temperature case. By introducing the complete set $|n\rangle$, we have

$$\mathrm{Tr}[e^{-\beta\hat{H}}] = \sum_{n=0}^{1}\langle n|e^{-\beta\hat{H}}|n\rangle \tag{7.32}$$

$$= 1 + e^{-\beta\omega}, \tag{7.33}$$

and

$$\mathrm{Tr}[e^{-\beta\hat{H}}bb^{\dagger}] = e^{-\beta\omega}. \tag{7.34}$$

Therefore, the number density of free fermion on the thermal background is expressed as

$$\langle n_F(\omega)\rangle = \frac{1}{e^{\beta\omega}+1}. \tag{7.35}$$

This result implies that the number density of fermion on the thermal background is described by the Fermi distribution function. By using following equation

$$\langle bb^{\dagger}\rangle = 1 - n_F(\omega), \tag{7.36}$$

we can express the two-point Green function as follows.

$$S^{(c)}(x-y) = \int \frac{d^4p}{(2\pi)^4}\rho(p)e^{-ip(x-y)}[\theta_c(x^0-y^0) - n_F(\omega)]. \tag{7.37}$$

The two-point Green functions of free scalar and fermion Eqs. (7.22) and (7.37) can be summarized as

$$G(\tau,\ \mathbf{x}) = \int \frac{d^4p}{(2\pi)^4}\rho(p)e^{ipx}[\theta(\tau) + \eta n(p^0=\omega)], \tag{7.38}$$

$$n(\omega) \equiv \frac{1}{e^{\beta\omega}-\eta}. \tag{7.39}$$

where

$$\eta = \begin{cases} -\frac{1}{2} & \text{(boson)} \\ 1 & \text{(Weyl fermion)} \end{cases}, \tag{7.40}$$

In this calculation, we have used $t = i\tau$. The Fourier transformation of $G(\tau, \mathbf{x})$ is given by

$$\tilde{G}(\omega_n,\ \mathbf{p}) = \int_0^{\beta}\int d^3x e^{i\omega_n\tau - i\mathbf{p}\cdot\mathbf{x}}G(\tau,\ \mathbf{x}). \tag{7.41}$$

Very interestingly, from the Kubo-Martin-Schwinger relation Eqs. (7.1) and (7.28), we obtain following expressions:

$$\eta e^{i\omega_n \beta} = 1, \tag{7.42}$$

$$\omega_n = \begin{cases} \frac{2\pi n}{\beta} & \text{(Boson)} \\ \frac{(2n+1)\pi}{\beta} & \text{(Fermion)} \end{cases} \tag{7.43}$$

Then the Green functions becomes

$$\begin{aligned} \tilde{G}(\omega_n,\ \tau) &= \int_0^\beta d\tau \int d^3x e^{i\omega_n \tau - i\mathbf{p}\cdot\mathbf{x}} G(\tau,\ \mathbf{x}) \\ &= \frac{1}{\omega_n^2 + \mathbf{p}^2 + m^2}. \end{aligned} \tag{7.44}$$

We can then define the propagator as

$$G(\tau, \mathbf{x}) \equiv i\Delta(-i\tau, \mathbf{x}). \tag{7.45}$$

Then we can express $\Delta(x)$ is given by

$$\Delta(x) = \frac{1}{\beta} \sum_{n=-\infty}^{n=+\infty} \int \frac{d^3\mathbf{p}}{(2\pi)^3} e^{-i\omega_n \tau - i\mathbf{p}\cdot\mathbf{x}} \frac{-i}{\mathbf{p}^2 + m^2 + \omega_n^2}. \tag{7.46}$$

This implies that we can compute some physical quantities on the thermal background by using following Feynman Rules:

$$\text{Boson propagtor}: \ \frac{1}{p^2 + m^2},\ p^\mu = \left(\frac{2\pi i n}{\beta},\ \mathbf{p}\right) \tag{7.47}$$

$$\text{Fermion propagator}: \ \frac{1}{\not{p} + m},\ p^\mu = \left(\frac{(2n+1) i\pi}{\beta},\ \mathbf{p}\right) \tag{7.48}$$

$$\text{loop integral}: \ \frac{1}{\beta} \sum_{n=-\infty}^{n=+\infty} \int \frac{d^3k}{(2\pi)^3} \tag{7.49}$$

$$\text{Vertex function}: \ -i\beta(2\pi)^3 \delta(\sum_i \omega_i) \delta^{(3)}(\sum_i \mathbf{p}_i) \tag{7.50}$$

The vertex factor is completely same as the zero-temperature field theory. We can easily find above expressions that just the integration with respect to time is discretized due to the Kubo-Martin-Schwinger relation. In the following, we will compute the one-loop thermal effective potential with above mentioned Feynman Rules.

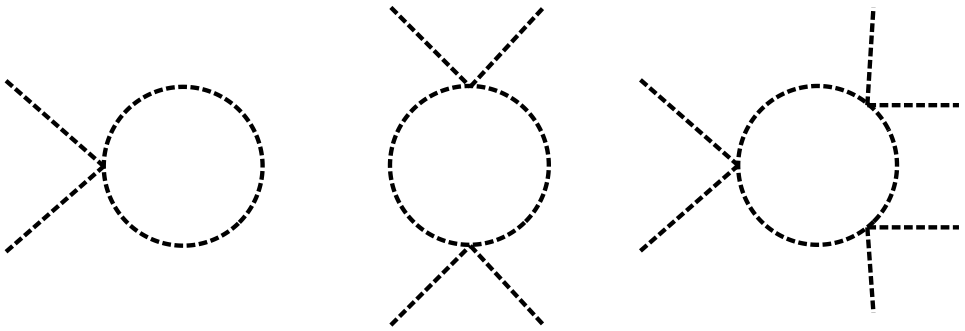

Figure 7.1: The one-loop Feynman diagram contributing to the $V_{\rm thermal}$ is shown. The external leg corresponds to the background field φ.

A scalar field contribution

Let us consider the scalar field contribution, where the tree-level Lagrangian is given by

$$\mathcal{L} = \frac{1}{2}\partial_\mu\phi\partial^\mu\phi - V(\phi), \tag{7.51}$$

$$V(\phi) = \frac{1}{2}m^2\phi^2 + \frac{\lambda}{4}\phi^4. \tag{7.52}$$

The one-loop effective potential can be calculated by computing the Feynman diagram indicated in Fig. 7.1. With taking into account following factors

$$\text{propagator} : \left(-\frac{1}{p^2+m^2}\right)^n, \tag{7.53}$$

$$\text{external leg} : \varphi^{2n}, \tag{7.54}$$

$$\text{vertex} : (-3\lambda)^n, \tag{7.55}$$

$$\text{symmetric factor} : \frac{1}{2n}, \tag{7.56}$$

$$\frac{1}{\beta}\sum_{n=-\infty}^{n=+\infty}\int\frac{d^3k}{(2\pi)^3}, \tag{7.57}$$

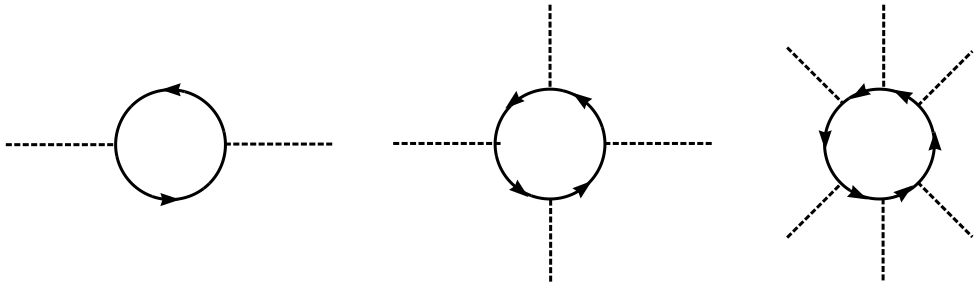

Figure 7.2: The one-loop Feynman diagram contributing to the $V_{\rm thermal}$ is shown. The internal line corresponds to the fermion field, while the external field corresponds to the background field φ.

for nth diagram, $V_{\rm thermal}$ of a scalar field contribution is calculated as

$$V_{1-\rm loop} = \frac{1}{\beta}\sum_{n=-\infty}^{\infty}\sum_{N=1}^{\infty}\int\frac{d^3p}{(2\pi)^3}\frac{1}{2N}\left(-\frac{3\lambda\varphi^2}{p^2+m^2}\right)^N, \tag{7.58}$$

$$= \frac{1}{\beta}\sum_{n=-\infty}^{\infty}\sum_{N=1}^{\infty}\int\frac{d^3p}{(2\pi)^3}\log\left(1+\frac{3\lambda\varphi^2}{p^2+m^2}\right), \tag{7.59}$$

$$= \frac{1}{2\beta}\sum_{n=-\infty}^{\infty}\int\frac{d^3p}{(2\pi)^3}\log(p^2+m^2+3\lambda\varphi^2). \tag{7.60}$$

The momentum p is defined in Eq. (7.47). The extension of the multi-compoent scalar field system is straightforward.

A fermion contribution

Let us consider the following Lagrangian:

$$\mathcal{L} = i\bar{\psi}\partial\!\!\!/\psi - \bar{\psi}M_F(\varphi)\psi, \tag{7.61}$$

where $M_F(\varphi) \propto \varphi$. This coupling usually comes from a Yukawa coupling. With taking into account following factors

$$\text{vertex} : \left(M_F^2\right)^n, \tag{7.62}$$

$$\text{symmertric factor} : -\frac{1}{2n}. \tag{7.63}$$

for nth diagram, V_{thermal} of a fermion contribution is given by

$$V_{\text{thermal}} = -\frac{n_F}{2\beta} \sum_{n=-\infty}^{n=\infty} \int \frac{d^3p}{(2\pi)^3} \log(p^2 + M_F^2), \tag{7.64}$$

where

$$n_F = \begin{cases} 4 & \text{(Dirac fermion)} \\ 2 & \text{(Weyl fermion)} \end{cases}. \tag{7.65}$$

Note that Feynman diagrams having odd external legs vanishes because the trace of odd numbers of gamma matrices or Pauli matrices are zero.

A gauge field contribution

Finally, we consider the contribution from gauge boson. When the background field φ is charged under the gauge symmetry, the covariant derivative term $D_\mu\varphi$ leads to following Lagrangian:

$$\mathcal{L} = -\frac{1}{4}\text{Tr}(F_{\mu\nu}F^{\mu\nu}) + \frac{M(\varphi)^2}{2} A_{a\mu}A^{b\mu}. \tag{7.66}$$

By choosing the Landau gauge, gauge field propagator can be expressed as

$$\Pi^\mu_\nu \equiv -\frac{1}{p^2}\Delta^\mu_\nu, \tag{7.67}$$

$$\Delta^\mu_\nu \equiv \delta^\mu_\nu - \frac{p^\mu p_\nu}{p^2}. \tag{7.68}$$

In this gauge, $\Delta^\mu_\nu\Delta^\nu_\rho = \Delta^\mu_\rho$ and $p_\mu\Pi^\mu_\nu = 0$ are satisfied. With taking into account following factors

$$\text{vertex} : (-M^2(\varphi))^n, \tag{7.69}$$

$$\text{symmetric factor} : \frac{1}{2n}, \tag{7.70}$$

for nth diagram, V_{thermal} of a gauge bosons contribution is given by

$$V_{\text{thermal}} = \frac{3}{2\beta} \sum_{n=-\infty}^{\infty} \int \frac{d^3p}{(2\pi)^3} \log(p^2 + M^2(\varphi)). \tag{7.71}$$

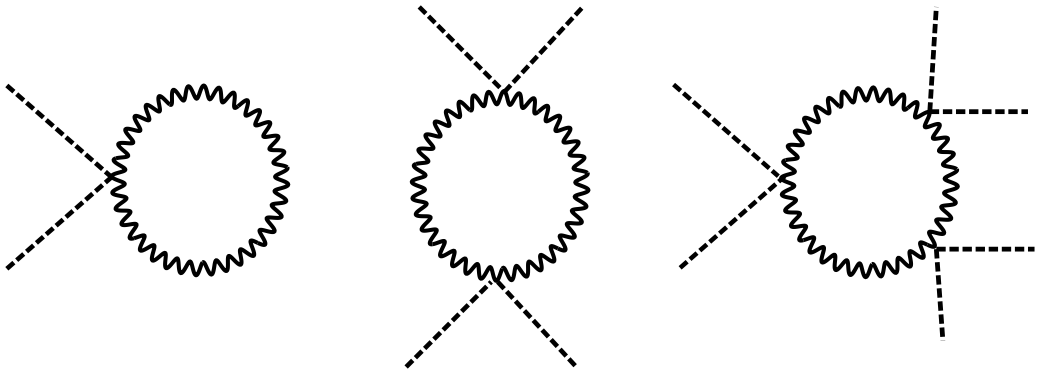

Figure 7.3: The one-loop Feynman diagram contributing to the $V_{\rm thermal}$ is shown. The internal line corresponds to the gauge bosons, while the external field corresponds to the background field φ.

In this expression, the factor 3 comes from $\mathrm{Tr}\Delta$, and p is defined in Eq. (7.47). If φ is charged under several gauge symmetries, $M(\varphi)$ becomes non-diagonal matrix. In such case, we should diagonalize the mass matrix. We will explicitly calculate this in the next Appendix.

If particles appearing inside the loop have additional degrees of freedoms, we should multiply this factor in the corresponding expressions.

7.2 Appendix B: Field dependent masses for electroweak gauge bosons

Here, we explicitly calculate the field dependent masses for $\mathrm{SU(2)_W \times U(1)_Y}$ gauge bosons. By taking the background field of the SM-like Higgs as Eq. (2.62), interactions with SM-like Higgs and gauge bosons are given by

$$\frac{g_2^2}{4}W_\mu^a W^{b\mu}\left(0,\ \frac{h_{\rm SM}}{\sqrt{2}}\right)\sigma^a\sigma^b\begin{pmatrix}0\\ \frac{h_{\rm SM}}{\sqrt{2}}\end{pmatrix}+\frac{1}{4}\left(0,\ \frac{h_{\rm SM}}{\sqrt{2}}\right)\begin{pmatrix}g_2W_\mu^3 g_1 B^\mu & 0\\ 0 & -g_2W_\mu^3 g_1 B^\mu\end{pmatrix}\begin{pmatrix}0\\ \frac{h_{\rm SM}}{\sqrt{2}}\end{pmatrix}$$
$$+\frac{g_1^2}{4}B_\mu B^\mu\left(0,\ \frac{h_{\rm SM}}{\sqrt{2}}\right)\begin{pmatrix}0\\ \frac{h_{\rm SM}}{\sqrt{2}}\end{pmatrix}. \tag{7.72}$$

In the $(W^1_\mu, W^2_\mu, W^3_\mu, B_\mu)$ basis, above expression can be rewritten as

$$(W^1_\mu,\ W^2_\mu,\ W^3_\mu,\ B_\mu)\begin{pmatrix} g_2^2\frac{h_{\rm SM}^2}{4} & 0 & 0 & 0 \\ 0 & g_2^2\frac{h_{\rm SM}^2}{4} & 0 & 0 \\ 0 & 0 & g_2^2\frac{h_{\rm SM}^2}{4} & -g_2g_1\frac{h_{\rm SM}^2}{4} \\ 0 & 0 & -g_2g_1\frac{h_{\rm SM}^2}{4} & g_1^2\frac{h_{\rm SM}^2}{4} \end{pmatrix}\begin{pmatrix} W^{1\mu} \\ W^{2\mu} \\ W^{3\mu} \\ B^\mu \end{pmatrix}. \tag{7.73}$$

By acting an orthogonal matrix for (W^3_μ, B_μ), we can diagonalize the mass matrix:

$$(W^1_\mu,\ W^2_\mu,\ Z_\mu,\ A_\mu)\begin{pmatrix} g_2^2\frac{h_{\rm SM}^2}{4} & 0 & 0 & 0 \\ 0 & g_2^2\frac{h_{\rm SM}^2}{4} & 0 & 0 \\ 0 & 0 & (g_1^2+g_2^2)\frac{h_{\rm SM}^2}{4} & 0 \\ 0 & 0 & 0 & 0 \end{pmatrix}\begin{pmatrix} W^{1\mu} \\ W^{2\mu} \\ Z^\mu \\ A^\mu \end{pmatrix}. \tag{7.74}$$

When we consider the resummation effect, we should include the temperature corrections on the field dependent mass. In that case, the field dependent mass given by Eq. (7.73) is improved by the following expression:

$$(W^1_\mu,\ W^2_\mu,\ W^3_\mu,\ B_\mu)\begin{pmatrix} g_2^2\frac{h_{\rm SM}^2}{4}+\Pi_W & 0 & 0 & 0 \\ 0 & g_2^2\frac{h_{\rm SM}^2}{4}+\Pi_W & 0 & 0 \\ 0 & 0 & g_2^2\frac{h_{\rm SM}^2}{4}+\Pi_W & -g_2g_1\frac{h_{\rm SM}^2}{4} \\ 0 & 0 & -g_2g_1\frac{h_{\rm SM}^2}{4} & g_1^2\frac{h_{\rm SM}^2}{4}+\Pi_B \end{pmatrix}\begin{pmatrix} W^{1\mu} \\ W^{2\mu} \\ W^{3\mu} \\ B^\mu \end{pmatrix}. \tag{7.75}$$

By diagonalizing this matrix, we obtain Eqs. (4.18) and (5.9) with given Π_W and Π_B. Note that the photon becomes massive due to the finite-temperature corrections.

Bibliography

[1] F. Csikor, Z. Fodor and J. Heitger, *Endpoint of the hot electroweak phase transition*, *Phys. Rev. Lett.* **82** (1999) 21 [hep-ph/9809291].

[2] A. I. Bochkarev and M. E. Shaposhnikov, *Electroweak Production of Baryon Asymmetry and Upper Bounds on the Higgs and Top Masses*, *Mod. Phys. Lett.* **A2** (1987) 417.

[3] K. Kajantie, M. Laine, K. Rummukainen and M. E. Shaposhnikov, *The Electroweak phase transition: A Nonperturbative analysis*, *Nucl. Phys.* **B466** (1996) 189 [hep-lat/9510020].

[4] M. S. Turner and F. Wilczek, *Relic gravitational waves and extended inflation*, *Phys. Rev. Lett.* **65** (1990) 3080.

[5] A. Kosowsky, M. S. Turner and R. Watkins, *Gravitational radiation from colliding vacuum bubbles*, *Phys. Rev.* **D45** (1992) 4514.

[6] A. Kosowsky, M. S. Turner and R. Watkins, *Gravitational waves from first order cosmological phase transitions*, *Phys. Rev. Lett.* **69** (1992) 2026.

[7] A. Kosowsky and M. S. Turner, *Gravitational radiation from colliding vacuum bubbles: envelope approximation to many bubble collisions*, *Phys. Rev.* **D47** (1993) 4372 [astro-ph/9211004].

[8] M. S. Turner, E. J. Weinberg and L. M. Widrow, *Bubble nucleation in first order inflation and other cosmological phase transitions*, *Phys. Rev.* **D46** (1992) 2384.

[9] M. Hindmarsh, S. J. Huber, K. Rummukainen and D. J. Weir, *Gravitational waves from the sound of a first order phase transition*, *Phys. Rev. Lett.* **112** (2014) 041301 [1304.2433].

[10] J. T. Giblin and J. B. Mertens, *Gravitional radiation from first-order phase transitions in the presence of a fluid*, *Phys. Rev.* **D90** (2014) 023532 [1405.4005].

[11] M. Hindmarsh, S. J. Huber, K. Rummukainen and D. J. Weir, *Numerical simulations of acoustically generated gravitational waves at a first order phase transition*, *Phys. Rev.* **D92** (2015) 123009 [1504.03291].

[12] M. Hindmarsh, S. J. Huber, K. Rummukainen and D. J. Weir, *Shape of the acoustic gravitational wave power spectrum from a first order phase transition*, *Phys. Rev.* **D96** (2017) 103520 [1704.05871].

[13] M. Kamionkowski, A. Kosowsky and M. S. Turner, *Gravitational radiation from first order phase transitions*, *Phys. Rev.* **D49** (1994) 2837 [astro-ph/9310044].

[14] C. Caprini and R. Durrer, *Gravitational waves from stochastic relativistic sources: Primordial turbulence and magnetic fields*, *Phys. Rev.* **D74** (2006) 063521 [astro-ph/0603476].

[15] C. Caprini, R. Durrer and G. Servant, *The stochastic gravitational wave background from turbulence and magnetic fields generated by a first-order phase transition*, *JCAP* **0912** (2009) 024 [0909.0622].

[16] A. Kosowsky, A. Mack and T. Kahniashvili, *Gravitational radiation from cosmological turbulence*, *Phys. Rev.* **D66** (2002) 024030 [astro-ph/0111483].

[17] G. Gogoberidze, T. Kahniashvili and A. Kosowsky, *The Spectrum of Gravitational Radiation from Primordial Turbulence*, *Phys. Rev.* **D76** (2007) 083002 [0705.1733].

[18] P. Niksa, M. Schlederer and G. Sigl, *Gravitational Waves produced by Compressible MHD Turbulence from Cosmological Phase Transitions*, *Class. Quant. Grav.* **35** (2018) 144001 [1803.02271].

[19] N. Seto, S. Kawamura and T. Nakamura, *Possibility of direct measurement of the acceleration of the universe using 0.1-Hz band laser interferometer gravitational wave antenna in space*, *Phys. Rev. Lett.* **87** (2001) 221103 [astro-ph/0108011].

[20] G. M. Harry, P. Fritschel, D. A. Shaddock, W. Folkner and E. S. Phinney, *Laser interferometry for the big bang observer*, *Class. Quant. Grav.* **23** (2006) 4887.

[21] M. Trodden, *Electroweak baryogenesis*, *Rev. Mod. Phys.* **71** (1999) 1463 [hep-ph/9803479].

[22] D. E. Morrissey and M. J. Ramsey-Musolf, *Electroweak baryogenesis*, *New J. Phys.* **14** (2012) 125003 [1206.2942].

[23] Z. Chacko, H.-S. Goh and R. Harnik, *The Twin Higgs: Natural electroweak breaking from mirror symmetry*, *Phys. Rev. Lett.* **96** (2006) 231802 [hep-ph/0506256].

[24] E. Ma, *Verifiable radiative seesaw mechanism of neutrino mass and dark matter*, *Phys. Rev.* **D73** (2006) 077301 [hep-ph/0601225].

[25] Particle Data Group collaboration, M. Tanabashi et al., *Review of Particle Physics*, *Phys. Rev. D* **98** (2018) 030001.

[26] P. F. de Salas, D. V. Forero, C. A. Ternes, M. Tortola and J. W. F. Valle, *Status of neutrino oscillations 2018: 3σ hint for normal mass ordering and improved CP sensitivity*, *Phys. Lett.* **B782** (2018) 633 [1708.01186].

[27] I. Esteban, M. C. Gonzalez-Garcia, A. Hernandez-Cabezudo, M. Maltoni and T. Schwetz, *Global analysis of three-flavour neutrino oscillations: synergies and tensions in the determination of $\theta_2 3, \delta_C P$, and the mass ordering*, *JHEP* **01** (2019) 106 [1811.05487].

[28] Planck collaboration, N. Aghanim et al., *Planck 2018 results. VI. Cosmological parameters*, 1807.06209.

[29] M. Cirelli, N. Fornengo and A. Strumia, *Minimal dark matter*, *Nucl. Phys.* **B753** (2006) 178 [hep-ph/0512090].

[30] R. Barbieri, L. J. Hall and V. S. Rychkov, *Improved naturalness with a heavy Higgs: An Alternative road to LHC physics*, *Phys. Rev.* **D74** (2006) 015007 [hep-ph/0603188].

[31] E. Ma, *Common origin of neutrino mass, dark matter, and baryogenesis*, *Mod. Phys. Lett.* **A21** (2006) 1777 [hep-ph/0605180].

[32] L. Lopez Honorez, E. Nezri, J. F. Oliver and M. H. G. Tytgat, *The Inert Doublet Model: An Archetype for Dark Matter*, *JCAP* **0702** (2007) 028 [hep-ph/0612275].

[33] T. Hambye, F. S. Ling, L. Lopez Honorez and J. Rocher, *Scalar Multiplet Dark Matter*, *JHEP* **07** (2009) 090 [0903.4010].

[34] E. M. Dolle and S. Su, *The Inert Dark Matter*, *Phys. Rev.* **D80** (2009) 055012 [0906.1609].

[35] L. Lopez Honorez and C. E. Yaguna, *The inert doublet model of dark matter revisited*, *JHEP* **09** (2010) 046 [1003.3125].

[36] L. Lopez Honorez and C. E. Yaguna, *A new viable region of the inert doublet model*, *JCAP* **1101** (2011) 002 [1011.1411].

[37] M. Gustafsson, S. Rydbeck, L. Lopez-Honorez and E. Lundstrom, *Status of the Inert Doublet Model and the Role of multileptons at the LHC*, *Phys. Rev.* **D86** (2012) 075019 [1206.6316].

[38] A. Goudelis, B. Herrmann and O. Stal, *Dark matter in the Inert Doublet Model after the discovery of a Higgs-like boson at the LHC*, *JHEP* **09** (2013) 106 [1303.3010].

[39] A. Arhrib, Y.-L. S. Tsai, Q. Yuan and T.-C. Yuan, *An Updated Analysis of Inert Higgs Doublet Model in light of the Recent Results from LUX, PLANCK, AMS-02 and LHC*, *JCAP* **1406** (2014) 030 [1310.0358].

[40] A. Dasgupta and D. Borah, *Scalar Dark Matter with Type II Seesaw*, *Nucl. Phys.* **B889** (2014) 637 [1404.5261].

[41] M. A. Daz, B. Koch and S. Urrutia-Quiroga, *Constraints to Dark Matter from Inert Higgs Doublet Model*, *Adv. High Energy Phys.* **2016** (2016) 8278375 [1511.04429].

[42] D. Borah and A. Gupta, *New viable region of an inert Higgs doublet dark matter model with scotogenic extension*, *Phys. Rev.* **D96** (2017) 115012 [1706.05034].

[43] D. Borah, P. S. B. Dev and A. Kumar, *TeV scale leptogenesis, inflaton dark matter and neutrino mass in a scotogenic model*, *Phys. Rev.* **D99** (2019) 055012 [1810.03645].

[44] A. Ahriche, A. Jueid and S. Nasri, *Radiative neutrino mass and Majorana dark matter within an inert Higgs doublet model*, *Phys. Rev.* **D97** (2018) 095012 [1710.03824].

[45] D. Mahanta and D. Borah, *Fermion dark matter with N_2 leptogenesis in minimal scotogenic model*, *JCAP* **1911** (2019) 021 [1906.03577].

[46] T. Hugle, M. Platscher and K. Schmitz, *Low-Scale Leptogenesis in the Scotogenic Neutrino Mass Model*, *Phys. Rev.* **D98** (2018) 023020 [1804.09660].

[47] W.-C. Huang, H. Ps and S. Zeiner, *Scalar Dark Matter, GUT baryogenesis and Radiative neutrino mass*, *Phys. Rev.* **D98** (2018) 075024 [1806.08204].

[48] S. Baumholzer, V. Brdar and P. Schwaller, *The New νMSM ($\nu\nu$MSM): Radiative Neutrino Masses, keV-Scale Dark Matter and Viable Leptogenesis with sub-TeV New Physics*, *JHEP* **08** (2018) 067 [1806.06864].

[49] D. Borah, A. Dasgupta and S. K. Kang, *Leptogenesis from Dark Matter Annihilations in Scotogenic Model*, 1806.04689.

[50] D. Mahanta and D. Borah, *TeV Scale Leptogenesis with Dark Matter in Non-standard Cosmology*, 1912.09726.

[51] LUX collaboration, D. S. Akerib et al., *Results from a search for dark matter in the complete LUX exposure*, *Phys. Rev. Lett.* **118** (2017) 021303 [1608.07648].

[52] PandaX-II collaboration, A. Tan et al., *Dark Matter Results from First 98.7 Days of Data from the PandaX-II Experiment*, *Phys. Rev. Lett.* **117** (2016) 121303 [1607.07400].

[53] PandaX-II collaboration, X. Cui et al., *Dark Matter Results From 54-Ton-Day Exposure of PandaX-II Experiment*, *Phys. Rev. Lett.* **119** (2017) 181302 [1708.06917].

[54] XENON collaboration, E. Aprile et al., *First Dark Matter Search Results from the XENON1T Experiment*, *Phys. Rev. Lett.* **119** (2017) 181301 [1705.06655].

[55] E. Aprile et al., *Dark Matter Search Results from a One Tonne×Year Exposure of XENON1T*, 1805.12562.

[56] T. A. Chowdhury, M. Nemevsek, G. Senjanovic and Y. Zhang, *Dark Matter as the Trigger of Strong Electroweak Phase Transition*, *JCAP* **1202** (2012) 029 [1110.5334].

[57] D. Borah and J. M. Cline, *Inert Doublet Dark Matter with Strong Electroweak Phase Transition*, *Phys. Rev.* **D86** (2012) 055001 [1204.4722].

[58] G. Gil, P. Chankowski and M. Krawczyk, *Inert Dark Matter and Strong Electroweak Phase Transition*, *Phys. Lett.* **B717** (2012) 396 [1207.0084].

[59] J. M. Cline and K. Kainulainen, *Improved Electroweak Phase Transition with Subdominant Inert Doublet Dark Matter*, *Phys. Rev.* **D87** (2013) 071701 [1302.2614].

[60] N. Blinov, S. Profumo and T. Stefaniak, *The Electroweak Phase Transition in the Inert Doublet Model*, *JCAP* **1507** (2015) 028 [1504.05949].

[61] F. P. Huang and J.-H. Yu, *Exploring inert dark matter blind spots with gravitational wave signatures*, *Phys. Rev.* **D98** (2018) 095022 [1704.04201].

[62] X. Liu and L. Bian, *Dark matter and electroweak phase transition in the mixed scalar dark matter model*, *Phys. Rev.* **D97** (2018) 055028 [1706.06042].

[63] K. Fujikura, K. Kamada, Y. Nakai and M. Yamaguchi, *Phase Transitions in Twin Higgs Models*, *JHEP* **12** (2018) 018 [1810.00574].

[64] D. Borah, A. Dasgupta, K. Fujikura, S. K. Kang and D. Mahanta, *Observable Gravitational Waves in Minimal Scotogenic Model*, *JCAP* **08** (2020) 046 [2003.02276].

[65] MEG collaboration, A. M. Baldini et al., *Search for the lepton flavour violating decay $\mu^+ \to e^+\gamma$ with the full dataset of the MEG experiment*, *Eur. Phys. J.* **C76** (2016) 434 [1605.05081].

[66] SINDRUM collaboration, U. Bellgardt et al., *Search for the Decay mu+ —¿ e+ e+ e-*, *Nucl. Phys.* **B299** (1988) 1.

[67] SINDRUM II collaboration, C. Dohmen et al., *Test of lepton flavor conservation in mu —¿ e conversion on titanium*, *Phys. Lett.* **B317** (1993) 631.

[68] T. Toma and A. Vicente, *Lepton Flavor Violation in the Scotogenic Model*, *JHEP* **01** (2014) 160 [1312.2840].

[69] W. J. Marciano and A. I. Sanda, *Exotic Decays of the Muon and Heavy Leptons in Gauge Theories*, *Phys. Lett. B* **67** (1977) 303.

[70] ATLAS, CMS collaboration, G. Aad et al., *Measurements of the Higgs boson production and decay rates and constraints on its couplings from a combined ATLAS and CMS analysis of the LHC pp collision data at $\sqrt{s} = 7$ and 8 TeV*, *JHEP* **08** (2016) 045 [1606.02266].

[71] R. Barbieri and G. F. Giudice, *Upper Bounds on Supersymmetric Particle Masses*, *Nucl. Phys.* **B306** (1988) 63.

[72] R. Barbieri and A. Strumia, *The 'LEP paradox'*, in *4th Rencontres du Vietnam: Physics at Extreme Energies (Particle Physics and Astrophysics)*, 7, 2000, hep-ph/0007265.

[73] F. Zwicky, *Die Rotverschiebung von extragalaktischen Nebeln*, *Helv. Phys. Acta* **6** (1933) 110.

[74] V. Rubin, N. Thonnard and J. Ford, W.K., *Rotational properties of 21 SC galaxies with a large range of luminosities and radii, from NGC 4605 /R = 4kpc/ to UGC 2885 /R = 122 kpc/*, *Astrophys. J.* **238** (1980) 471.

[75] R. Massey, T. Kitching and J. Richard, *The dark matter of gravitational lensing*, *Rept. Prog. Phys.* **73** (2010) 086901 [1001.1739].

[76] K. GRIEST and J. SILK, *No more neutrino cold dark matter*, *Nature* **343** (1990) 26.

[77] E. Witten, *Cosmic Separation of Phases*, *Phys. Rev. D* **30** (1984) 272.

[78] N. Craig, A. Katz, M. Strassler and R. Sundrum, *Naturalness in the Dark at the LHC*, *JHEP* **07** (2015) 105 [1501.05310].

[79] G. Burdman, Z. Chacko, H.-S. Goh and R. Harnik, *Folded supersymmetry and the LEP paradox*, *JHEP* **02** (2007) 009 [hep-ph/0609152].

[80] A. Falkowski, S. Pokorski and M. Schmaltz, *Twin SUSY*, *Phys. Rev.* **D74** (2006) 035003 [hep-ph/0604066].

[81] S. Chang, L. J. Hall and N. Weiner, *A Supersymmetric twin Higgs*, *Phys. Rev.* **D75** (2007) 035009 [hep-ph/0604076].

[82] N. Craig and K. Howe, *Doubling down on naturalness with a supersymmetric twin Higgs*, *JHEP* **03** (2014) 140 [1312.1341].

[83] A. Katz, A. Mariotti, S. Pokorski, D. Redigolo and R. Ziegler, *SUSY Meets Her Twin*, *JHEP* **01** (2017) 142 [1611.08615].

[84] M. Badziak and K. Harigaya, *Supersymmetric D-term Twin Higgs*, *JHEP* **06** (2017) 065 [1703.02122].

[85] M. Badziak and K. Harigaya, *Minimal Non-Abelian Supersymmetric Twin Higgs*, *JHEP* **10** (2017) 109 [1707.09071].

[86] M. Badziak and K. Harigaya, *Asymptotically Free Natural Supersymmetric Twin Higgs Model*, *Phys. Rev. Lett.* **120** (2018) 211803 [1711.11040].

[87] P. Batra and Z. Chacko, *A Composite Twin Higgs Model*, *Phys. Rev.* **D79** (2009) 095012 [0811.0394].

[88] M. Geller and O. Telem, *Holographic Twin Higgs Model*, *Phys. Rev. Lett.* **114** (2015) 191801 [1411.2974].

[89] R. Barbieri, D. Greco, R. Rattazzi and A. Wulzer, *The Composite Twin Higgs scenario*, *JHEP* **08** (2015) 161 [1501.07803].

[90] M. Low, A. Tesi and L.-T. Wang, *Twin Higgs mechanism and a composite Higgs boson*, *Phys. Rev.* **D91** (2015) 095012 [1501.07890].

[91] C. Csaki, M. Geller, O. Telem and A. Weiler, *The Flavor of the Composite Twin Higgs*, *JHEP* **09** (2016) 146 [1512.03427].

[92] E. Ma, *Pathways to naturally small neutrino masses*, *Phys. Rev. Lett.* **81** (1998) 1171 [hep-ph/9805219].

[93] A. Merle and M. Platscher, *Running of radiative neutrino masses: the scotogenic model revisited*, *JHEP* **11** (2015) 148 [1507.06314].

[94] J. A. Casas and A. Ibarra, *Oscillating neutrinos and muon —¿ e, gamma*, *Nucl. Phys.* **B618** (2001) 171 [hep-ph/0103065].

[95] E. Lundstrom, M. Gustafsson and J. Edsjo, *The Inert Doublet Model and LEP II Limits*, *Phys. Rev.* **D79** (2009) 035013 [0810.3924].

[96] ATLAS collaboration, M. Aaboud et al., *Combination of searches for invisible Higgs boson decays with the ATLAS experiment*, *Phys. Rev. Lett.* **122** (2019) 231801 [1904.05105].

[97] D. Borah and A. Dasgupta, *Leftright symmetric models with a mixture of keVTeV dark matter*, *J. Phys.* **G46** (2019) 105004 [1710.06170].

[98] X. Miao, S. Su and B. Thomas, *Trilepton Signals in the Inert Doublet Model*, *Phys. Rev.* **D82** (2010) 035009 [1005.0090].

[99] A. Datta, N. Ganguly, N. Khan and S. Rakshit, *Exploring collider signatures of the inert Higgs doublet model*, *Phys. Rev.* **D95** (2017) 015017 [1610.00648].

[100] P. Poulose, S. Sahoo and K. Sridhar, *Exploring the Inert Doublet Model through the dijet plus missing transverse energy channel at the LHC*, *Phys. Lett.* **B765** (2017) 300 [1604.03045].

[101] M. Hashemi and S. Najjari, *Observability of Inert Scalars at the LHC*, 1611.07827.

[102] A. Belyaev, G. Cacciapaglia, I. P. Ivanov, F. Rojas and M. Thomas, *Anatomy of the Inert Two Higgs Doublet Model in the light of the LHC and non-LHC Dark Matter Searches*, 1612.00511.

[103] A. Belyaev, T. R. Fernandez Perez Tomei, P. G. Mercadante, C. S. Moon, S. Moretti, S. F. Novaes et al., *Advancing LHC probes of dark matter from the inert two-Higgs-doublet model with the monojet signal*, *Phys. Rev.* **D99** (2019) 015011 [1809.00933].

[104] D. Borah, S. Sadhukhan and S. Sahoo, *Lepton Portal Limit of Inert Higgs Doublet Dark Matter with Radiative Neutrino Mass*, 1703.08674.

[105] D. Borah, D. Nanda, N. Narendra and N. Sahu, *Right-handed neutrino dark matter with radiative neutrino mass in gauged B L model*, *Nucl. Phys.* **B950** (2020) 114841 [1810.12920].

[106] M. Sher, *Electroweak Higgs Potentials and Vacuum Stability*, *Phys. Rept.* **179** (1989) 273.

[107] G. C. Branco, P. M. Ferreira, L. Lavoura, M. N. Rebelo, M. Sher and J. P. Silva, *Theory and phenomenology of two-Higgs-doublet models*, *Phys. Rept.* **516** (2012) 1 [1106.0034].

[108] D. Dercks and T. Robens, *Constraining the Inert Doublet Model using Vector Boson Fusion*, *Eur. Phys. J.* **C79** (2019) 924 [1812.07913].

[109] I. F. Ginzburg and I. P. Ivanov, *Tree-level unitarity constraints in the most general 2HDM*, *Phys. Rev.* **D72** (2005) 115010 [hep-ph/0508020].

[110] M. Aoki, S. Kanemura, M. Kikuchi and K. Yagyu, *Renormalization of the Higgs Sector in the Triplet Model*, *Phys. Lett.* **B714** (2012) 279 [1204.1951].

[111] A. Vicente and C. E. Yaguna, *Probing the scotogenic model with lepton flavor violating processes*, *JHEP* **02** (2015) 144 [1412.2545].

[112] P. Gondolo and G. Gelmini, *Cosmic abundances of stable particles: Improved analysis*, *Nucl. Phys.* **B360** (1991) 145.

[113] K. Griest and D. Seckel, *Three exceptions in the calculation of relic abundances*, *Phys. Rev. D* **43** (1991) 3191.

[114] G. Belanger, F. Boudjema, A. Pukhov and A. Semenov, *micrOMEGAs 3: A program for calculating dark matter observables*, *Comput. Phys. Commun.* **185** (2014) 960 [1305.0237].

[115] D. Kirzhnits and A. D. Linde, *Macroscopic Consequences of the Weinberg Model*, *Phys. Lett. B* **42** (1972) 471.

[116] S. Weinberg, *Perturbative Calculations of Symmetry Breaking*, *Phys. Rev. D* **7** (1973) 2887.

[117] L. Dolan and R. Jackiw, *Symmetry Behavior at Finite Temperature*, *Phys. Rev. D* **9** (1974) 3320.

[118] T. Matsubara, *A New approach to quantum statistical mechanics*, *Prog. Theor. Phys.* **14** (1955) 351.

[119] S. Weinberg, *The quantum theory of fields. Vol. 2: Modern applications*. Cambridge University Press, 8, 2013.

[120] M. E. Carrington, *The Effective potential at finite temperature in the Standard Model*, *Phys. Rev.* **D45** (1992) 2933.

[121] P. B. Arnold and O. Espinosa, *The Effective potential and first order phase transitions: Beyond leading-order*, *Phys. Rev.* **D47** (1993) 3546 [hep-ph/9212235].

[122] R. R. Parwani, *Resummation in a hot scalar field theory*, *Phys. Rev. D* **45** (1992) 4695 [hep-ph/9204216].

[123] P. Basler, M. Krause, M. Muhlleitner, J. Wittbrodt and A. Wlotzka, *Strong First Order Electroweak Phase Transition in the CP-Conserving 2HDM Revisited*, *JHEP* **02** (2017) 121 [1612.04086].

[124] A. D. Linde, *Infrared Problem in Thermodynamics of the Yang-Mills Gas*, *Phys. Lett.* **96B** (1980) 289.

[125] D. J. Gross, R. D. Pisarski and L. G. Yaffe, *QCD and Instantons at Finite Temperature*, *Rev. Mod. Phys.* **53** (1981) 43.

[126] P. B. Arnold, *The Electroweak phase transition: Part 1. Review of perturbative methods*, in *8th International Seminar on High-energy Physics (Quarks 94) Vladimir, Russia, May 11-18, 1994*, pp. 71–86, 1994, hep-ph/9410294.

[127] J. Callan, Curtis G. and S. R. Coleman, *The Fate of the False Vacuum. 2. First Quantum Corrections*, *Phys. Rev. D* **16** (1977) 1762.

[128] S. R. Coleman, *The Fate of the False Vacuum. 1. Semiclassical Theory*, *Phys. Rev. D* **15** (1977) 2929.

[129] A. D. Linde, *Fate of the False Vacuum at Finite Temperature: Theory and Applications*, *Phys. Lett.* **100B** (1981) 37.

[130] J. R. Espinosa, T. Konstandin, J. M. No and G. Servant, *Energy Budget of Cosmological First-order Phase Transitions*, *JCAP* **1006** (2010) 028 [1004.4187].

[131] P. Binetruy, A. Bohe, C. Caprini and J.-F. Dufaux, *Cosmological Backgrounds of Gravitational Waves and eLISA/NGO: Phase Transitions, Cosmic Strings and Other Sources*, *JCAP* **1206** (2012) 027 [1201.0983].

[132] C. Caprini et al., *Science with the space-based interferometer eLISA. II: Gravitational waves from cosmological phase transitions*, *JCAP* **1604** (2016) 001 [1512.06239].

[133] J. Ellis, M. Lewicki and J. M. No, *On the Maximal Strength of a First-Order Electroweak Phase Transition and its Gravitational Wave Signal*, *JCAP* **04** (2019) 003 [1809.08242].

[134] D. Cutting, M. Hindmarsh and D. J. Weir, *Vorticity, kinetic energy, and suppressed gravitational wave production in strong first order phase transitions*, *Phys. Rev. Lett.* **125** (2020) 021302 [1906.00480].

[135] J. Ellis, M. Lewicki and J. M. No, *Gravitational waves from first-order cosmological phase transitions: lifetime of the sound wave source*, 2003.07360.

[136] P. J. Steinhardt, *Relativistic Detonation Waves and Bubble Growth in False Vacuum Decay*, *Phys. Rev.* **D25** (1982) 2074.

[137] S. J. Huber and M. Sopena, *An efficient approach to electroweak bubble velocities*, 1302.1044.

[138] L. Leitao and A. Megevand, *Hydrodynamics of phase transition fronts and the speed of sound in the plasma*, *Nucl. Phys.* **B891** (2015) 159 [1410.3875].

[139] G. C. Dorsch, S. J. Huber and T. Konstandin, *Bubble wall velocities in the Standard Model and beyond*, *JCAP* **1812** (2018) 034 [1809.04907].

[140] J. M. Cline and K. Kainulainen, *Electroweak baryogenesis at high wall velocities*, 2001.00568.

[141] S. J. Huber and T. Konstandin, *Gravitational Wave Production by Collisions: More Bubbles*, *JCAP* **0809** (2008) 022 [0806.1828].

[142] R. Jinno and M. Takimoto, *Gravitational waves from bubble collisions: An analytic derivation*, *Phys. Rev.* **D95** (2017) 024009 [1605.01403].

[143] R. Jinno and M. Takimoto, *Gravitational waves from bubble dynamics: Beyond the Envelope*, *JCAP* **1901** (2019) 060 [1707.03111].

[144] R. Jinno, S. Lee, H. Seong and M. Takimoto, *Gravitational waves from first-order phase transitions: Towards model separation by bubble nucleation rate*, *JCAP* **1711** (2017) 050 [1708.01253].

[145] C. Kilic and S. Swaminathan, *Can A Pseudo-Nambu-Goldstone Higgs Lead To Symmetry Non-Restoration?*, *JHEP* **01** (2016) 002 [1508.05121].

[146] L. Delle Rose, C. Marzo and A. Urbano, *On the fate of the Standard Model at finite temperature*, *JHEP* **05** (2016) 050 [1507.06912].

[147] S. Bruggisser, B. Von Harling, O. Matsedonskyi and G. Servant, *Baryon Asymmetry from a Composite Higgs Boson*, *Phys. Rev. Lett.* **121** (2018) 131801 [1803.08546].

[148] S. Bruggisser, B. Von Harling, O. Matsedonskyi and G. Servant, *Electroweak Phase Transition and Baryogenesis in Composite Higgs Models*, *JHEP* **12** (2018) 099 [1804.07314].

[149] D. Croon, V. Sanz and G. White, *Model Discrimination in Gravitational Wave spectra from Dark Phase Transitions*, *JHEP* **08** (2018) 203 [1806.02332].

[150] D. Comelli and J. R. Espinosa, *Bosonic thermal masses in supersymmetry*, *Phys. Rev.* **D55** (1997) 6253 [hep-ph/9606438].

[151] K. Rummukainen, M. Tsypin, K. Kajantie, M. Laine and M. E. Shaposhnikov, *The Universality class of the electroweak theory*, *Nucl. Phys.* **B532** (1998) 283 [hep-lat/9805013].

[152] K. Farakos, K. Kajantie, K. Rummukainen and M. E. Shaposhnikov, *3-D physics and the electroweak phase transition: Perturbation theory*, *Nucl. Phys.* **B425** (1994) 67 [hep-ph/9404201].

[153] K. Kajantie, M. Laine, K. Rummukainen and M. E. Shaposhnikov, *Generic rules for high temperature dimensional reduction and their application to the standard model*, *Nucl. Phys.* **B458** (1996) 90 [hep-ph/9508379].

[154] K. Kajantie, M. Laine, K. Rummukainen and M. E. Shaposhnikov, *High temperature dimensional reduction and parity violation*, *Phys. Lett.* **B423** (1998) 137 [hep-ph/9710538].

[155] J. R. Espinosa, *Dominant two loop corrections to the MSSM finite temperature effective potential*, *Nucl. Phys.* **B475** (1996) 273 [hep-ph/9604320].

[156] K. Funakubo and E. Senaha, *Two-loop effective potential, thermal resummation, and first-order phase transitions: Beyond the high-temperature expansion*, *Phys. Rev.* **D87** (2013) 054003 [1210.1737].

[157] M. Laine and M. Losada, *Two loop dimensional reduction and effective potential without temperature expansions*, *Nucl. Phys.* **B582** (2000) 277 [hep-ph/0003111].

[158] R. Barbieri, L. J. Hall and K. Harigaya, *Minimal Mirror Twin Higgs*, *JHEP* **11** (2016) 172 [1609.05589].

[159] Planck collaboration, P. A. R. Ade et al., *Planck 2015 results. XIII. Cosmological parameters*, *Astron. Astrophys.* **594** (2016) A13 [1502.01589].

[160] R. H. Cyburt, B. D. Fields, K. A. Olive and T.-H. Yeh, *Big Bang Nucleosynthesis: 2015*, *Rev. Mod. Phys.* **88** (2016) 015004 [1505.01076].

[161] Z. Chacko, N. Craig, P. J. Fox and R. Harnik, *Cosmology in Mirror Twin Higgs and Neutrino Masses*, *JHEP* **07** (2017) 023 [1611.07975].

[162] N. Craig, S. Koren and T. Trott, *Cosmological Signals of a Mirror Twin Higgs*, *JHEP* **05** (2017) 038 [1611.07977].

[163] C. Csaki, E. Kuflik and S. Lombardo, *Viable Twin Cosmology from Neutrino Mixing*, *Phys. Rev.* **D96** (2017) 055013 [1703.06884].

[164] Z. Chacko, D. Curtin, M. Geller and Y. Tsai, *Cosmological Signatures of a Mirror Twin Higgs*, 1803.03263.

[165] M. Farina, *Asymmetric Twin Dark Matter*, *JCAP* **1511** (2015) 017 [1506.03520].

[166] N. Craig and A. Katz, *The Fraternal WIMP Miracle*, *JCAP* **1510** (2015) 054 [1505.07113].

[167] I. Garcia Garcia, R. Lasenby and J. March-Russell, *Twin Higgs WIMP Dark Matter*, *Phys. Rev.* **D92** (2015) 055034 [1505.07109].

[168] M. Freytsis, S. Knapen, D. J. Robinson and Y. Tsai, *Gamma-rays from Dark Showers with Twin Higgs Models*, *JHEP* **05** (2016) 018 [1601.07556].

[169] V. Prilepina and Y. Tsai, *Reconciling Large And Small-Scale Structure In Twin Higgs Models*, *JHEP* **09** (2017) 033 [1611.05879].

[170] J. I. Kapusta and C. Gale, *Finite-temperature field theory: Principles and applications*, Cambridge Monographs on Mathematical Physics. Cambridge University Press, 2011, 10.1017/CBO9780511535130.

[171] A. Klein et al., *Science with the space-based interferometer eLISA: Supermassive black hole binaries*, *Phys. Rev.* **D93** (2016) 024003 [1511.05581].

[172] K. Yagi and N. Seto, *Detector configuration of DECIGO/BBO and identification of cosmological neutron-star binaries*, *Phys. Rev.* **D83** (2011) 044011 [1101.3940].

[173] S. Hild et al., *Sensitivity Studies for Third-Generation Gravitational Wave Observatories*, *Class. Quant. Grav.* **28** (2011) 094013 [1012.0908].

[174] H. Kudoh, A. Taruya, T. Hiramatsu and Y. Himemoto, *Detecting a gravitational-wave background with next-generation space interferometers*, *Phys. Rev.* **D73** (2006) 064006 [gr-qc/0511145].

[175] J. R. Ellis, K. A. Olive and C. Savage, *Hadronic Uncertainties in the Elastic Scattering of Supersymmetric Dark Matter*, *Phys. Rev. D* **77** (2008) 065026 [0801.3656].

[176] A. Bottino, F. Donato, N. Fornengo and S. Scopel, *Interpreting the recent results on direct search for dark matter particles in terms of relic neutralino*, *Phys. Rev. D* **78** (2008) 083520 [0806.4099].

[177] W. Porod and F. Staub, *SPheno 3.1: Extensions including flavour, CP-phases and models beyond the MSSM*, *Comput. Phys. Commun.* **183** (2012) 2458 [1104.1573].

[178] C. Wainwright, S. Profumo and M. J. Ramsey-Musolf, *Gravity Waves from a Cosmological Phase Transition: Gauge Artifacts and Daisy Resummations*, *Phys. Rev.* **D84** (2011) 023521 [1104.5487].

[179] C.-W. Chiang and E. Senaha, *On gauge dependence of gravitational waves from a first-order phase transition in classical scale-invariant $U(1)'$ models*, *Phys. Lett.* **B774** (2017) 489 [1707.06765].

[180] C. L. Wainwright, S. Profumo and M. J. Ramsey-Musolf, *Phase Transitions and Gauge Artifacts in an Abelian Higgs Plus Singlet Model*, *Phys. Rev.* **D86** (2012) 083537 [1204.5464].